



PEOPLE'S DEMOCRATIC REPUBLIC OF ALGERIA
MINISTRY OF HIGHER EDUCATION AND SCIENTIFIC RESEARCH



UNIVERSITY OF SAAD DAHLAB BLIDA 1
FACULTY OF TECHNOLOGY
MECHANICAL ENGINEERING DEPARTMENT

To obtain the Master's Degree in Mechanical Engineering, Major:
Materials Engineering
Laboratory for studies and research in industrial technology

Title

Lubricated a dry sliding properties of select 2D Materials

By:

Menari Ikram

Proposed and led by:

Dr. Nemri yacine

Co-promoter:

Dr. Benamor Abdessabour

University year: 2022/2023

summary

Chapter I: recherche bibliographic of two demonsional materials

I .1.Introduction.....	3
I.2.Different of two dimensional materials.....	4
I.2.1 Graphene.....	5
I.2.2 Graphene oxide (GO).....	6
I.2.3 MXenes - MBenes Based 2D Materials.....	7
I.2.4 Bororphene.....	10
I.2.5 Bismuthene.....	11
I.2.6. The transition metal dichalcogenides (TMDCs).....	12
I.2.7. The 2D material Nano-filament	14
CHAPTER II:PROPERTIES AND LUBRICATION	
II.Introduction.....	16
II.2.The properties of 2D materials.....	17
II.2.1. Graphene properties.....	17
II .2.2.The Mbenes properties	20
II.2.3. Mxene properties.....	21
II .2.4.properties of borophene.....	21
II .3.The lubrications.....	27
II .3.1.Role of 2D materials in friction and wear reduction mechanisms.....	28
II .3.2.Tribofilm.....	28
II .3.3.Other possible roles.....	29
II.4.Tribology of 2d materials.....	30
II .4.1.Graphene and Graphene-Family.....	30
II .5.Graphene liquid lubrication.....	35
II .6.Mxenes lubrication.....	39
II .7.External Factors.....	43

II .8. Discussing generally of the synthesis and characterization of nano- filament derived from multiple materials procures of titanium family	47
II .8.1.The Properties.....	50
II .8.2.The .Mechanisms.....	50

CHAPTER III:EXPERIMENTAL PART ELABORATION AND CHARACTERIZATION

III .1.Introduction.....	59
III .2.Materials.....	59
III.3.Stability tests.....	59
III.4.Methods.....	62
III.4.1. Oillubrication.....	62
III.4.2. Dry lubrication.....	62
III .5.Understanding steps by thesemethods.....	63
III .5.1.Spray coating.....	64
III.5.2.Drop casting.....	64
III .5.3.immersion.....	64
III.5.4.immersion assisted by ultrasonication.....	64
III.6. Preparation coating of nanofilament derived from TiB ₂ dry lubricantion.....	65
III .6.1.Spray coating.....	65
III .6.2.Test with dropcasting.....	70
III .6.3.Method the immersion assisted byultrasonication.....	71
III .6.4.Another method immersion by laboratoryoven.....	72
III.6.5.generally laboratory materials are used.....	80
Chapter IV Results and discussion	
IV.1 Introduction.....	87
IV .2 Spray coating testing.....	87
IV .2 .1 the first and second test results.....	88
IV .2.2 Discusses the results of tribological testing.....	88
IV .2 .3 optical microscope as part of investigation.....	89

<i>IV .2.4 discusses the results.....</i>	89
<i>IV.3 Oil lubrication.....</i>	90
<i>IV .3.1 discusses the tribological tests.....</i>	90
<i>IV .3.2microscope optical results.....</i>	91
<i>IV .3.3 discusses the results.....</i>	92
<i>IV .3.4 different concentration between TiB2 and Cr2CTx.....</i>	95
<i>IV .4.the wear rate tests.....</i>	97
<i>IV .5. Calculate different wear rate.....</i>	98

CONCLUSION GENERAL

List of tables and figures

Figure I.1: Graphene the first example of a big family.....	5
Figure I.2: (a) Typical preparation of graphene oxide (GO). Pristine graphite powder is reacted with in strong oxidant. Upon oxidation and purification.....	6
Figure I.3: Three different formulas (M_2XT_x , $M_3X_2T_x$, and $M_4X_3T_x$) and compositions (mono-MMxenes and double-M Mxenes)	7
Figure I.4: Three structures of borophene.....	8
Figure I.5: Top and side views of (A) 2D β -Bi and (B) α -Bi . 2D, two dimensional.	10
Figure I.6: Composition of TMDCs.....	12
Figure I.7: known layered TMDs in the periodic table highlighted with shadow.....	13
Figure II.1 : Compositions, properties, synthesis, film preparation, and patterning of MXenes for integrated MXene- based nanoelectronics.....	21
Figure II.2: (a) Absorption coefficient of borophene and (b) reflectivity alongside the different two directions. Reprinted with permission	25
Figure II.3 : (a) β 12 borophene is in contact with 2D semiconductor atoms. The electron injection monolayer β 12 borophene shows its path ($A \rightarrow B \rightarrow C \rightarrow D \rightarrow E$) by the red arrow.....	25
Figure II.4 : (a) The total lattice thermal conductivity of borophene as a function of temperature by using the iterative (solid line) and relaxation time approximation (RTA) solution of phonon Boltzmann transport equation (PBTE).....	27
Figure II.5: (a) A lateral force image of graphene/PDMS sample done under a low load after two scratch tests; the black arrows indicate the scratch direction.....	32
Figure II.6: (a) COF of CVD deposited monolayer graphene versus sliding cycles with changing applied normal load. (b) Average COF at different applied normal load. (c) The COF versus sliding cycles along the sliding track. (d) Topography of the sliding track obtained with SEM	35

Figure II 7: (a) Curves of COF versus time, (b) average COF under different test conditions, and (c–e) topography of wear tracks obtained with SEM, (f–h) 3D morphologies of the wear track surfaces, and (i–k) 2D line profiles of the wear tracks on Si substrates.36

Figure II 8: (a) Schematic diagram of the electrophoretic deposition fabrication process. (b) COF of GO, MoS2 and GO-MoS2 films versus time under ambient condition with 3 N normal load. (c) Influence of normal load on average COF of different films. (d) Cross-sectional transmission electron microscopy (TEM) image depicted from the tribofilm. (e) High resolution transmission electron microscopy (HRTEM) image shows that GO nanoflakes wrapping around MoS2 nanoflakes.38

Figure II.9: (a) Frictional force while SAFM probe sliding against graphene with the lubrication of water. The corresponding COF was 0.0003. Reproduced with permission . (b) Friction forces between AFMcolloidal probeand composite MAC/rGO film..... 39

Figure II.10: (a) Schematic diagram of friction tests using AFM. (b) Friction of Mica, Ti3C2, and Nb2C under different pressure. (c) Adhesion force of Mica, Ti3C2, and Nb2C under different preloading forces. (d) Friction of Mica, Ti3C2, and Nb2C under different temperatures. (e) Adhesion force of Mica, Ti3C2, and Nb2C under different temperatures. (f) Schematic diagram of friction principle and structure of Ti3C241

Figure II.11: (a) SEM image of cross-sectional Ti3C2 coatings with a thickness of 200 nm. (b) COF curves of copper and Ti3C2 coatings under different loads. (c) Wear rate of copper and Ti3C2 coatings under different loads. (d) Cross-section image of MXene coating with a thickness of 100 nm. (e) COF curves of MXene coating and reference. (f) A comparison of normalized wear life and COF in this work with other 2D materials when they are used as solid lubricants. (a-c) Reproduced with permission42

FigureII.12: (a) Friction coefficient of Ti3C2 under different concentrations. (b) Friction coefficient under different applied loads with various contents of Ti3C2. (c) EDS analysis of worn surfaces on steels lubricated by 1.0 wt% Ti3C2 base oil43

Figure II.13: (a) The preparation process of Ti3C2Tx/EP composite. (b) The wear rate of EP with different Ti3C2Tx contents from 0 to 3.0 wt%. (c) COF curves over time ofas-prepared coatings under different sliding speeds from 0.03 to 0.8 ms⁻¹ (d) COF curves over time of as-prepared coatings at the speed of 0.4 ms⁻¹. (e) The wearrate of as-prepared coatings at the speed of 0.4 ms⁻¹43

FigureII.14: Tribological properties of as-prepared coatings under different environments. (a) and (b) Air. (c) and (d) Relative humidity of 80%. (e) and (f) Vacuum..... 47

FigureII.15: Characterization of 2D material	51
FigureII.16: TCO Flake morphology.....	52
Figure II.17: XRD patterns and DFT-generated 1DL structure	53
Figure II.18: ABF STEM micrograph of a bundle of individual 1DL NFs	55
Figure II.19: Low angle annular dark field STEM micrograph of sample	56
Figure II.20: STEM characterization of TiC-derived NFs	56
Figure III.1: Propanol +TiB ₂ ; a) in few seconds and b) after 15 min.....	60
Figure III.2: Acetone+TiB ₂ ; a) in few seconds and b) after 15 min	60
Figure III.3: Water+TiB ₂ ; a) in few seconds and b) after 15 min	61
Figure III.4: Ethanol+TiB ₂ ; a) in few seconds and b) after 15 min	61
FigureIII.5: (a) sample ultrasonically cleaned in ethanol; (b)solution mixed in ultrasonication; (c)coating sample.....	65
Figure III.6: coating tests of 100 Cr6 with different shape that aren't achieved.....	66
Figure III.7: The spray coating in the fifth test were achieved	66
Figure III.8: For the sixth test of spray coating are not achieved.....	67
Figure III.9: After spray coating with a closer, more detailed look.....	68
Figure III.10: After spray coating with a closer, more detailed look.....	69
FigureIII.11: coating surface of stainless steel 430C with drop casting succed.....	70
Figure III.12: coating surface of 430C with drop casting failed.....	70
FigureIII.13: method of immersion the sample assisted by ultrasonication.....	71
FigureIII.14: coating results of the surface 430C.....	71
FigureIII.15: solution subjected to ultrasonication	72
FigureIII.16: coating surface with 7.5mg TiB ₂ powder results by laboratory oven.....	73
FigureIII.17: coating surface with 5mg of TiB ₂ powder results by laboratory oven.....	73

FigureIII.18: coating surface with concentration 2.5mg of TiB ₂	74
FigureIII.19 coating surface with concentration 1 mg TiB ₂ powder mixed with 5 ml of water.....	74
FigureIII.20: different coating results with (a):5mg TiB ₂ ;(b) 2.5mgTiB ₂ ;(c)1mgTiB ₂	75
FigureIII.21: results of coating with 7.5mg concentration TiB ₂ of ethanol.....	76
FigureIII.22: TiB ₂ misured.....	77
FigureIII.23: 0.5%TiB ₂ solution with homoginization	78
FigureIII.24: 0.25%Cr ₂ CTx solution on magentic stirrer	79
Figure III.25: mixed the solution 0.25%Cr ₂ CTx on homoginization	79
FigureIII.26: polisher image.....	80
FigureIII.27: the ultrasonication image	81
FigureIII.28: magentic stirrer image	81
FigureIII.29: :(a) homoginization image ; (b) laboratory oven	82
FigureIII.30: Lubricant:Paraffin oil.....	83
FigureIII.31: ethanol.....	84
Figure III.32: a)tribometry images; b) optical microscope	85
Fig. IV .1: Friction coefficient variation versus sliding distance. 1N load.....	88
Fig. IV .2: Friction coefficient variation versus sliding distance. 2N load.....	90
Figure IV .3: (a) and (c) show the surfaces of the steel ball against nanofilament derived from TiB ₂	91
Figure IV .4 : Friction coefficient variation versus time of (A) Cr ₂ CTX%; (B) TiB ₂ %.....	91
Figure IV .5: Microscope optical of Cr ₂ CTX 2D in multiple concentrations; (a) reference sample; (b) 0.1%Cr ₂ CTX; (c) 0.5%Cr ₂ CTX; (d) 1%Cr ₂ CTX.....	92
Figure IV .6: Microscope optical of nfs derived from TiB ₂ in multiple concentrations.....	94

Figure IV 7: Microscope optical of balls Cr ₂ CTx; (a) sample REF ; (b) 0.1% Cr ₂ CTx ; (c) 0.5% Cr ₂ CTx ; (d) 1% Cr ₂ CTx.....	95
Figure IV .8: Microscope optical of TiB ₂ (a) sample ref; (b) 0.1%TiB ₂ ; (c) 0.25%TiB ₂ ; (d) 0.5% TiB ₂ ; (e) 0.75%TiB ₂ ; (f) 1% TiB ₂	96
Figure IV. 9: The coefficient friction (μ) versus additive concentration (Wt. %) between TiB ₂ and Cr ₂ CTx.....	96
Figure IV. 10: Coefficient friction versus concentration both of (A) Cr 2 Ctx % and (B) TiB 2 also (c) concentration 0.5 % TiB 2 of the wear rate test.....	97
Table 1: the wear rate in different concentration of materials.....	98
Figure IV .11: The wear rate ($\text{mm}^2 / \text{N.m}$) $\times 10^{-7}$ calculated versus additive concentration W.t% of TiB ₂ +A.O.....	99
Figure IV .12: the wear rate ($\text{mm}^2 / \text{N.m}$) $\times 10^{-7}$ calculated versus additive concentration W.t% between TiB ₂ and Cr ₂ CTx.....	99

THANKS

I would like to take this opportunity to express my sincere gratitude to the individuals and organizations who have played a significant role in the completion of this memoire. First and foremost, I am deeply grateful to my supervisor, Mr.yacine Nemri, for unwavering support, invaluable guidance, and insightful feedback throughout the research process.

Their expertise and dedication have been instrumental in shaping this work. I am also thankful to co-supervisor Mr. Abdessabour Benamor, the participants of this study, whose willingness to share their experiences and insights provided the foundation for my research.

dedication

my heartfelt appreciation goes to my dear family and friends for their unconditional love, encouragement, and understanding throughout this journey. Their constant belief in me has been a source of motivation and inspiration. I am truly grateful for all the support I have received, and without it, this memoire would not have been possible.

Also I am grateful to Mr.Abdessabour benamor for hes belief in this project, combined with hes exceptional knowledge and insights, have shaped it into what it is today. hes mentorship and encouragement have not only helped me navigate challenges but also inspired me to push my limits and strive for excellence.

Abstract

The objective of this work generally about elaboration of new material called dimensional nanofilament derived from TiB_2 ; this study focuses on fabricating a solid lubricant using a novel materials called nanofilament TiB_2 1D through spray coating and Cr_2CTx 2D in oil lubrication . The primary objective is to investigate the lubrication properties of this new materials by subjecting the resulting samples to tribological testing and to exhibits excellent lubrication performance, specifically in terms of reducing friction and wear. By conducting comprehensive tribological tests, the researchers seek to gain insights into the potential of this new solid lubricants for practical applications aimed at minimizing friction and wear.

résumé

L'objectif de ce travail porte généralement sur l'élaboration d'un nouveau matériau appelé nanofilament dimensionnel dérivé de TiB_2 ; cette étude se concentre sur la fabrication d'un lubrifiant solide utilisant un matériau novateur appelé nanofilament TiB_2 1D par pulvérisation et le Cr_2CTx 2D en lubrification à l'huile.

L'objectif principal est d'étudier les propriétés de lubrification de ce nouveau matériau en soumettant les échantillons obtenus à des essais tribologiques, afin de démontrer d'excellentes performances de lubrification, notamment en termes de réduction du frottement et de l'usure. En menant des tests tribologiques approfondis, les chercheurs cherchent à mieux comprendre le potentiel de ces nouveaux lubrifiants solides pour des applications pratiques visant à minimiser le frottement et l'usure.

الملخص

يركز هذا الهدف من هذا العمل عمومًا هو تطوير مادة جديدة تسمى نانوأسلاك ثنائية الأبعاد مشتقة من D بأبعاد 1 TiB2 الدراسة على تصنيع مزيج تشحيم صلب باستخدام مادة مبتكرة تسمى نانوأسلاك ثنائية الأبعاد في تشحيم الزيت Cr2CTx بالرش.

الهدف الرئيسي هو دراسة خصائص التشحيم لهذه المادة الجديدة من خلال إجراء اختبارات التحلل التدريجي للعينات المحضرة، بهدف إظهار أداء التشحيم الممتاز، بما في ذلك تقليل الاحتكاك والتآكل. من خلال إجراء اختبارات التحلل التدريجي المتعمقة، يسعى الباحثون إلى فهم أفضل لإمكانات هذه المواد التشحيم الصلبة الجديدة للتطبيقات العملية التي تهدف إلى تقليل الاحتكاك والتآكل.

Introduction general

Two-dimensional materials have gained significant attention in recent years due to their unique properties and potential applications in various fields.

Lubrication plays a critical role in minimizing friction and wear in mechanical systems, improving their efficiency and longevity. Conventional lubricants, although effective, often have limitations such as high viscosity, limited stability, and environmental concerns. Therefore, there is a growing demand for the development of new solid lubricants that can offer superior performance and overcome the drawbacks of traditional lubrication methods. In this context, the present study aims to investigate the lubrication properties of a new material called 1D nanofilament derived from TiB_2 . The fabrication of TiB_2 1D nanofilaments involves a novel approach using spray coating techniques, which allows for the deposition of a thin layer of nanofilament TiB_2 with enhanced dimensional characteristics. Additionally, the inclusion of Cr_2CTx 2D, another two-dimensional material, in oil lubrication further enhances the lubrication performance of the system. The primary objective of this research is to evaluate the tribological behavior of the TiB_2 1D nanofilament-based solid lubricant.

The unique properties of 2D materials and their potential applications have sparked intense research interest worldwide. Scientists and engineers are exploring novel approaches to harness the remarkable properties of 2D materials in diverse fields. The discovery and development of new 2D materials and their integration into functional devices hold great promise for technological advancements and innovative solutions to various challenges. In this context, this review aims to provide a comprehensive overview of the field of 2D materials, covering their synthesis, characterization, properties, and mechanisms. By understanding the fundamental aspects and exploring the potential of 2D materials.

Chapter I: recherche bibliographique of two demonsional materials

I .1. Introduction:

Two-dimensional (2D) substances are a category of nanomaterials which have dimensions (XY plane) out of doors of the nanometric length variety and atomic-scale thicknesses which are type of independent planar material have a large size to thickness ratio, they show many unique physicochemical characteristics. such as : High specific surface area to enhance ion adsorption and enhanced capacity, exclusion of weak van der Waals interactions, localization of electron known as quantum confinement, also with flexible transistor ; and photodetectors^[1].

The first study start with use of layered materials whose structure involves the stacking of individual platelets has a very long history. Graphite is one of the allotrope forms of carbon that is popularly used in pencils and other writing materials. It is highly conductive and is used in numerous industrial applications. Until relatively recently, research and applications of layered materials involved their bulk solids. It was the mechanical exfoliation of a single graphene layer from graphite in 2004 by Geim, Novoselov, and co-workers ^[2]. That focused the attention of the scientific community on the study of single or few layers of these materials ^[3].

However ; the research didn't stop on graphene they figured out a several types of 2D materials has similar properties as graphene For example the graphene oxide ; Mbenes ; carbonitrides (MXene) ; transition metal dichalcogined (TMDCs).

I.2.Different of two dimensional materials :

I.2.1 Graphene :

For a long time, it was believed that two-dimensional (2D) crystals did not exist because they could not withstand thermal fluctuations. Several past attempts to make atomic films of other materials have failed because the films become unstable and tend to separate and clump together rather than form perfect layers. Although theoretical studies of graphite fullerenes, and nanotubes were performed using single-layer graphite as the starting material that was first demonstrated in 1991, scientists succeeded in isolating single-layer graphene for the first time in 2004. Which was one of the first truly two-dimensional materials (**one atom thick carbon in an atomic -scale sp²- bonded hexagonal arrangement**), isolated in nature by Andre Geim's group, at Manchester University. ^[4]

The reported technique for obtaining real one atom thick layers with almost macroscopic lateral dimensions is really simple). This causes a variety of flakes to form on the surface. Most of these flaky materials are composed of more than ten layers ^[5].

Also Graphene is a promising electrocatalytically active material due to its unique properties of high electrical conductivity and large surface area. Owing to the low catalytic activity of pristine graphene, those with large planar conjugated structures are usually initially coupled with electrocatalytically active components through intermolecular interactions. And the stability of graphene can also be explained by the hypothesis of small out-of-plane waves. Another part of the explanation is that a 2D crystal is never a completely self-contained system. It is always in contact with the edge-clamped substrate, thus stabilizing the structure. First example of figure shows the big family of graphene. ^[6,7]

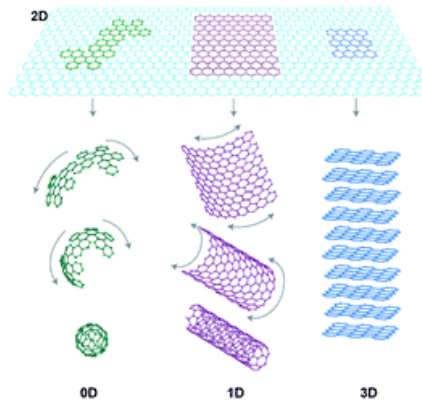


Figure I.1: Graphene the first example of a big family.

I.2.2 Graphene oxide (GO) :

Following the creation of graphene, substantial research on two-dimensional materials began in the first year of this century. Due to their height of a few atoms, two-dimensional materials are characterized by an inherently high surface-to-volume ratio. Additionally, unlike graphene, a semimetal with a band gap of zero or almost zero, these materials typically have semiconducting characteristics. Both of these characteristics make them strong contenders for the next wave of gas detectors. The first graphene-like substance to be examined and utilized to detect target gases was graphene oxide, an intermediary in the creation of graphene, which was followed by MoS₂ in the early 2010s [8].

Graphite may be exfoliated using a chemical process that has been known for 150 years to create graphene oxide (GO). Since GO is a possible precursor that can be processed in a solution for the mass manufacture of graphene, it is a two-dimensional (2D) sheet with distinctive dimensions that are distributed across two different length scales. Although the lateral dimensions of the functionalized carbon sheets might range from a few nanometers to hundreds of micrometers, their apparent thickness is around 1 nm [9].

Consists of many oxygen groups that are chemically bound to the carbon lattice, leading to fault regions, making it chemically inhomogeneous as well. Its crystal structure also includes large amounts of flaws and oxygen content, making it one of the finest materials for electrochemical sensors. Another graphene-based material with significant optical characteristics appropriate for biomedical applications, as well as one that can be functionalized easily, is called Nano-GO. It also has a greater degree of oxidation [10].

GO has regained widespread attention as a solution-processable precursor for the large-scale production of graphene for use in products such as transparent conductors, chemical sensors, biosensors, polymer; composites, batteries, and supercapacitors .

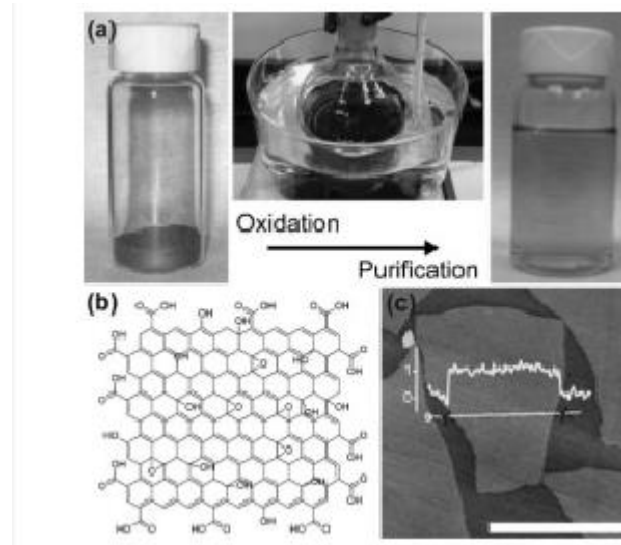


Figure I.2: (a) Typical preparation of graphene oxide (GO). Pristine graphite powder is reacted with in strong oxidant. Upon oxidation and purification. A stable light brown suspension of GO is obtained. (b) Structural model of GO. which is composed of a partially broken sp^2 -carbon network with phenol hydroxyl and epoxide groups on the basal plane and carboxylic acid groups at the edges. (c) AFM image of a GO sheet. The apparent thickness of a single sheet is around 1nm. The bar shows $5\mu\text{m}$.

I.2.3 MXenes - MBenes Based 2D Materials:

The synthesis of MXenes usually takes place in the MAX phase, which involves the use of layered ternary carbides. The molecular formula for this process is $MN_{+1}AX_n$. The various elements that are commonly used in the production of these materials include M, A, Cd, Al, Ga, Sn, P, S, and X. Some of the most common types of MXenes that have been reported are Ti_3C_2X , Ti_2CT_x , Nb_2CT_x , V_2CT_x , and Ti_3CNT_x . Other MXenes that have been shown to have excellent properties include $Mo_2Ti_2C_3Tx$, Ta_4C_3Tx , Nb_4C_3Tx , and Ti_3CNT_x [11].

With high light transmission and flexibility, MXenes sheets play an important role in the manufacture of high-efficiency solar cells, photodetectors, light-emitting diodes and liquid crystal displays (LCDs) after modulating the work function of MXenes, it is also used to form electrode B in thin film transistors, FETs, and logic devices ; Including various applications. The unique properties of MXenes sheets make them an ideal material for use in modern

electronics. Their high light transmission and flexibility allow them to be used in solar cells, photodetectors, light-emitting diodes, and LCDs, while their ability to modulate their work function allows them to be used as electrode B in thin film transistors, FETs, and logic devices. MXenes sheets are incredibly versatile due to their unique properties. They can be used for a variety of applications, from solar cells to photodetectors to light-emitting diodes. They can also be used to form electrodes for thin film transistors, FETs, and logic devices. Furthermore, they are able to modulate their work function, making them even more useful. MXenes have recently been used in energy harvesting, energy conversion, and energy storage tools, batteries, supercapacitors, Hence the high electrical energy and water splitting properties, which are considered to be very suitable for electrical and optoelectronic applications ¹².

These MXenes are composed of a transition metal (M) and an inorganic 2D sheet (X) which are connected by chemical bonds. The MXenes can have various surface terminations, such as OH, F, and O, which determine the properties of the MXenes. For example, the acidic fluorides MXenes, which are commonly made in aqueous solutions, have OH, F, and O terminations on their surfaces. These molecules are abbreviated as $M_{n+1}X_nT_x$, where T denotes the surface termination, and they come in different forms, such as M_2XT_x , $M_3X_2T_x$, and $M_4X_3T_x$ ^[13]. (Figure shows three different formulas of them):

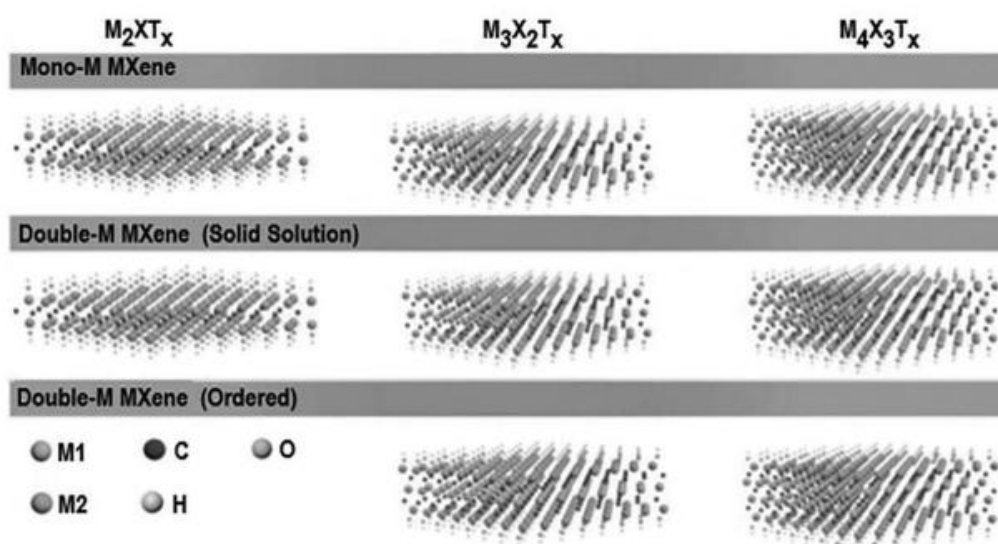


Figure I.3: Three different formulas (M_2XT_x , $M_3X_2T_x$, and $M_4X_3T_x$) and compositions (mono-M MXenes and double-M MXenes) of MXenes.

MXenes offer outstanding electronic characteristics, as demonstrated by computational and experimental studies, and are attractive candidate materials for electrochemistry, energy

storage, and electrocatalysis. The unique structure of MXenes, which consists of two-dimensional transition metal carbides and nitrides, gives them a combination of properties that make them useful for a wide range of applications. These include their ability to retain electrical conductivity even in extreme environments, their high chemical stability, and their ability to act as electronic bridges between two surfaces. Additionally, their transition metal content means that their electrical conductivity can be tuned to fit a variety of needs.

Additionally, **MBenes**, a related 2D material, offer similar properties as MXenes which making them a promising and relatively new addition to the MXene family; also attractive for use in a variety of applications, such as electrocatalysis, energy storage, and electrochemistry [14].

Comprehensive research summarized **MBenes**, which attracted more interest from researchers after extensive empirical and theoretical studies showed exciting results: energy conversion potential and characteristic electrochemical storage [14].

Ade and Hillebrecht [15] released the first publication on MBenes in 2015, identifying them as MXene derivatives. Many academics have since carried out theoretical and practical studies on the synthesis and use of MBenes 2D MBenes, although being a very new and underexplored class of nanomaterials, which are promising family of nanomaterials; MAB-MBenes have a different stoichiometry than MAX-MXenes and the layer intercalation patterns of MAB-MBenes are also different than MAX-MXenes. This means that MAB-MBenes cannot be directly attached to MAX-MXenes and must be treated separately for energy storage and catalytic reactions.

And with Chemical etching which is a type of surface treatment that uses an acid or a base to remove material from the surface of an object. When applied to an MAB phase, it selectively removes the material in certain areas, leaving behind the desired layered MBenes structure. Therefore, we nimbly expect 2D MBenes to pursuit their facile counterparts 2D MXenes in upcoming years ; this has opened up the possibility of further tuning the properties of MXenes and MBenes by controlling their stoichiometry. By adjusting the stoichiometry, it is possible to create materials with different physical, chemical and mechanical properties, which can be used in various applications . While around 30 different MXenes have already been successfully synthesized . We hypothesize that MBenes with different chemical compositions can also be synthesized due to the rapid progress on MXenes and their chemical and structural diversity [16,17].

I.2.4 Bororophene:

Bororophene can be used to develop new materials with high thermal and electrical conductivity, making it ideal for a variety of applications. Additionally, the unique structure which is honeycomb of bororophene makes it extremely strong and flexible, by B80 boron making it a potential candidate for use in a variety of industries. from aerospace to electronics. It shows in bororophene structures triangular .

The research team of (L-S WANG) was the first to experimentally confirm the planarity of boron clusters. A further experiment showed that B36 was the most stable boron cluster and had the highest symmetry since it is the smallest boron to have six fold symmetry this made it a prime candidate to be used as a building block for extended two-dimensional boron sheets [18].

Interestingly, two teams of researchers achieved high-vacuum bororophene phase synthesis on silver surfaces in 2015. Among the three bororophene phases created (Figure illustrates distinct bororophene structures), an earlier hypothesis showed the $\sqrt{3}\times\sqrt{3}$ sheet, or 12, to be the ground state on the Ag (111) surface, [19].

While the $\sqrt{3}\times\sqrt{3}$ bororophene was predicted by the Zeng team in 2012, it was not discovered until now .

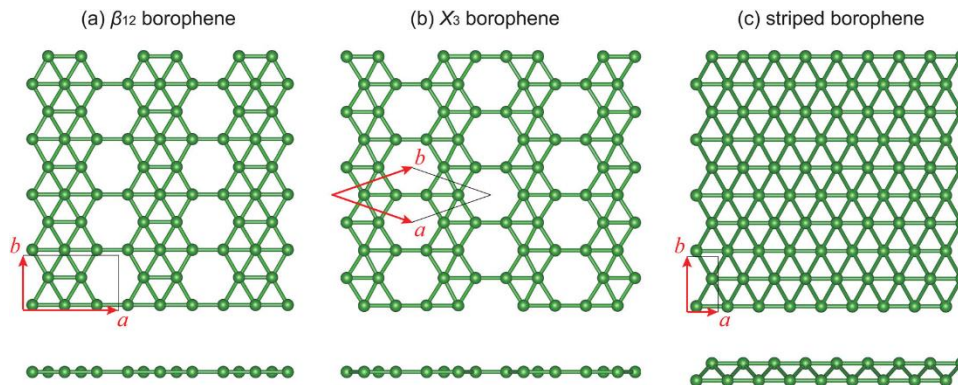


Figure I.4: Three structures of bororophene

The β_{12} phase has a greater Young's modulus and a higher carrier density than graphene the metal conductivity of bororophene is unique among bulk B allotropes and is caused by its delocalized multicenter bonding. Dirac electronic states have also been found in the bororophene

β 12 and χ 3 phases. Well, theoretically, 2D B sheets should have great mechanical characteristics and superconductivity with an extremely high critical value. Borophene is projected to perform better due to its enhanced electronic density along ridgelines and metallic structure, which can offer electrons for chemical binding. It is worthwhile to assess its selectivity and sensing capability. Ranjan et al. described one of the finest real-time sensing applications of borophene, in which ammonia sensing was done on free-standing borophene sheets [20].

I.2.5 Bismuthene:

In the past few years, there has been an explosive growth of interest in 2D materials, such as graphene, this wave of interest made a good reason for the exploration of these nanomaterials, and one of them called bismuthene.

Bismuth on various surfaces has been investigated for decades, and the latest study expands on that earlier work [21]. The shift of materials from metallic conductors to semiconductors while simultaneously reducing the number of layers, as well as the consequent optical, electrocatalytic, and electrical characteristics, is an essential component of these materials that warrants further research. This review will go through the characteristics of 2D layered elemental VA (group 15, pnictogens) materials .

Graphite has the pseudo-layered structure of bismuth, but the atoms are folded and are not all on the same plane. Bismuth is a covalent semimetal. The effective mass of magnesium is significantly lower than that of electrons, the mean free route for phonons is longer than that of electrons, the charge carrier mobility is faster, it has the lowest thermal conductivity except for mercury, and it has a significant magneto resistance effect [22].

- **Band structure**

Bi is a heavy element, and its SOC effect is strong enough to affect the band structures of both the 2D α - and β -phase (semiconductors) bismuthene. This means that the band gaps of these materials can be manipulated easily, which gives them potential for a wide variety of applications in electronics; Figure shows views sides of 2D α - and β -phase bismuthene [23].

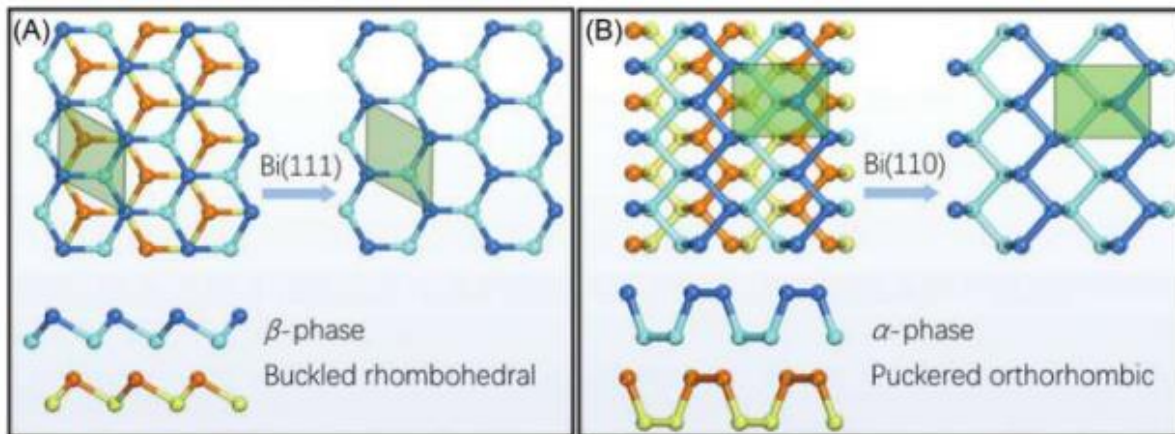


Figure 5: Top and side views of (A) 2D β -Bi and (B) α -Bi. 2D, two-dimensional. Source: Reproduced with permission from X. Liu, S. Zhang, S. Guo, et al., *Advances of 2D bismuth in energy sciences*, *Chem. Soc. Rev.* 49(1) (2020) 263.

I.2.6. The transition metal dichalcogenides (TMDCs):

A new class of materials called transition metal dichalcogenides (TMDCs) has properties that make them very attractive for studying novel physical phenomena and for using in a variety of applications. Nanoelectronics and nanophotonics have seen a strong resurgence in interest over the past few years, as has sensing and actuation at the nanoscale; TMDC has a long and fruitful history. Their structure was first determined by Linus Pauling in 1923 .^[24]

By the end of the 1960s, about 60 species of TMDC were known, at least 40 of which had a hierarchical structure . Robert Frindt originally described the use of tapes to produce ultrathin MoS₂ layers in 1963, and the first monolayer MoS₂ suspensions were created in 1986. Reshef Tenne et al research helped to lay the groundwork for the development of graphene and other two-dimensional materials, which have allowed for the development of technologies that take advantage of the unique properties of these materials. The research has enabled the exploration of new applications in various fields, including electronics, optics, and energy; starting the discovery of WS₂ nanotubes and nested particles until they paved the way for new research into TMDCs .

- **Composition TMDs:**

Commonly marked as MX₂ (M: transition metal elements from group IVB to group VIII; X: S, Se and Te elements of group VIA) (Figure of composition TMDCs), are typical 2D layered nanomaterials. Each TMD monolayer contains three atom layers, forming an “X–M–X”

sandwich structure. The adjacent monolayers, with a distance of 6–7 Å, are held together by weak van der Waals forces, which makes them readily isolated [25].

Legend:
 M: transition metal elements from group IVB to group VIII
 X: S, Se and Te elements of group VIA

Figure I.6: Composition of TMDCs.

- **Structure :**

Depending on the coordination sphere of the transition metal atom, different types of TMDCs can form. For example, octahedral TMDCs; tetrahedral, and trigonal prismatic, among others. The two common structural phases are characterized by either trigonal prismatic (2H) or octahedral (1T) coordination of metal atoms ; These structural phases can also be viewed in terms of different stacking orders of the three atomic planes (chalcogen–metal–chalcogen) forming the individual layers of these materials. In phase 2H, chalcogen atoms are stacked in the direction perpendicular to the layer in a stacking named ABA, in which different atomic planes occupy the same position A [26].

The already known layered TMDs are outlined in a periodic table with shadow background (**in the figure**), and a majority of their 2D counterparts have been theoretically predicted and experimentally synthesized.

IIIB	IVB	VB	VIB	VIIIB	VIII			IB	IIB	VIA
21 Sc	22 Ti	23 V	24 Cr	25 Mn	26 Fe	27 Co	28 Ni	29 Cu	30 Zn	16 S
39 Y	40 Zr	41 Nb	42 Mo	43 Tc	44 Ru	45 Rh	46 Pd	47 Ag	48 Cd	34 Se
57 La	72 Hf	73 Ta	74 W	75 Re	76 Os	77 Ir	78 Pt	79 Au	80 Hg	52 Te

Figure I.7: known layered TMDs in the periodic table highlighted with shadow.

- **The TMDs monolayers like :**

Group VIB present the 2D metals with layered structure which consist of a transition metal dechalcogenide (TMDCs) As one of the most widely studied in the twentieth century like (**MoS₂**, **WS₂**, **MoSe₂**, **WSe₂**, **MoTe₂**, **WTe₂**) and By studying the band structure of MoS₂, researchers have been able to gain insights into its tribological properties, such as friction and wear^[27].

I.2.7. The 2D material Nano-filament:

Recently the scientists explored the potential of synthesizing titanium carbides, phosphides, nitrides, silicides and borides into two-dimensional flakes by subjecting them to tetramethylammonium hydroxide solution which is new and interesting 2D material.

they conclude The nanofilaments were shown to have a high surface area and good electrical conductivity which makes them ideal for use as electrodes in lithium-ion and lithium-sulphur systems which they used scanning electron microscopy and other analytical methods to measure the composition of the flakes are carbon containing anatase-based layers that are, in turn, comprised of $6 \times 10 \text{ \AA}^2$ nanofilaments were composed of carbon-containing anatase layers.

The team found that heating the ten distinct Ti-based precursor powders in Tetramethylammonium Hydroxide (TMAH) at varying temperatures resulted in the synthesis of two-dimensional materials with non-layered, inexpensive materials, near ambient temperatures. This technique offers a simple, affordable, reasonably high-yield, near ambient, completely scalable, one-pot, bottom-up approach for synthesizing 2D anatase-based titanium carbo-oxide films constituted of nanofilaments.

Since 2D materials are known to have unique properties compared to their bulk counterparts, the synthesis of such materials could potentially lead to the development of novel materials and technologies. However, to do so requires a deeper understanding of the chemical and physical processes involved in the synthesis of 2D materials furthermore should make more study and large-scale synthesis of 2D materials from non-layered solids which is difficult and challenging. [28].

CHAPTER II: PROPERTIES AND LUBRICATION

II.Introduction:

The remarkable advancements in the field of materials science have led to the discovery and exploration of two-dimensional (2D) materials, which possess exceptional properties at the atomic scale. These materials have garnered immense interest among researchers due to their potential applications in various industries. In particular, the properties and lubrication behavior of 2D materials have become a subject of significant attention, offering promising avenues for technological breakthroughs in fields such as nanotechnology, electronics, and energy storage. In this chapter, we delve into the fascinating realm of 2D materials, with a specific focus on their properties and lubrication characteristics. Lubrication, which involves reducing friction and wear between two surfaces in relative motion, plays a pivotal role in numerous mechanical systems, from micro electromechanical systems (MEMS) to macroscopic machinery.

While traditional lubricants, such as oils and greases, have been extensively used to enhance efficiency and durability, the emergence of 2D materials presents a new frontier for lubrication science, offering novel possibilities to revolutionize tribology the study of friction, wear, and lubrication. Before exploring the lubrication aspects, it is crucial to grasp the fundamental properties of 2D materials. These materials, with their atomic-thin nature, exhibit extraordinary characteristics that deviate from their bulk counterparts.

Graphene, the first isolated 2D material, serves as an excellent example, displaying remarkable mechanical strength, exceptional electrical conductivity, and thermal stability. Additionally, other 2D materials, such as transition metal dichalcogenides (TMDs) and others, possess their own unique sets of properties, making them intriguing subjects of study. Understanding the lubrication behavior of 2D materials requires a comprehensive examination of their interfacial interactions and the mechanisms governing their friction and wear properties. The interplay between atomic structure, surface morphology, and adhesion forces dictates the lubrication performance of these materials.

Furthermore, the application of 2D materials as additives to traditional lubricants has shown great promise in enhancing performance and extending service life. In this chapter, we will explore the various characterization techniques employed to study the properties of 2D materials, including atomic force microscopy (AFM), transmission electron microscopy (TEM), and Raman spectroscopy, among others. We will also delve into the state-of-the-art research on the lubrication behavior of 2D materials, covering topics such as frictional properties, wear resistance, and tribochemical reactions. Additionally, we will discuss the

challenges and opportunities in the development of 2D-based lubricants and their potential impact on various industries. Over all, the investigation of the properties and lubrication behavior of 2D materials presents an intriguing frontier that holds immense potential for scientific advancements and technological breakthroughs. By harnessing the unique attributes of these materials and unraveling their fundamental mechanisms, researchers aim to revolutionize lubrication science and pave the way for the development of next-generation lubricants. In the following sections, we will embark on a detailed exploration of these intriguing materials, their properties, and their lubrication applications, with the ultimate goal of contributing to the growing body of knowledge in this exciting field.

II.2.The properties of 2D materials:

II.2.1. Graphene properties :

Is the thinnest material known, its strong carbon bonds make graphene the strongest material known, as well. Graphene is considered as the “most important material in the next century” since it is 300 times stronger than steel, has a much harder structure than diamond, and is a better heat conductor than diamond. In addition, graphene can be easily stretched and easily coated on the surface of many materials in various forms. Owing to all these extraordinary properties, graphene is expected to be used in a lot of fields such as automotive and aerospace sector, electrical-electronics sector, robot production, solar cells, energy storage, telecommunication, biochemistry, and medicine . Graphene sheets are produced by using several methods.²⁹

- **Properties Elastic of graphene :**

Modulus (Lee et al., 2008), very high thermal conductivity ($5.1 \times 10^3 \text{ W m}^{-1} \text{ K}^{-1}$) (Balandin et al., 2008), highest intrinsic electrical conductivity compared with other carbon NMs ($6 \times 10^5 \text{ S m}^{-1}$) (Du et al., 2008), high aspect ratio of flakes (ratio of lateral dimensions to the thickness of 104 and higher) and high intrinsic flexibility (Fasolino et al., 2007; Zhang et al., 2011) are some of the most important characteristics of GFMs. These characteristics attribute functional properties to these NMs such as electrical semi-conductivity, unique photonic/optical transportation, anisotropic transport, low permeability, and fluorescence quenching. For all these reasons applications of GFMs are increasing rapidly (Britnell et al., 2013; El-Kady and Kaner, 2013; Tetsuka et al., 2012; Mao et al., 2013; Shahil and Balandin, 2012). GO is one of the most popular graphene derivatives (Bianco et al., 2013). It exhibits various properties that make them attractive for different applications. An important feature of GO is its chemical

reactivity and its capacity for chemical functionalization. Their functionalization involves the surface oxygen functional groups that can participate in various chemical reactions allowing for example the growth of metallic nanoparticles.

Moreover, GO surface can be also modified using covalent bonding between nanoparticle precursors and metal oxides, as described for titanium dioxide (TiO₂) by Peter et al. (2015) that tried to determine the influence of synthesis conditions and thermal treatment of two GO–TiO₂ composites on their morphostructural and photocatalytic characterization. TiO₂ was also used by Jastrzębska et al. (2016) describing the influence of the modification of the electrostatic properties of TiO₂ nanoparticles by their deposition on the surface of rGO.

- **chemical properties :**

Theoretically, graphene is a two-dimensional (2D) flat layer with single atomic thickness consisting of sp²-hybridized carbon, in other words, it has aromatic nature possessing highly dense p-electron clouds both above and below the layer. Specific surface area of 2965 m²/g was theoretically calculated for infinite single-layer graphene and a large specific surface area as 2600 m²/g has been cited in different literature. Practically, graphene films (sheets) synthesized by chemical vapor deposition (CVD) and cleavage methods are presenting the nanomaterials having almost ideal structure with a low density of structural defects, except the edges of the layer. In these graphene films (sheets), the lateral size and number of stacked layers can be controlled by the selection of the size of the substrate and the deposition/cleavage conditions, although certain limitations in the controls of the size, structural perfection, and stacked layer number cannot be avoided, for example, whether a large enough sized single crystal of a substrate metal, whether single crystalline graphite to be cleaved is available, etc. Even by taking these practical limitations into consideration, however, the size of an aromatic plane is extraordinary large, in comparison to the conventional aromatic compounds, and the graphene layer creates extended p-electron clouds that can interact with p-electron clouds of other aromatic compounds and also with other cationic species. On the other hand, the so-called reduced graphene oxide (rGO) nanoflakes prepared from various kinds of graphite through their oxidation, exfoliation, and reduction contain different functional groups, mainly oxygen-containing groups, and many structural defects in the layers. On these rGO flakes, the extension of p-electron clouds is highly limited due to the limited size of the flake and also the presence of functional groups even inside of the layer. However, it has to be pointed out that the presence of functional groups makes the modification of flakes easier, for example, control of

hydrophilicity, functionalization through various chemical bonds, etc. On both graphene and rGO, functionalization is possible, even on both above and below the layer.³⁰

- **Hydrogenation the chemical properties of monolayer graphene :**

Are expected to be largely different from bulk graphite, although graphite is known as a chemically inert material. The chemical stability of graphene in specific atmospheres is particularly important for its applications in nanodevices.

1- Layer modification Ideal graphene layer has various features, high chemical stability, highly electrical and thermal conductivities, high mechanical properties with flexibility, etc. For practical applications of graphene and related materials in various fields, some modifications of these layers are often required by keeping these characteristics of graphene layers. On rGO-related materials, these modifications are mostly performed during the preparation processes by calling “functionalization,” In this section, the modification of graphene layers is explained by focusing on the graphene films synthesized by CVD.

2 -Oxygenation Oxidation of graphite in acidic solution has been carried out for the production of flexible graphite sheets through oxidation, thermal exfoliation and compression. Oxidation in oxygen gas has been studied as the process for gasification of carbon materials, particularly coal. Now Oxidation in acidic solution is commonly used as the preparation process for graphene oxide (GO) for the precursor of reduced graphene oxide (rGO). The oxidation products in acidic solutions have various functional groups, such as -OH, -COOH, etc., at the edges of graphene layers and at the defects in layers.^[30]

- **Thickness of graphene:**

The thickness of graphene is a vexed question. The common description of graphene as a 2D material implies extension in two dimensions but not in the third (i.e. zero thickness). Indeed, the very definition of the thickness of graphene is complicated from a quantum mechanics point of view, as it pertains to defining the diameter of atoms. The Yakobson paradox arose through the attribution of values as low as 0.6 Å to the thickness – and hence 6 Young’s moduli as high as 5 TPa. It is interesting to see how the similar issue of the size of atoms was addressed a century ago. Sir William Bragg proposed the hypothesis that atoms of a given element could be considered to be spheres with a fixed radius. However, the crystal structures of some metals and compounds led to proposals that some atoms have lower symmetry than spherical. Wyckoff re-examined the question and concluded that the hypothesis of constant radii (or other

shapes with fixed sizes) must be rejected but that the evidence supported atomic radii that vary more or less according to their environment. [31]

II .2.2.The Mbenes properties :

- **Electrochemical properties:**

Metal borides have unique electrochemical properties, including high chemical stability, low cost, and excellent electronic interaction between metal and boron atoms. Nanostructuring metal borides can enhance their properties by increasing surface area, reaction rate kinetics, accessibility to catalytic centers, and electronic structure tunability. Studies show that metal boride-based nanostructures exhibit improved performance in hydrogen evolution reactions (HER) due to boron's role in transferring electrons to d-orbitals. For instance, nanovanadium diboride (VB₂) and a single-phase ternary solid solution of Cr_{1-x}Mo_xB₂ have shown excellent HER performance. Metal-boride-derived 2D nanostructures are also gaining increasing attention for oxygen evolution reactions (OER) electrocatalysis. Studies suggest that during the OER process, surface oxidation states change, leading to the formation of a surface layer on a core-shell structure. Amorphous cobalt boride nanosheets and heterostructures of Ni-Co-B and Ni-Fe-B nanosheets have shown good performance towards OER electrocatalysis. Additionally, the presence of heteroatoms can increase active catalytic site density, reduce charge-transfer resistance, and favor electronic state tuning. Nickel boride nanosheets/functionalized multiwalled carbon nanotubes (Ni_xB/f-MWCT) have shown excellent catalytic performance for both OER and HER, outperforming noble metal-free bifunctional catalysts such as IrO₂/Pt/C. These high-performing electrocatalysts encourage the search for other metal boride-derived 2D nanostructures with even higher electrocatalytic activity. [32] [33]

- **Transport Properties:**

Although metal-boride-derived 2D nanostructures have been extensively studied for their synthesis, their transport properties have not been fully characterized. Theoretical studies have predicted the transport properties of specific 2D metal-boride nanostructures, particularly in the areas of superconductivity and electronic surface states. However, due to the lack of experiments on monolayer materials, the discussion remains limited to theoretical predictions. To provide insight for researchers in this field, we can look to the experimental transport properties of thin films. Similar to the study of transport in metal-boride nanosheets, the study of few-monolayer metal borides can draw upon previous research on quasi-2D materials such

as transition-metal chalcogenides and boron nitride. The study of transport in metal-boride nanosheets is heavily influenced by research on graphene, which was the first 2D material to be extensively studied. While numerous other materials can be formed into monolayers, research on these materials has followed in the footsteps of graphene. [34]

II.2.3. Mxene properties :

As briefly illustrated in the right area of Figure, MXenes have several unique properties including high electrical conductivity, work function (WF) tunability, superconductivity, and surface plasmons. MXene films exhibit high conductivity, which is desired for contact material applications. For instance, the electrical conductivity of Ti_3C_2Tx films can reach 25,000 S cm⁻¹ under optimized synthesis conditions. In addition, the WF of MXenes can theoretically be tuned between 2 and 8 eV, which is a substantially larger range than traditional metals. This indicates that MXenes can be practically engineered as either ohmic or Schottky contacts in a variety of electronic devices . Furthermore, Ti_3C_2Tx flakes have been verified to have a high-breakdown current density. The concurrent outstanding electrical conductivity and high-breakdown current density make MXenes very promising as interconnect materials in integrated circuits Besides, Nb_2CTx MXenes with well-controlled surface groups have been demonstrated to have superconducting properties, illustrating the potential of fabricating MXene-based superconducting quantum devices. Thanks to their ability to support surface plasmons, MXenes also have promising potential in sensing applications (photo-, chemical, and biosensing) [35]

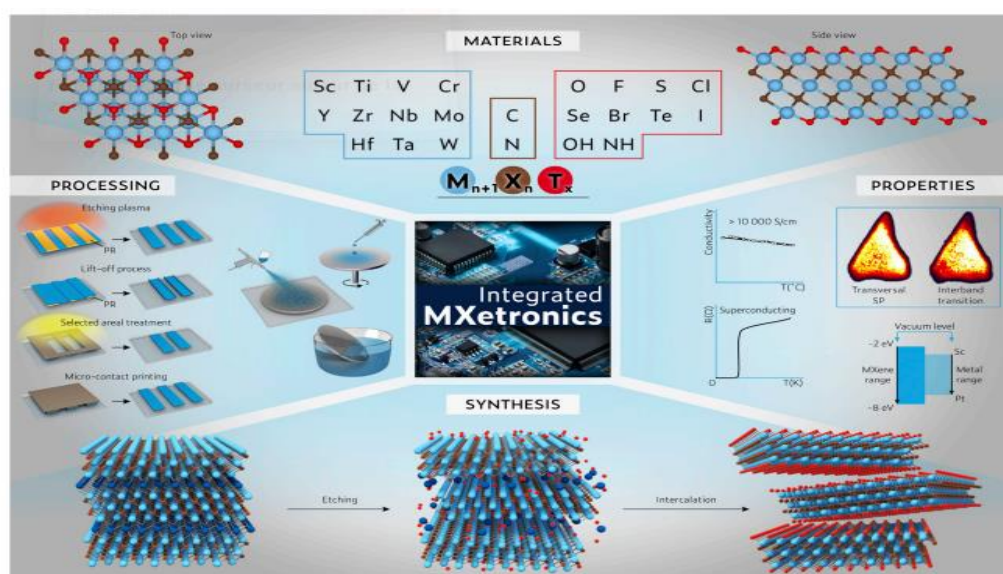


Figure II.1 : Compositions, properties, synthesis, film preparation, and patterning of MXenes for integrated MXene- based nanoelectronics.

- **Mechanical properties**

Through selective peeling of the aluminium layer in Ti_3AlC_2 phase using hydro-fluoric acid, a novel 2D transition metal carbide and nitride (MXene) was created, which sparked a lot of attention. Exfoliation of the MAX phase (abbreviated later) that is firmly bound inside a 2D layer and kept together through weak van der Waals contact may be used to make MXenes. The MAX phase formula is $M_{n+1}AX_n$ ($n = 1, 2, 3$), where M is a transition metal, A is a group IIIA or IVA element, and X would either be a carbon or nitrogen atom. With increase in the value of n, the production of MXene and MAX may be reduced. The $Ti_{n+1}N_n$ has a greater production rate than $Ti_{n+1}C_n$, implying that nitrogen-containing MXene has a lower durability than carbon-containing MXene. The MXene material possesses metal and ceramic properties, with great stiffness and high strength. Corrosion resistance, strong electrical conductivity, and good thermal conductivity are all features of this material. MXene also exhibits high hydrophilicity, adaptability, and plasticity and has increasingly become a 2D materials research focus. According to experimental data, the modulus of elasticity of monolayer $Ti_3C_2(OH)_2$ is around 300 GPa, which is lower than graphene, equivalent to several transition metal carbides, but larger than most oxides and multilayer clays. The bonding here between M_2X and the terminating group improves the mechanical characteristics. Single-layer M_2X , in-plane elasticity is estimated to be between 42 and 199 $N\ m^{-1}$, that is less stiff as compared to graphene (341 $N\ m^{-1}$) and monolayer h-BN (276 $N\ m^{-1}$). Young's modulus of MXene ($Ti_3C_2T_x$) is observed as 0.33 ± 0.03 TPa, which is more than the phosphorus (0.166 TPa). However, h-BN has a higher value of Young's modulus in the comparison of other 2D materials.

II .2.4.properties of borophene :

- **Optical properties :**

Borophene has a unique crystal structure that leads to a significant in-plane anisotropy in its optical properties. This feature makes borophene a promising material for applications in photovoltaics, flexible electronics, and displays. Tai et al. measured the optical bandgap of borophene to be 2.25 eV, which closely matches the theoretical value of 2.07 eV obtained from first-principles calculations. They also observed strong photoluminescence, indicating that borophene is a direct bandgap semiconductor. Wang et al. explain that for direct bandgap semiconductors like borophene, photons with energy above the bandgap energy can be easily absorbed or emitted, while for indirect bandgap semiconductors, an additional phonon must be emitted or absorbed to balance the energy, reducing the efficiency of the absorption or emission

process. Figure II.3 shows that borophene has different absorption peaks in the two crystallographic directions, with major absorption peaks at around 10.36 and 3.65 eV along the a direction, and up to 10.31, 8.29, and 1.09 eV along the b direction. The reflectivity of borophene is less than 30% along the A direction and higher than 40% along the b direction in the visible region. Along the A direction, borophene has high transmittance and electrical conductivity, but low optical conductivity in the visible region. These properties make borophene suitable for applications in flexible electronics, photovoltaics, and displays. Adamska et al. found that borophene is an anisotropic metal with weak absorbance in the visible region, thickness-dependent optical transparency, and strong energy. Tatullo et al. showed that borophene has high optical transparency in the visible range, while Lherbier et al. demonstrated its strong photosensitivity to surface modifications. [36] [37]

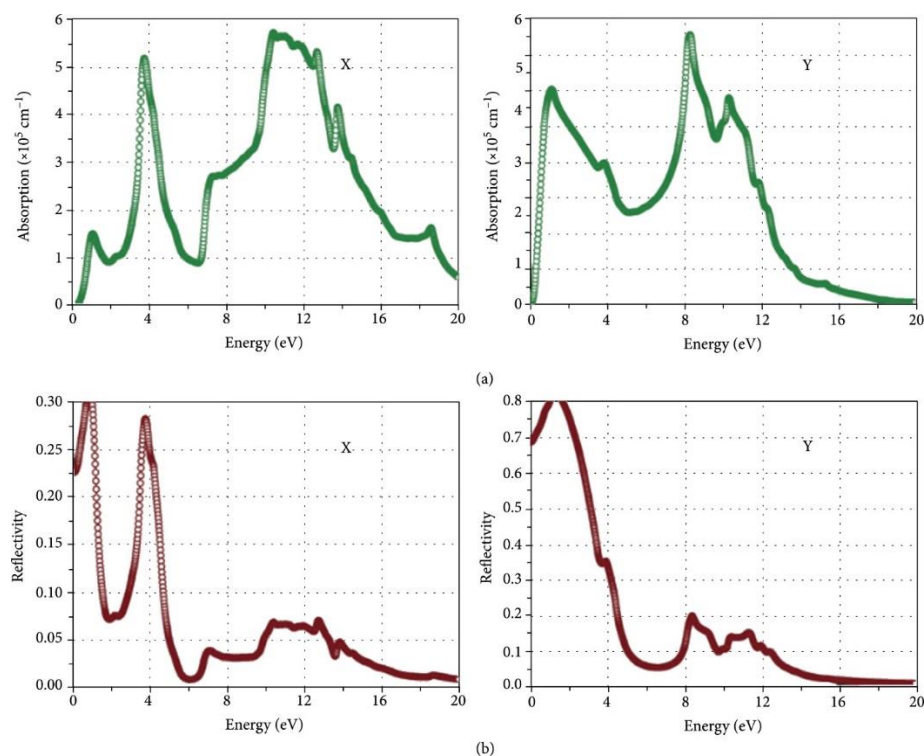


Figure II.2: (a) Absorption coefficient of borophene and (b) reflectivity alongside the different two directions. Reprinted with permission from Ref. Copyright 2016 Royal Society of Chemistry.

- **Semiconducting Properties:**

In recent years, due to the rapid development of the electronic industry, the traditional silicon technology can no longer meet the requirements of the semiconductors . Hence, looking for a new semiconductor material to promote the development of the electronic industry is a crucial factor. Through research, Yang et al. found that borophene can form ideal contact with 2D semiconductor and effectively reduce the contact resistance, which can further improve the related performance of 2D transistor .^[38]

Jie et al. studied experimentally and systematically that the tunnel barrier was nearly zero after borophene making effective contact with various 2D semiconductors. It is shown in Figures II.3 (a) – (d). The valid channel barrier height is given as the barrier height difference that must be overcome when the Fermi energy of the carrier in the metal is the same as that of the heterostructure. As shown in Figure II.3 (e), all of the tunnel barriers in the 2D layer in contact with borophene are zero, only graphene is 0.10 eV. Earlier findings have accorded that there is a tunnel barrier between the 2D material and bulk metal, so it can be seen that zero tunneling barrier is an irreplaceable favorable condition of borophene as a semiconductor contact layer.

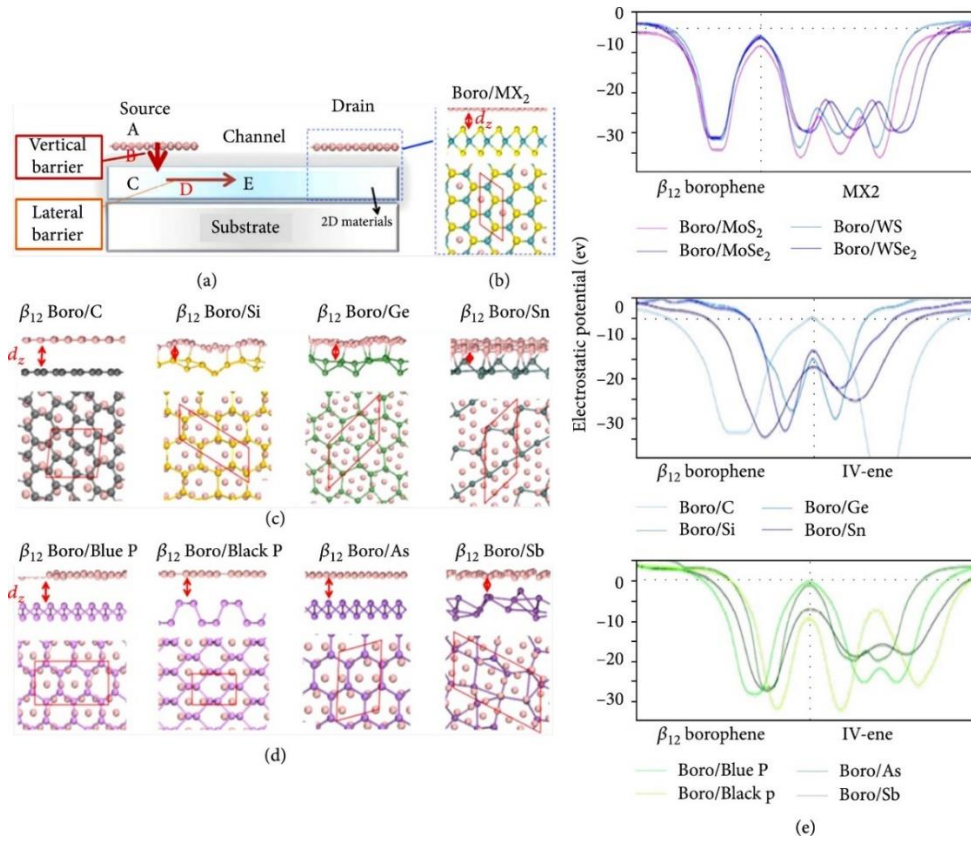


Figure II.3 : (a) β_{12} borophene is in contact with 2D semiconductor atoms. The electron injection monolayer β_{12} borophene shows its path (A \rightarrow B \rightarrow C \rightarrow D \rightarrow E) by the red arrow. Lateral and top viewpoints of the utmost steady structure: (b) β_{12} borophene gets to MX_2 (M for Mo or W; X for S or Se); (c, d) β_{12} borophene gets to the group IV-enes. (e) The balanced electrostatic potential with zz position for β_{12} borophene/2D material interactions. Reprinted with permission from Copyright 2017 Royal Society of Chemistry.

The research on borophene is just beginning. With the development of the research on borophene, borophene not only has the above excellent properties but also may have novel atomic structure, excellent physical and chemical properties, and more interesting quantum effects, providing more possibilities for borophene-based applications in the future.

- **Mechanical properties:**

Previous research has examined the effect of strain on the mechanical properties of borophene, focusing on two types: B1 and B2. B1 has a puckered surface with repeated corrugations along a direction, while B2 is a planar structure containing vacancies. These structures exhibit different behaviors when subjected to strain. B1 has optimized lattice parameters of $a = 1.614 \text{ \AA}$ and $b = 2.863 \text{ \AA}$, while B2 has $a = 2.928 \text{ \AA}$ and $b = 5.069 \text{ \AA}$. Borophene displays highly anisotropic mechanical properties, with different yield points along the a and b directions. For

B1, the yield points were found to be $\epsilon_a = 0.10$ and $\epsilon_b = 0.15$, and $\epsilon_a = 0.21$ and $\epsilon_b = 0.18$, respectively. Under uniaxial tension, B1 exhibited a maximum stress of 27.46 N m^{-1} at $\epsilon_a = 0.10$, which was higher than the stress along the b direction (12.95 N m^{-1} at $\epsilon_b = 0.15$). This difference can be attributed to the presence of strong σ bonds along the a direction, whereas weaker multicenter bonds are involved along the b direction. The Young's moduli for B1 were determined to be 354 N m^{-1} along the a direction (E_a) and 145 N m^{-1} along the b direction (E_b), whereas B2 had values of 147 N m^{-1} and 123 N m^{-1} , respectively. Moreover, the influence of loading direction and point vacancies on the mechanical response of monolayer borophene sheets has been investigated by Mortazavi and colleagues. They considered five different structures of single-layer borophene (S1 to S5). Elastic moduli were similar for all structures when stretched along the zigzag or armchair direction, except for S1, which exhibited higher elastic moduli of 382 GPa nm along the armchair direction and 163 GPa nm along the zigzag direction. When borophene sheets were uniaxially stretched along the armchair direction, the length of the B-B bonds in that direction increased with increasing strain levels, while the length of the B-B bonds along the zigzag direction remained the same or slightly decreased. ^{[39][40]}

- **Thermal properties:**

Thermal properties of two-dimensional materials are crucial for many potential applications in electronics and thermal management. The thermal conductivity, specific heat capacity, and thermal expansion coefficient are important properties that affect heat transfer and energy dissipation in these materials. For example, borophene, a two-dimensional material composed of boron atoms, has a very high thermal conductivity due to its unique structure, which allows for efficient heat transfer through the material. Additionally, borophene has a low coefficient of thermal expansion, which makes it suitable for use in high-temperature applications where dimensional stability is critical. Understanding the thermal properties of two-dimensional materials like borophene is essential for designing and optimizing materials for various applications in the fields of electronics and thermal. ^[41]

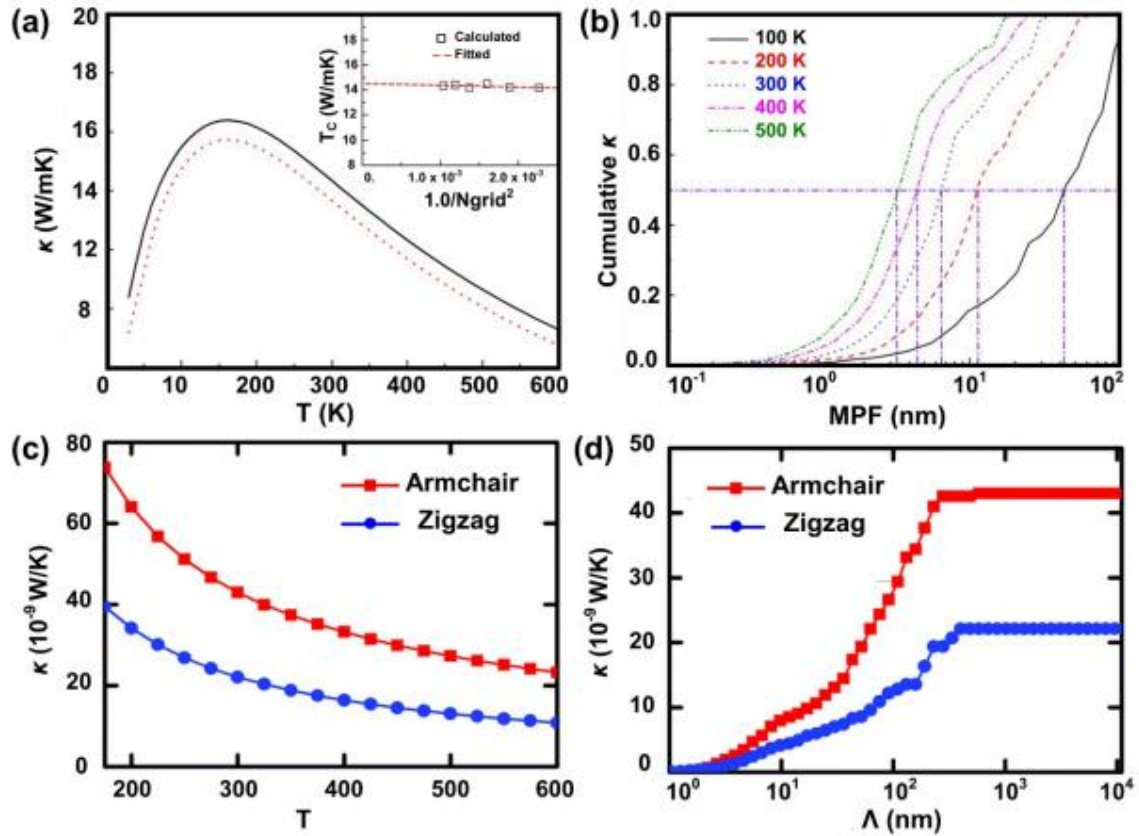


Figure II.4 : (a) The total lattice thermal conductivity of borophene as a function of temperature by using the iterative (solid line) and relaxation time approximation (RTA) solution of phonon Boltzmann transport equation (PBTE). (Inset) The dependence of lattice thermal conductivity of borophene on the phonon q -grid using iterative approach (300 K). (b) The accumulative lattice thermal conductivity of borophene versus phonon mean free path (MFP) at various temperatures. Reproduced with permission from Copyright 2016, Springer Nature. (c) The temperature dependent lattice thermal conductivity of borophene. (d) The cumulative thermal conductivity at 300 K. Reproduced with permission from ref. Copyright 2016, The Royal Society of Chemistry.

In a study conducted by Xiao and colleagues, the thermal transport properties of buckling α -borophene sheets were investigated using first-principles calculations and the phonon Boltzmann transport equation. The lattice constant of the borophene sheet was $a = 4.37 \text{ \AA}$, and the vertical distance from the plane was 0.173 \AA . The findings of the study showed that the thermal conductivity of borophene initially increased with temperature up to 150 K but decreased as the temperature exceeded 150 K (Figure II.6). This behavior was attributed to enhanced phonon-phonon scattering at higher temperatures. The lattice thermal conductivity (κ_l) of α -borophene was significantly lower (14.3 W mK^{-1}) than that of graphene (around 3500 W mK^{-1}), indicating its thermal insulating properties. Surprisingly, more than 70% of the thermal conductivity of borophene was contributed by high-frequency phonon modes. This

is in contrast to other 2D materials like graphene, silicene, and phosphorene, where low-frequency phonon modes dominate the transport properties. The unique contribution of high-frequency phonon modes to the transport properties of borophene arises from their interactions with three acoustic phonon modes and among themselves, as well as the limited anharmonic phonon-phonon scattering leading to a large phonon relaxation time. The primary phonon transmission process was identified as the scattering between the out-of-plane flexural acoustic mode (FA) and other modes such as $FA + FA/TA/LA/OP \leftrightarrow TA/LA/OP$. The effect of size on the thermal conductivity of borophene was evaluated by measuring the accumulative thermal conductivity with respect to the phonon mean free path (MFP). At temperatures of 100, 200, 300, 400, and 500 K, the MFPs corresponding to 50% accumulation conductivity of borophene were approximately 41, 11, 6.4, 4.5, and 3.3 nm, respectively. This behavior differs from graphene, where nearly half of the thermal conductivity is contributed by phonons with MFPs longer than 1 μm . The findings suggest that the diffusion transport of phonons in borophene may be possible if its domain size is larger than a few nanometers, indicating that nanostructuring borophene with nanoinclusions and grain boundaries could be a way to tune its thermal conductivity. [42]

II .3.The lubrications:

The investigated 2D nanomaterials used as lubricant additives can be categorized into three groups: graphene family, metal dichalcogenides, and other materials. Graphene has been extensively studied both theoretically and experimentally due to its exceptional mechanical, chemical, and electrical properties. Research on the tribological properties of graphene and its derivatives as lubricant additives was first published in 2011 . Besides its application as an oil lubricant additive, graphene-based nanomaterials have also shown promise as additives in water-based media and grease . The addition of graphene family nanomaterials can effectively enhance lubricating performance in different base media by creating a protective film and separating the contact surfaces . [43] [44]

II .3.1.Role of 2D materials in friction and wear reduction mechanisms:

Numerous studies have been devoted to understanding the underlying mechanisms of 2D materials as lubricant additives in effort to promote their wider application. Generally, the evolution of the protection of the lubricants can be divided into four aspects:

- 1) Entering the contact area of sliding surfaces;
- 2) Forming a tribofilm;
- 3) Filling the pits and gaps of the contact area;
- 4) Affecting the fluid drag and viscosity. The four proposed mechanisms are schematically expressed .The 2D materials discussed above play a key role in these processes.

5) Entering the contact area of sliding surfaces and providing efficient lubricating 2D materials

Entering the contact area of sliding surfaces and providing efficient lubrication 2D materials

With a sheet-like shape and small size have the advantage of easily entering the contact area between rubbing surfaces. The incorporation of nanoparticles in these 2D materials further improves their ability to penetrate the gaps between the contact surfaces, enabling effective lubrication. When two surfaces come into contact and experience normal forces during rubbing, the 2D nanomaterials within the contact area are also subjected to pressure. The relative motion between the surfaces generates shear stress on these materials. Consequently, the easy shearing of interlayers within the multilayer 2D material creates a sliding system with the rubbing contact . In comparison to direct hard contact, the friction force in the sliding system is significantly reduced, resulting in efficient lubrication. ^[45]

II .3.2.Tribofilm:

The formation of a tribofilm occurs in two stages during lubrication at the contact area of sliding surfaces. In the initial stage, the high surface energy and easy shearing properties allow the materials to readily adsorb onto the substrate surface, forming a protective film (referred to as a physical film) without involving any chemical reactions. The primary function of this film is to separate the contacting surfaces, preventing direct contact and reducing friction and wear. As sliding continues, the physical film eventually ruptures, generating a significant amount of heat and initiating a tribochemical reaction between the lubricant and substrate. This reaction leads to the formation of a new tribofilm, which gradually replaces the physical film. Unlike

the physical film, the tribofilm is not limited to the localized contact surfaces but also extends into the substrate matrix, significantly improving the tribological performance . [46]

II .3.3.Other possible roles:

In addition to the aforementioned functions, 2D materials used as lubricant additives have other roles in enhancing tribological performance. Certain materials like graphene exhibit high chemical stability, making them impermeable to liquids (such as water) and gases (such as oxygen) . When these materials adsorb onto a substrate, they can act as a barrier, preventing chemical attacks from the lubricant or other reactive elements present in the system. This helps slow down corrosion and oxidation, reducing wear on the sliding surface and extending its lifespan. [47]

Recent nanoscale experiments have revealed that even when reduced to a single atomic layer, these materials exhibit remarkably low surface friction when in contact with other surface. Apart from weak interlayer interaction, the regular atomic arrangement in these materials can also contribute to achieving super-low friction, known as superlubricity .Moreover, studies on few-layered 2D materials have shown that the static friction force initially increases over a few atomic periods before reaching a steady value. This transient behavior and the subsequent improvement in the steady-state of friction decrease as the number of 2D layers increases, particularly when the material is loosely attached to a substrate .

Atomistic simulations by Li et al. successfully reproduced experimental findings on layer-dependent friction and transient frictional strengthening in graphene nanosheets. These simulations revealed that the evolution of static friction arises from the inherent tendency of thinner and less-constrained graphene to rearrange its configuration due to its higher flexibility. The pinning state and synchrony of stick-slip motion of individual atoms at the tip interface increase as the local pinning state and comprehensive commensurability expand in frictional sliding on graphene nanosheets.Furthermore, Lee et al. investigated the nanotribological properties of selected 2D materials (graphene, MoS₂, h-BN, and NbSe₂) obtained through mechanical exfoliation. The study showed that the friction of all four 2D materials was higher than that of their bulk counterparts. This increased friction was attributed to the low bending stiffness of the thinnest layers, known as the puckering effect. A simplified model of a tip sliding across an elastic membrane was employed to understand the role of sheet stiffness in friction. The contact between the tip and the top surface leads to local puckering due to adhesion, resulting from the low bending stiffness of the sheet relative to its in-plane stiffness.

The out-of-plane puckering contributes to increased friction by enlarging the tip-sheet contact area and requiring additional work to shift the puckered region. As the sheet becomes thinner, the puckering effect becomes more prominent. Additionally, graphene, MoS₂, and h-BN exhibit significantly lower friction (~1 nN) compared to NbSe₂ (~7 nN). [48]

Zhou et al. also demonstrated that transition metal dichalcogenides (TMDCs) with smaller vertical interlayer force constants (lower elastic modulus) exhibit higher friction when colliding with AFM tips. It is worth noting that the unique electrical properties and electron-phonon coupling of 2D materials are believed to influence their frictional behavior, releasing kinetic energy during frictional sliding through electronic or phononic means .

the mechanisms underlying the frictional action of 2D materials can be described as follows: Firstly, due to their small size, nanosheets are capable of penetrating the gaps between rubbing surfaces. When subjected to normal force and relative motion between the surfaces, the interlayers of the nanosheets experience shear stress, resulting in their sliding and consequently reducing friction and wear. Secondly, a tribofilm is formed at the contact area of the sliding surfaces . Initially, this tribofilm acts as a protective barrier, preventing direct contact between the rubbing surfaces. However, as sliding continues and heat is generated, a tribochemical reaction occurs at the contact surfaces between the lubricants and the substrate. This reaction leads to the rupture of the protective film and the formation of a new film . This new film significantly enhances the tribological behavior . Additionally, the high temperatures generated during sliding can cause the nanosheets to melt, allowing them to fill in micro-holes, gaps, and concave areas on the contact surfaces, thereby reducing friction and wear [49].

II.4. Tribology of 2d materials :

II .4.1.Graphene and Graphene-Family:

Possesses remarkable properties such as stiffness, strength, thermal conductivity, and impermeability to liquids and gases. Its exceptional physical and chemical attributes, coupled with its cost-effectiveness, make it a preferred candidate for nano-electromechanical and miniaturized devices. Despite being atomically thin, graphene exhibits high durability, with intrinsic strength of 130 GPa, fracture toughness of $4.0 \pm 0.6 \text{ MPa}\sqrt{\text{m}}$, and Young's Modulus of 1 TPa. Its superior strength and thermal stability (above 3000 W/m•K) make it ideal for ultra-thin protective coatings and as a solid lubricant in MEMS and NEMS applications. Additionally, graphene's impermeability to liquids and gases mitigates oxidative and corrosive activities that can damage rubbing surfaces. Even under extreme tribological conditions, such

as high pressure, temperature, and mechanical stress, graphene maintains long-lasting and highly efficient lubrication performance. Furthermore, at room temperature, graphene exhibits high electron mobility along the in-plane direction, which is crucial for its functionality in various applications. The electron-phonon interaction strength of graphene depends on sample thickness and local interactions with substrates, as demonstrated by angle-resolved photoemission spectroscopy and scanning tunneling spectroscopy. During the initial sliding phase of a tribological pair, there is typically a transient change in interfacial properties, known as "running-in." This change is often attributed to variations in interfacial roughness, wear of contact asperities, microstructure alterations, surface composition changes, and the presence of third bodies. In a study conducted by Zhao et al., a running-in phenomenon was observed in single-layer graphene grown on a copper substrate. Through repeated scratching with an atomic force microscope tip, the frictional force initially decreased by 32.6% after approximately 62 scratching cycles before reaching a stable state at 256 cycles. Interestingly, the graphene coating remained free from wear and damage. The underlying mechanism behind this observation was attributed to the plastic deformation and hardening of the copper substrate. Another study by Yao et al. investigated the antiwear performance of graphene on different substrates (PDMS, epoxy, SiO₂, and sapphire) using AFM nano-scale scratch experiments. The results showed that the maximum load-carrying capacity of graphene, which determines its anti-wear performance, is primarily influenced by the stiffness of the substrate. A stiffer substrate allows for higher load-carrying capacity. Finite Element Analysis simulations demonstrated that a rigid substrate effectively distributes the normal load, reducing in-plane stress and improving the overall load-carrying capacity of graphene. Additionally, the experimental results indicated that frictional shear stress during scratch tests may induce wear of graphene by reducing its equivalent strength. [49]

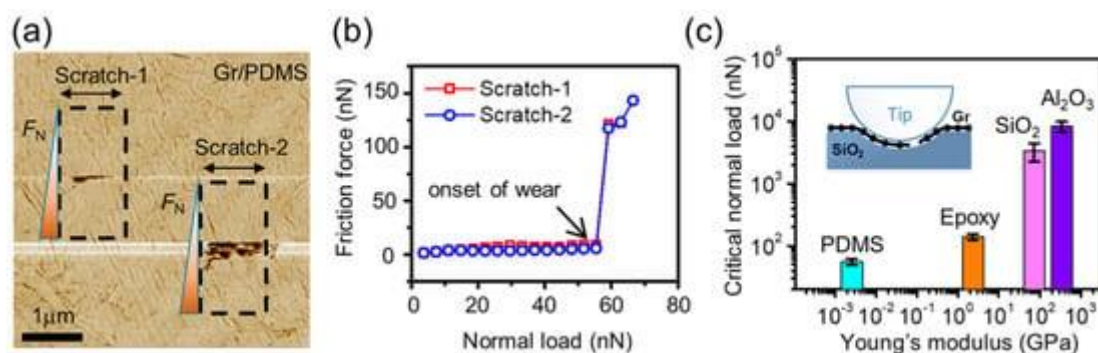


Figure II.5: (a) A lateral force image of graphene/PDMS sample done under a low load after two scratch tests; the black arrows indicate the scratch direction. (b) Variations of friction with the normal

load during the scratch tests in (a). (c) Critical normal loads of graphene on the substrates with different stiffnesses. [49] [50] [51]

Graphene, being an atomically thin material with low surface energy, has shown promise as a solid lubricant for mechanical systems at nano- and micro-scales. Many friction tests have been conducted at these scales to reveal the tribological performance and mechanisms of graphene. The atomic force microscope (AFM) is the most commonly used instrument for nano- and micro-scale friction tests. In the tests, the AFM tip is integrated with the end of a cantilever and measures attractive force, repulsive force, applied normal force, and friction force. Studies using AFM have shown that the tribological properties of graphene are greatly influenced by the interface interaction between the graphene and the substrate. The adhesion strength between graphene and the substrate greatly depends on the substrate morphology. No layer dependence of the friction performance was found with exfoliated graphene on smooth surfaces like graphite, h-BN, and mica, indicating that graphene could effectively reduce friction when it had good contact and strong adhesion with the substrate. However, on the surface with atomic roughness, adhesion force between graphene and substrate was reduced due to the less intimate contact, which led to higher friction attributed to the "puckering effect." The puckering effect is a commonly observed phenomenon in nanoscale friction tests that explains how, as the number of atomic layers decreased, the friction of graphene increased with lower graphene-substrate adhesion. But the trend vanished with higher graphene-substrate adhesion. The out-of-plane stiffness of graphene increased with the increased layer number, which suppressed the puckering induced by friction, therefore leading to lower friction. On the contrary, with higher graphene-substrate adhesion, the puckering of graphene was greatly suppressed, so the layer number of graphene had limited influence on the friction performance. Recent approaches have been proposed to eliminate the structural deformation on the friction of graphene. For example, some researchers treated the substrate with plasma to enhance the adhesion of graphene on the substrate through van der Waals force. Others achieved ultralow friction with highly aligned graphene on Ge (111) substrate, which was due to the suppressed deformation of graphene at the molecular level within the moire' superlattice structure. Single layer graphene exhibits anisotropic friction behavior, which was thought to be attributed to the periodic nanoscale ripples on graphene. The electron-phonon coupling also had influence on the frictional performance of graphene, as the strong electron-phonon coupling in the monolayer graphene was one of the origins of the higher friction compared to bi-layer or multilayer graphene. Most studies define friction with the coefficient of friction as the relation between lateral force and

normal force, but the complexity in friction is hard to be simply explained by this one parameter. Recent studies have investigated the frictional properties at a monolayer graphene step edge on graphite. The friction was divided into separate contributions of chemical and physical processes. It was found that the sliding motion was assisted by a force during the step-down process, while the chemical bonds provided a resistance force during the step-up motion. These studies indicated the opportunity to tune the friction force based on defined termination species and topographic features.

Graphene is known for its excellent friction reduction and wear resistance properties, and has been studied extensively for its potential use as a solid lubricant at the macro-scale, which is more valuable for engineering applications. Tribometers, such as ball/pin-on-plane in rotary and reciprocating modes, and block-on-ring, have been commonly used to investigate the macroscale tribological performance of graphene as a solid lubricant. Studies have shown that solution-deposited graphene nanoflakes can significantly reduce the friction and wear of steel tribopairs in ambient conditions. Small amounts of ethanol solution with graphene can reduce the coefficient of friction (COF) by a factor of 6 and reduce wear by almost 4 orders of magnitude. The friction is reduced by a protection layer with graphene nanoflakes, and the tribo-corrosion is suppressed, leading to a reduction in wear. The tribological performance of graphene has also been investigated with macroscale friction tests on chemical vapor deposition (CVD) deposited graphene under different external atmospheres. Results showed that the single layer graphene on a steel substrate lasted 6400 cycles and few-layer graphene lasted 47,000 cycles during friction test in hydrogen atmosphere, which were much longer than the lifetime in nitrogen atmosphere (500 cycles for single layer graphene). The longer lifetime of graphene in hydrogen atmosphere was attributed to the passivation of dangling bonds in a ruptured graphene by hydrogen. Humidity was also found to affect the response of graphene in pin-on-disk friction tests conducted in dry nitrogen atmosphere and air conditions with varying relative humidity. The discontinuous superlubricity between graphene layer and highly oriented pyrolytic graphite (HOPG) at the macroscale was observed. The extreme low friction with a COF of 0.001 was obtained with the transferred graphene nanoflakes on the steel counterpart ball sliding against HOPG. Recent studies have combined graphene with laser surface texturing techniques to further enhance the lubrication performance and lifetime to meet the needs of engineering applications. The enhanced lubrication performance and longer lifetime of graphene with laser surface texturing could be attributed to the laser-ablated microgrooves that act as reservoirs of graphene to provide a supply of graphene lubricant at the

sliding interface during the friction process. The real contact area between tribopairs is also reduced with laser surface texturing, leading to a lower COF. [52]

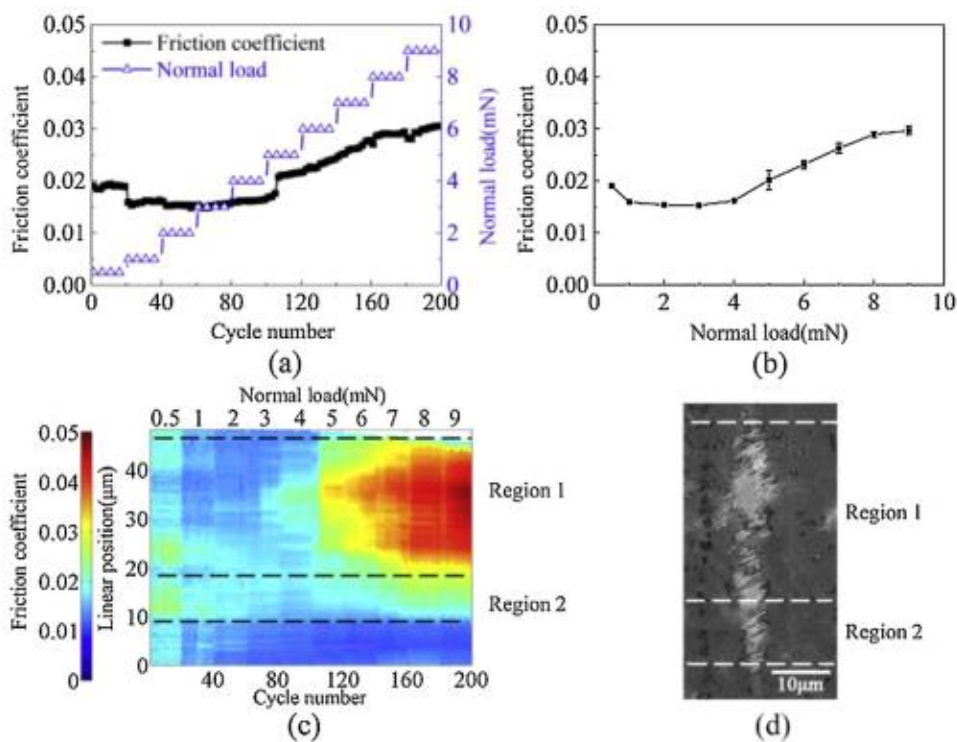


Figure II.6 : (a) COF of CVD deposited monolayer graphene versus sliding cycles with changing applied normal load. (b) Average COF at different applied normal load. (c) The COF versus sliding cycles along the sliding track. (d) Topography of the sliding track obtained with SEM.

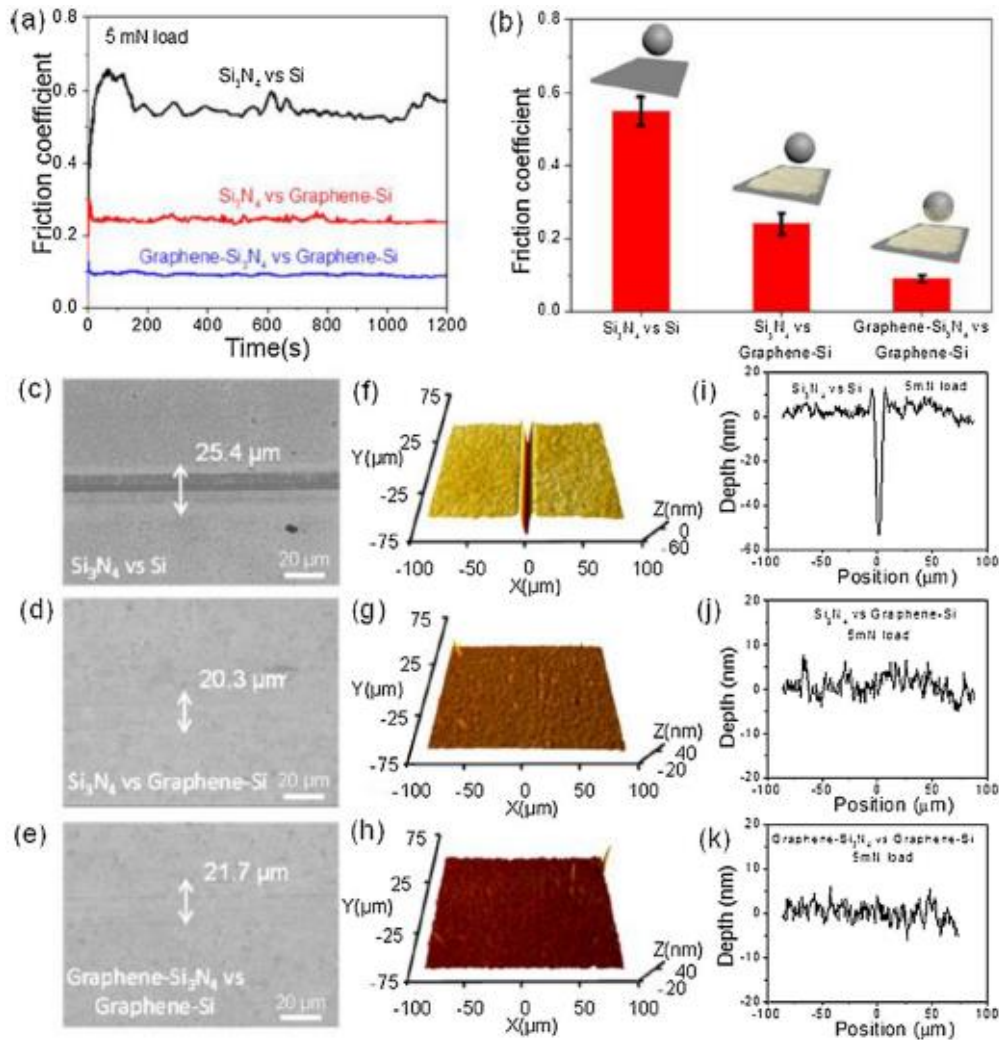


Figure II.7: (a) Curves of COF versus time, (b) average COF under different test conditions, and (c–e) topography of wear tracks obtained with SEM, (f–h) 3D morphologies of the wear track surfaces, and (i–k) 2D line profiles of the wear tracks on Si substrates. [53]

II .5.Graphene liquid lubrication:

Graphene has proven to be highly effective not only in solid lubrication, but also in liquid lubrication. The success of liquid lubrication in machinery depends on the lubricating properties of lubricants, which may not perform well enough on their own. There are many types of additives that can enhance the lubricating performance of lubricants, including friction modifiers, anti-wear additives, extreme pressure agents, anti-corrosion agents, antioxidants, and more. Among these, graphene stands out due to its 2D layer structure, which provides exceptional friction reduction and anti-wear properties that are difficult to find in other additives. Therefore, graphene has become increasingly popular as both a lubricant and a lubricating additive at multiple scales. At the nanoscale, graphene can offer super-low friction when incommensurate contact with specific liquid molecules is formed. Li et al. achieved

superlubricity at interfaces between graphene and hydrophobic self-assembled fluoroalkyl monolayers (SAFMs) with the lubrication of water. The tests were performed on AFM at a contact pressure of less than 14.5 MPa, and a super-low coefficient of friction (COF) of 0.0003 was obtained. This demonstrated that the friction between graphene and hydrophobic SAFMs in a water environment was extremely low. MD simulation revealed that a thin water layer intercalated between graphene and hydrophobic SAFMs, which was only several nanometers thick and so stable that it could not be squeezed out within this pressure range. The weak interaction between graphene and water allowed water molecules to slide easily on the graphene surface and contributed to superlubricity. Similarly, Mo et al. used rGO and multiply-alkylated cyclopentane (MAC) to create a composite film on a silicon plate and studied its tribological properties. The as-prepared composite films with various MAC concentrations in hexane were noted as 0.02 MAC/rGO, 0.08 MAC/rGO, and 0.16 MAC/rGO. The friction reduction property of MAC/rGO film was attributed to the long chain of MAC molecules, which formed a brush-like layer between the contact surfaces. This brush-like layer of MAC could swing and rearrange easily along the sliding direction under shear stress, which contributed to a very low shear resistance. This friction reduction strategy can also be applied to other surfaces, such as ceramic materials, metals, semiconductors, and more, by changing the rGO deposition technology. ^[54]

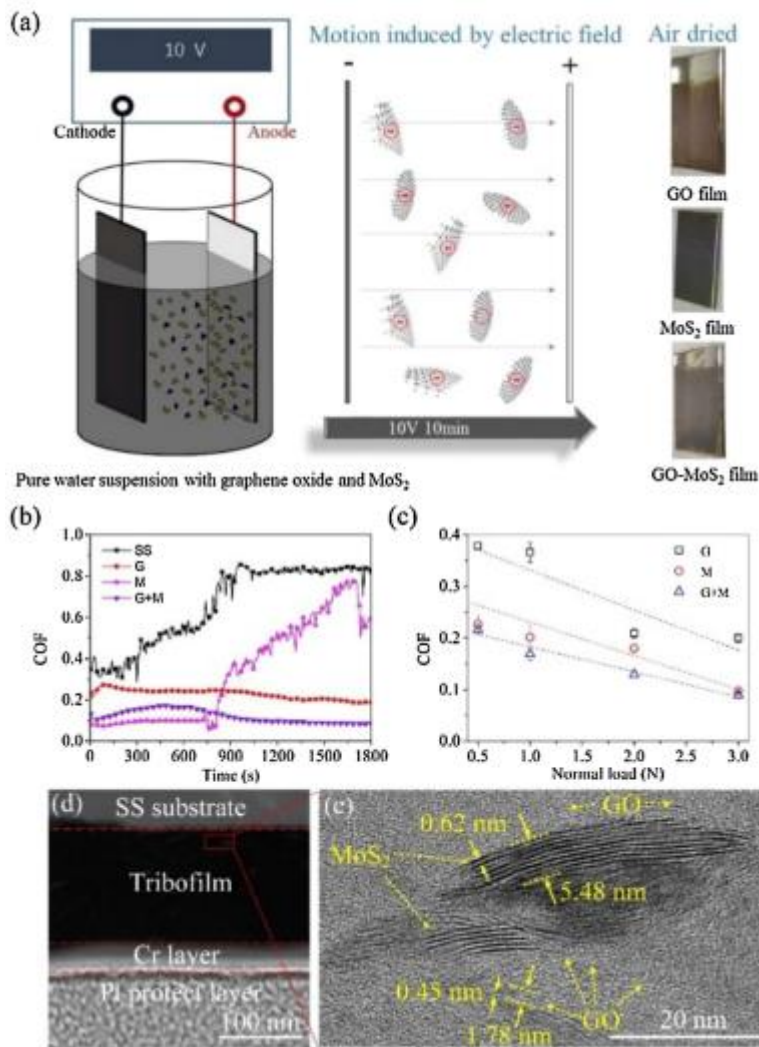


Figure II.8: (a) Schematic diagram of the electrophoretic deposition fabrication process. (b) COF of GO, MoS₂ and GO-MoS₂ films versus time under ambient condition with 3 N normal load. (c) Influence of normal load on average COF of different films. (d) Cross-sectional transmission electron microscopy (TEM) image depicted from the tribofilm. (e) High resolution transmission electron microscopy (HRTEM) image shows that GO nanoflakes wrapping around MoS₂ nanoflakes.

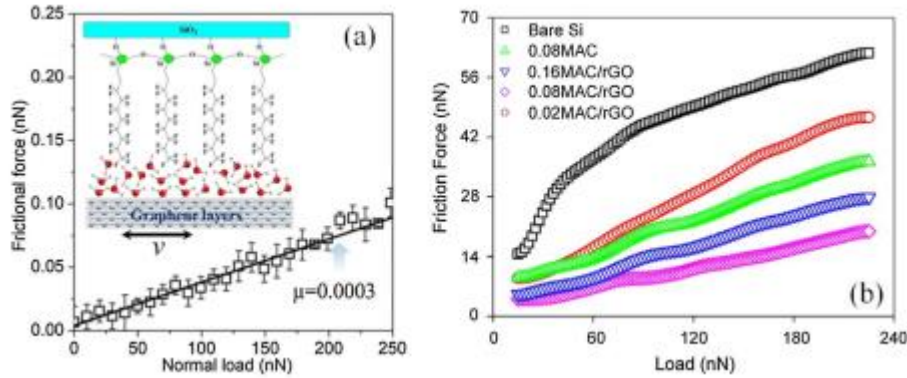


Figure II.9: (a) Frictional force while SAFM probe sliding against graphene with the lubrication of water. The corresponding COF was 0.0003. Reproduced with permission . (b) Friction forces between AFM colloidal probe and composite MAC/rGO film:

Graphene-family coatings with the lubrication of liquids :

Graphene-family materials are useful in developing surface coatings that can reduce friction and wear. One such application is the use of graphene-family coatings with the lubrication of liquids, which has been investigated and documented in recent years. Studies have shown that graphene oxide (GO) can greatly enhance the anti-wear property of coatings, thanks to its laminated structure and small size. GO can easily enter the contact area during rubbing motion and prevent surface asperities from direct contact. Furthermore, graphene-based coatings have demonstrated good lubricating performance with both water and oil lubrication. For example, the coefficient of friction (COF) between 440C stainless steel and reduced graphene oxide (rGO) coating with water lubrication was six times lower than that between 440C stainless steel surfaces. Additionally, the wear rate of a stainless steel plate sliding against an rGO-coated ball with water lubrication was three times lower than that against an uncoated ball with oil lubrication. Other studies have investigated the lubricating performances of polyimide and polyimide/FG coatings and epoxy-based composites with graphene and in situ liquid fillers under various lubricating conditions. In all cases, graphene-family materials have been found to improve lubricating performance and reduce friction and wear. [55][56]

II .6.Mxenes lubrication :

MXenes have excellent mechanical properties due to their strong M-X bond, which results in a high elastic constant and Young's modulus. Studies have shown that MXenes have superior mechanical properties compared to other 2D materials such as MoS₂ and graphene oxide. MXenes also exhibit outstanding lubrication properties due to their low-shear-resistance interlayers and excellent load-carrying ability. Various factors affect the mechanical properties of MXenes films, such as the size and quality of MXene sheets, the orientation of MXene sheets in films, the thickness, and the fabrication methods. Highly oriented MXene films can have tensile strength as high as 568 MPa. Additionally, MXenes-polymer composite films exhibit enhanced mechanical properties due to the superior mechanical behavior of MXenes and the interactions and cross-linking between MXenes and polymer chains. Studies have also demonstrated the lubrication potential of MXenes. Simulations and calculations have confirmed their lubrication properties, and different factors such as the interlayer distance, functionalization, and stacking type affect their tribological performance. Results have shown that larger interlayer distance, oxygen-functionalized M₂CO₂, and the mirror stack possess better tribological properties. MXenes can be used as solid lubricants, lubricant additives, and reinforcement phases in tribological applications. For example, Ti₂CO₂@MoS₂ heterostructure has been shown to have superlubricity and potential as an outstanding solid lubricant. MXenes can also be used as lubricant additives to reduce the coefficient of friction and wear of surfaces. Overall, MXenes exhibit excellent lubrication potential and can be used in various tribological applications.

- **Solid lubrication:**

MXenes are an excellent candidate for solid lubrication due to their weak interlayer interaction, ability to easily shear, formation of a tribo-layer, and self-lubricating ability. Micro- and macro-scale tribological behavior of MXenes and MXene-based composites have been investigated. Atomic force microscopy (AFM) and friction force microscopy (FFM) have been used to investigate the microscale tribological behavior of MXenes as solid lubricants. High pressure leads to high friction and adhesion force, while high temperature reduces the friction and adhesion force of Ti₃C₂ MXene. The friction and adhesion force of Ti₃C₂ and Nb₂C are positively correlated with pressure and negatively correlated with temperature. The increased contact area, increased oxygen content, and electron cloud density are the reasons for these influences. Surface dipole moment densities of the Ti₃C₂ and Nb₂C are responsible for the

difference in friction and adhesion force under the same conditions. The hydrophilicity of MXene surfaces significantly impacts the friction and adhesion force. Ti₃C₂ with worst hydrophilicity shows the lowest friction and adhesion force while TMA-Ti₃C₂ with the most hydrophilic surface exhibits the highest friction and adhesion force. The tribological properties of MXenes as a solid lubricant coating have been studied systematically. The thickness of the Ti₃C₂ MXene coating significantly reduces COFs and wear rates compared to copper disks. Carbonaceous transferred films and graphitized carbon are generated on the steel ball, which is the main reason for the good lubrication performance. The COF and wear rate of the Ti₃C₂ coating are significantly reduced compared to the ball bearing. MXenes show excellent lubricity and anti-wear performance, and can even achieve a superlubricity state at the macroscale. [57]

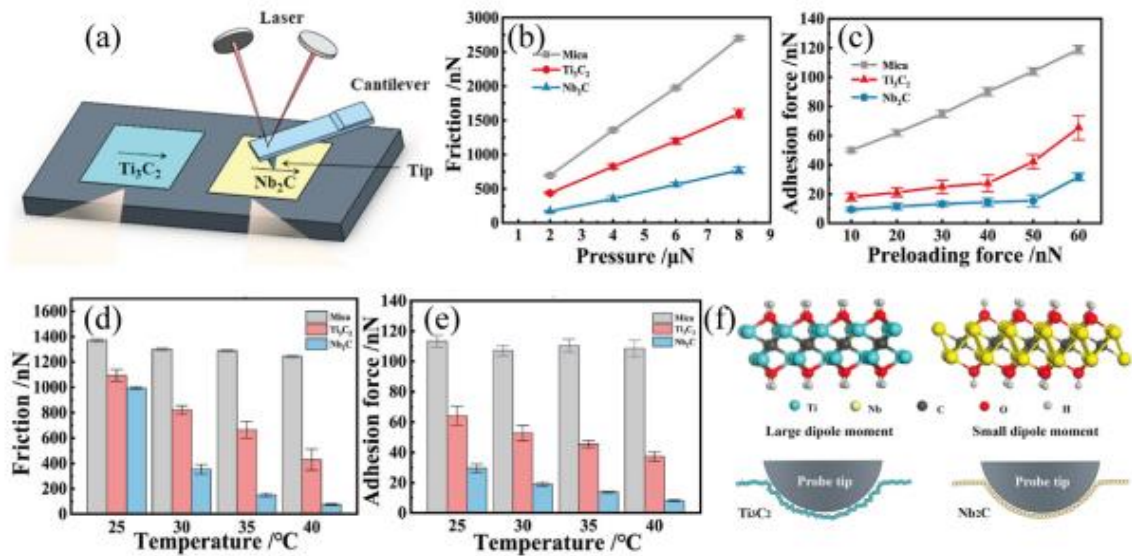


Figure II.10: (a) Schematic diagram of friction tests using AFM. (b) Friction of Mica, Ti₃C₂, and Nb₂C under different pressure. (c) Adhesion force of Mica, Ti₃C₂, and Nb₂C under different preloading forces. (d) Friction of Mica, Ti₃C₂, and Nb₂C under different temperatures. (e) Adhesion force of Mica, Ti₃C₂, and Nb₂C under different temperatures. (f) Schematic diagram of friction principle and structure of Ti₃C₂

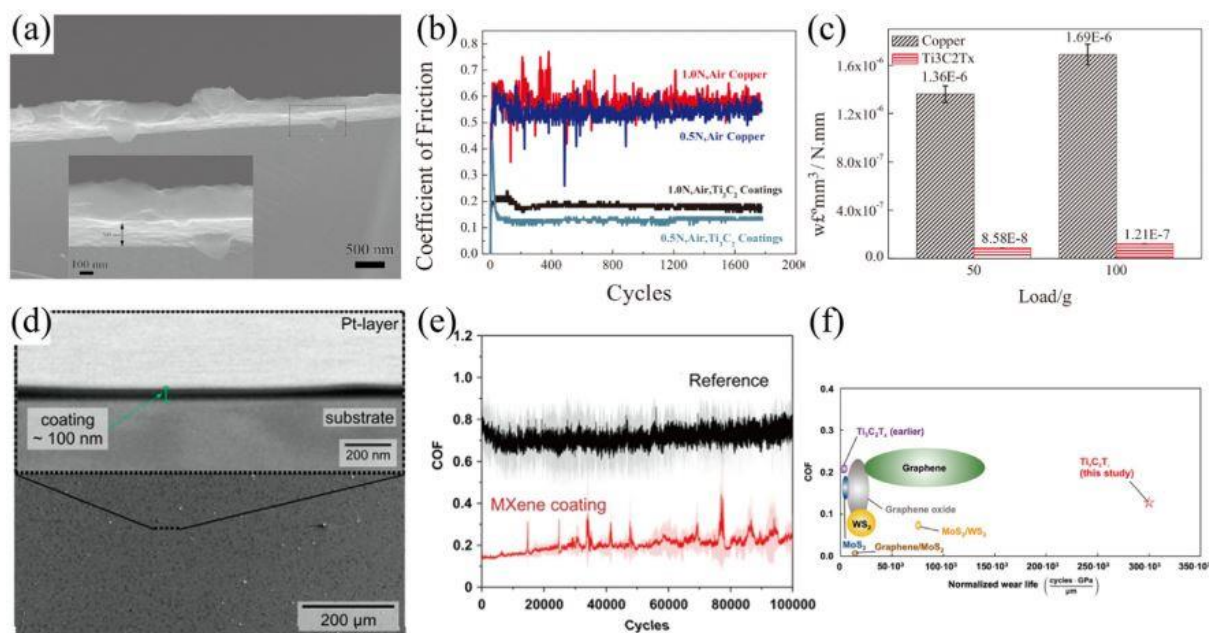


Figure II.11 : (a) SEM image of cross-sectional Ti₃C₂ coatings with a thickness of 200 nm. (b) COF curves of copper and Ti₃C₂ coatings under different loads. (c) Wear rate of copper and Ti₃C₂ coatings under different loads. (d) Cross-section image of MXene coating with a thickness of 100 nm. (e) COF curves of MXene coating and reference. (f) A comparison of normalized wear life and COF in this work with other 2D materials when they are used as solid lubricants. (a-c) Reproduced with permission .

- **Liquid lubrication :**

The paragraph is discussing the use of MXene as an additive in liquid lubrication. MXene is a material that has been shown to have excellent properties as a solid lubricant, but it can also be used as an additive in liquid lubricants to improve their performance. The paragraph describes several studies that have investigated the use of MXene as an additive in oil-based lubricants. One study, conducted by Yang et al. (2014), found that adding 2D Ti₃C₂ MXene to paraffin base oil greatly improved its friction reduction and anti-wear properties, especially at a concentration of 1.0 wt%. The researchers also found that under high applied loads (20 N – 30 N), the COFs remained unchanged, indicating that the formation of a Ti₃C₂ lubricant film prevented direct contact between the friction pairs and improved lubricating performance. Other studies have investigated the effect of etching time and temperature on MXene's performance as an additive in different base oils. Zhang et al. (2019) found that Ti₃C₂ (OH)₂ showed excellent tribological properties in 100SN base oil, while Liu et al. (2020) found that higher treatment temperatures led to higher exfoliation degrees and better lubrication performance in poly-alpha-olefin-8 oil (PAO8). One challenge with using MXene as an additive in oil-based lubricants is its poor dispersibility and stability. However, researchers have found

that surface modification can improve its dispersibility and stability in oil. For example, Huang et al. (2020) grafted tetradecylphosphonic acid (TDPA) onto the surface of 2D Ti₃C₂ and found that the modified MXene exhibited better tribological properties than unmodified MXene. Overall, these studies demonstrate that MXene has great potential as an additive in liquid lubrication, and that surface modification can further improve its performance. By using MXene as an additive, lubricants can be made more effective in reducing friction, wear, corrosion, and oxidation, which can lead to improved industrial production. [41]

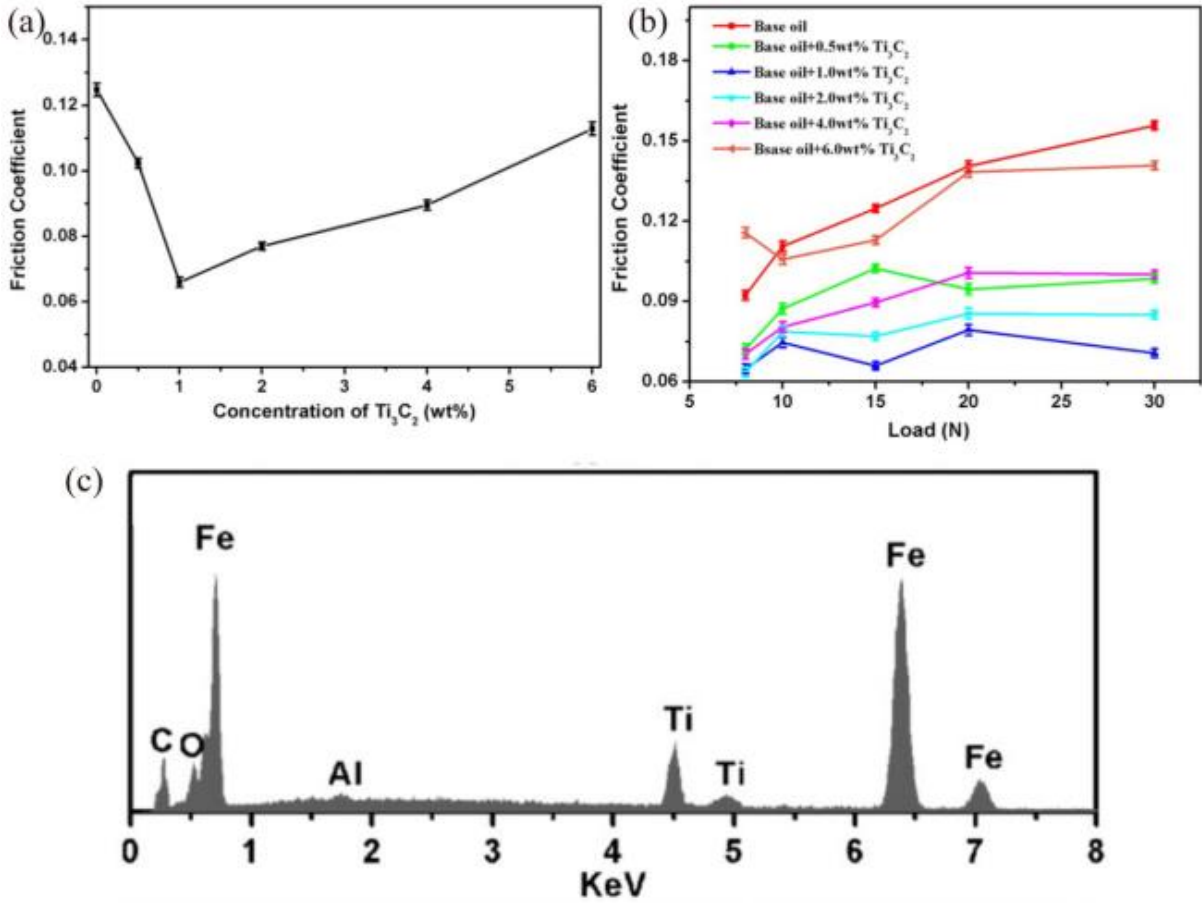


Figure II.12: (a) Friction coefficient of Ti₃C₂ under different concentrations. (b) Friction coefficient under different applied loads with various contents of Ti₃C₂. (c) EDS analysis of worn surfaces on steels lubricated by 1.0 wt% Ti₃C₂ base oil .

The lubrication mechanisms example of MXene-based materials are summarized into two categories:

- **nanoscale mechanisms and macroscale mechanisms:**

MXenes, which are transition metal carbides, nitrides, and carbonitrides, have abundant surface terminations that impact their tribological performance. The nanoscale mechanisms of MXene are complex and include various M-X bonds, layer numbers, and surface terminations. The hydrophilicity of Ti₃C₂T_x was found to impact its friction properties. Annealing treatment was performed to reduce the content of –OH termination of Ti₃C₂T_x and investigate its impact on friction behaviors. [57]

- **On the other hand, macroscale mechanisms of MXene-based materials:**

Can be divided into transfer film, physical deposition film, and chemical reaction film. The transfer film mechanism involves nanoparticles adhering and transferring onto the friction counterpart during the friction process, which usually occurs in solid lubrication. MXenes with large specific surface areas can form a physical absorption film or react at the friction surface to form a tribochemical reaction film. Transfer film lubrication mechanisms can result in ultra-long wear life. Secondary transfer mechanisms have also been observed in MXene-based materials.

Factors Influencing MXene Lubrication In the preceding sections, we provided an overview of the lubrication behavior of MXene in solid lubricants, liquid lubricants, and reinforcement phases.

MXene lubrication is a complex system, and its friction and wear properties are influenced by various factors. We categorize the influencing factors of MXene lubrication into two main parts: **external and internal factors**, and conduct a detailed analysis and comparison.

II .7.External Factors:

- **External factors can be categorized as follows: test parameters, friction counterparts, and environmental factors:**

Test Parameters: Our focus lies primarily on the parameters of applied load, sliding velocity, and test time. In the case of solid lubrication, the effect of applied load on lubricity exhibits irregular changes. Previous research has shown that the applied load may increase friction , reduce friction , reach an optimum load , or have no effect on friction Conversely, in terms of

lubricity, the applied load follows a regular pattern. High loads lead to increased wear and a shortened service life of solid lubricants. In the case of liquid lubrication, high loads typically result in increased friction and wear rates. However, the coefficient of friction (COF) and wear rate do not always align. For example, in systems involving Ti₃C₂ (OH)₂ in 100SN base oil and Ti₃C₂ in water, there is an optimum load for achieving the lowest COF, although the wear rate at this load is not the lowest. [57]

Sliding Velocity: Sliding velocity also plays a significant role in MXene lubrication. In solid lubrication, sliding velocity has minimal impact on lubricity, but it considerably reduces the service time as the sliding velocity increase. In liquid lubrication, the MXene-glycerol system exhibits an optimum sliding velocity of 0.075 m/s. In polymer composites, higher sliding velocities result in lower COF because more MXene nanoflakes exfoliate from the matrix, providing improved lubrication at the sliding interface. However, further experiments are required to fully understand the influence of sliding velocity on MXene lubrication.

Friction counterparts: Play a crucial role in the overall performance of the friction system, as different counterparts lead to varied tribological outcomes. In solid lubrication, friction tests have been conducted using various friction balls (such as steel ball, Al₂O₃ ball, Si₃N₄ ball, and PTFE ball) and disks (including steel, silicon, and copper) with coatings. Yin et al. examined the friction behavior of different polymer balls as friction components, where the PTFE ball demonstrated the lowest coefficient of friction (COF) due to its excellent self-lubricating properties. Additionally, when a stainless steel ball coated with a diamond-like carbon film was rubbed against silicon wafers with Ti₃C₂/ nanodiamond coating, it exhibited superlubricity. In liquid lubrication,). Notably, Yi et al. utilized Si₃N₄ ball and sapphire disk as friction counterparts, achieving a state of superlubricity in MXene-glycerol aqueous solution. Regarding phase-reinforced materials, Yan et al. utilized Al₂O₃ and Si₃N₄ balls as friction balls, but no significant differences in tribological behavior were observed between the two. Han et al. enhanced the antifriction and wear resistance of composites by subjecting the metal substrates to nitriding or micro-oxidation treatments.

In general, the selection of suitable friction counterparts significantly influences tribological performance. Optimal selection of friction counterparts can yield improved lubrication effects. Moreover, special treatments applied to friction counterparts can lead to exceptional performance and even achieve a state of superlubricity.

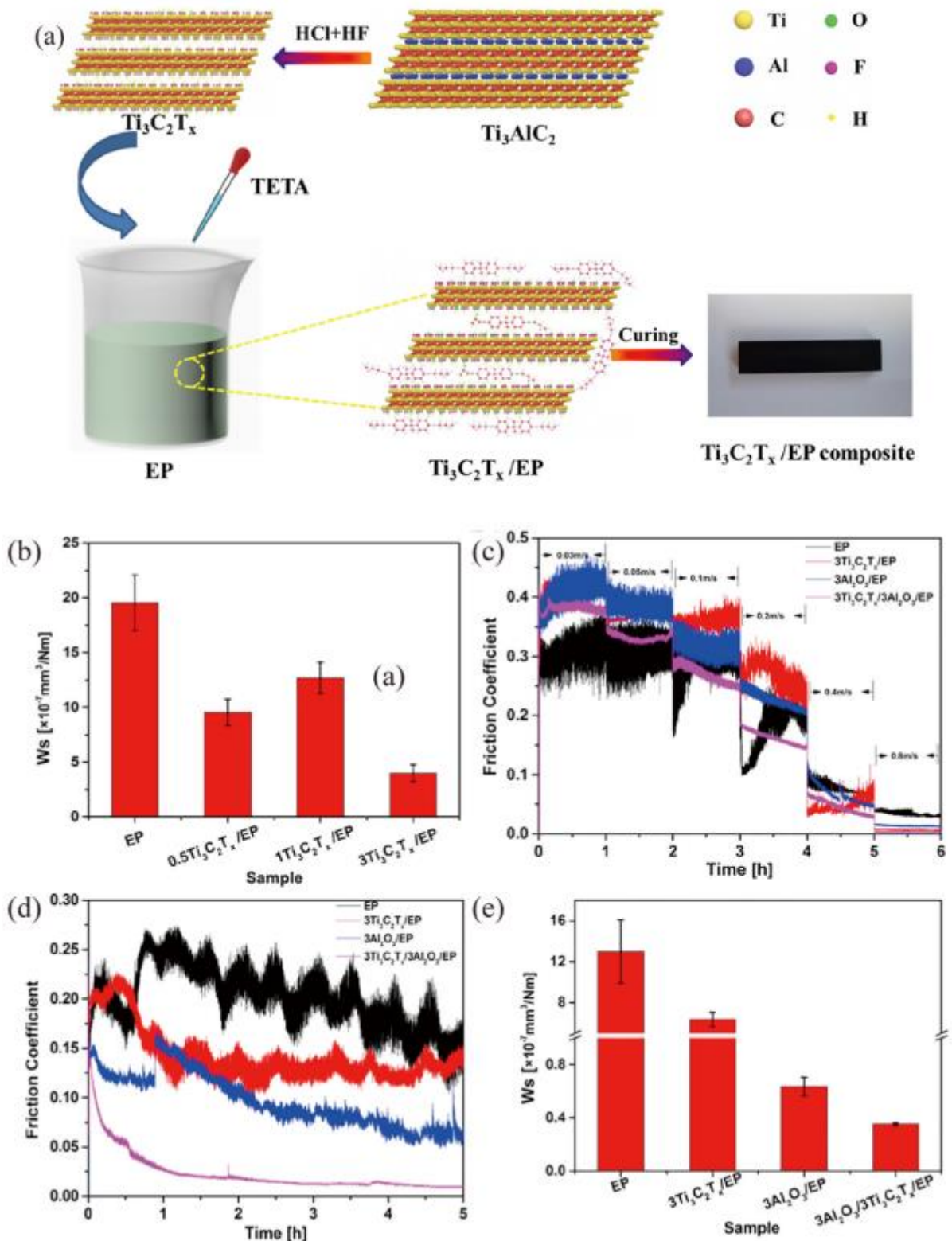
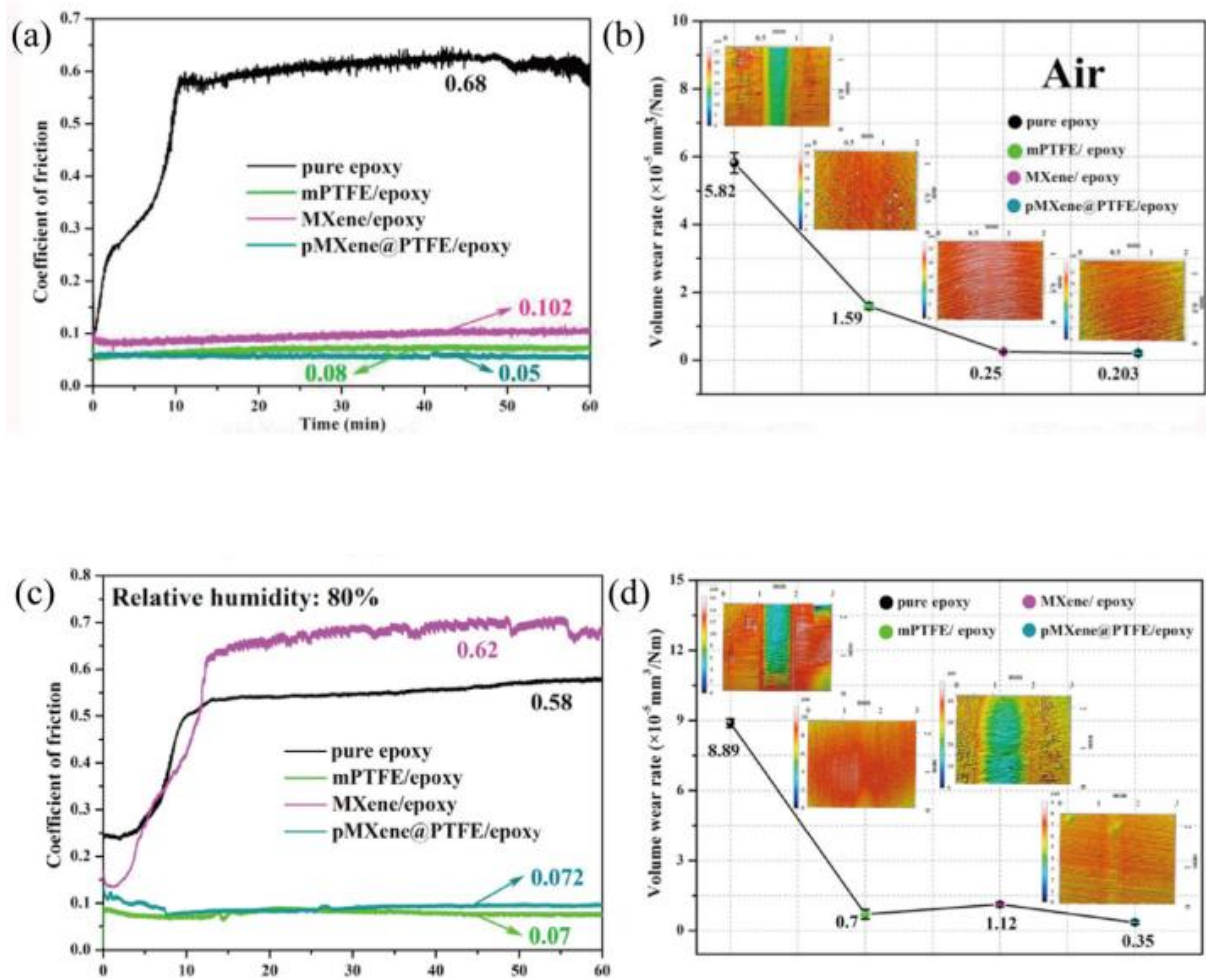


Figure II.13: (a) The preparation process of $\text{Ti}_3\text{C}_2\text{T}_x/\text{EP}$ composite. (b) The wear rate of EP with different $\text{Ti}_3\text{C}_2\text{T}_x$ contents from 0 to 3.0 wt%. (c) COF curves over time of as-prepared coatings under different sliding speeds from 0.03 to 0.8 ms^{-1} (d) COF curves over time of as-prepared coatings at the speed of 0.4 ms^{-1} . (e) The wear rate of as-prepared coatings at the speed of 0.4 ms^{-1}

Environmental factors:

Encompass temperature, relative humidity, atmosphere, and dry/wet friction, among others. Guo et al. conducted Atomic Force Microscopy (AFM) studies to examine the adhesion and friction behaviors of MXene nanosheets at different temperatures. They observed that MXene exhibits low adhesion and friction at higher temperatures, which can be attributed to structural changes. Marian et al. investigated the influence of relative humidity on the friction properties of MXene and found no significant benefits in terms of friction and/or wear at higher relative humidity levels. Lian et al. explored the tribological performance of Ti₃C₂-GO coatings under air and dry nitrogen atmospheres, while the team discussed the friction properties of pMXene@PTFE/epoxy composite coatings under dry air, humid air (RH = 80%), and vacuum environments. These studies revealed that MXene composites display environmental adaptability, demonstrating excellent lubrication effects in air, dry nitrogen, relative humidity of 80%, and vacuum environments.⁴¹



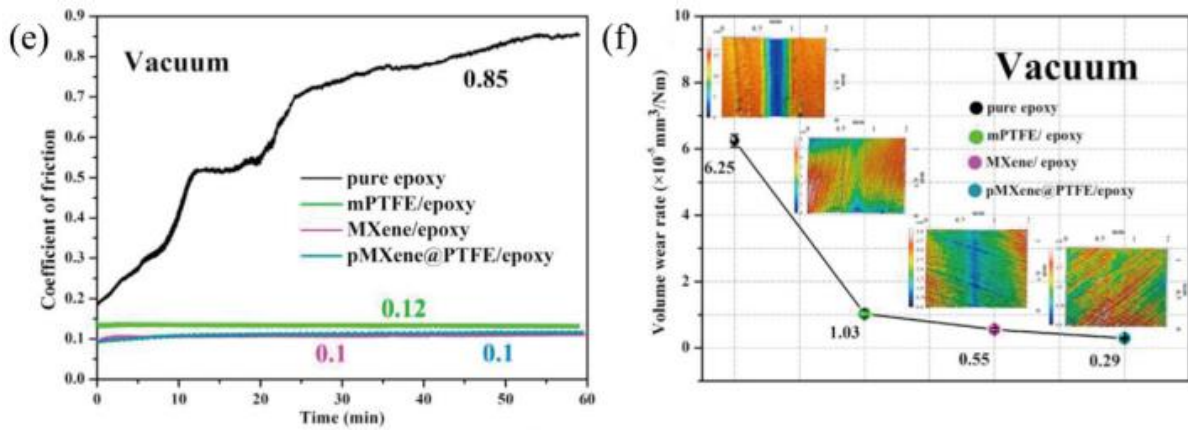


Figure II.14: Tribological properties of as-prepared coatings under different environments. (a) and (b) Air. (c) and (d) Relative humidity of 80%. (e) and (f) Vacuum . [57]

Internal factors:

Play a significant role in the friction behavior of MXene, including properties such as concentration, exfoliation degree, size (thickness), oxidation degree, surface groups, and hydrophilicity. The concentration of MXene has a notable impact on tribological properties, primarily in liquid lubrication and reinforced materials. Typically, there exists an optimal concentration that minimizes the coefficient of friction (COF) and wear rate . However, some reports have shown a gradual decrease in COF with increasing additive concentration without reaching a turning point. In certain studies, the COF and wear do not precisely correlate. Moreover, the optimal concentration varies across different tribological systems, ranging from 0.025% to 70% . The exfoliation degree and size of MXene also influence its tribological properties. Higher exfoliation degrees and smaller nanosheet sizes contribute to improved tribological performance. Furthermore, a moderate degree of oxidation tends to have a positive effect compared to no oxidation or complete oxidation . The influence of surface terminations on MXene lubrication, particularly at macroscales, has not been extensively explored and will be discussed in the section covering the lubrication mechanisms of MXene-based materials. [57]

II .8. Discussing generally of the synthesis and characterization of nano-filament derived from multiple materials procures of titanium family:

The Study on the synthesis and characterization of 2D flakes obtained from different precursors. which the nanofilaments being anatase-based and the synthesis process using Ti-containing precursors and TMAH ;The authors used scanning electron microscopy (SEM) to observe the 2D nature of the flakes derived from titanium carbide (TiC). The flakes varied in color and could be synthesized from non-layered precursors, suggesting a bottom-up approach. X-ray

diffraction (XRD) patterns confirmed the presence of 2D materials, and the peaks associated with the precursors were mostly absent. The authors also used transmission electron microscopy (TEM) to observe the flakes derived from different precursors, with some flakes reaching sizes greater than 1 μm . Selected area diffraction (SAD) patterns confirmed the structural characteristics of the flakes, and the presence of frayed fibers at the edges of the sheets indicated their alignment in specific directions. The authors acknowledge the possibility of amorphous regions and smaller flakes pointing in various directions.

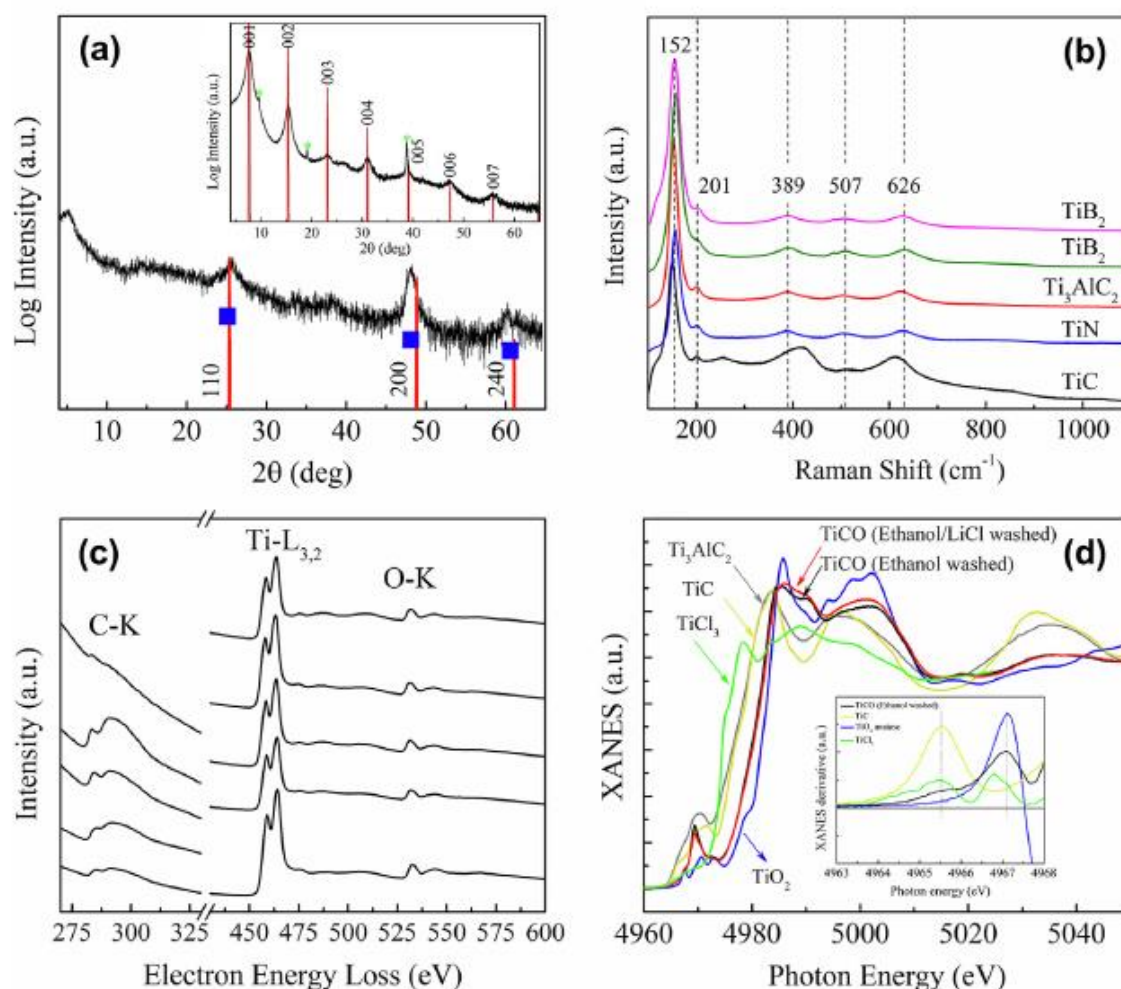


Figure II .15: Characterization of 2D material. (a) XRD patterns, on log scale, of filtered, vertically oriented, Ti_3AlC_2 -derived film in transmission mode. Inset shows pattern of horizontally oriented film. 5° 2θ peak is due to Kapton tape. Blue squares are 2θ locations determined from TEM-SAD patterns (Table S3). (b) Raman spectrum of FFs obtained from precursors indicated. All powders heated at 50°C for 3 d and washed with ethanol and water, except the top TiB_2 that was produced at 80°C for 2 d. All peaks belong to anatase. (c) Core loss EELS data measured from 5 individual particles. Graph shows

carbon –K edge at 280 eV energy loss, titanium –L3,2 peaks at 450 eV energy loss and oxygen –K edge at 530 eV energy loss. All spectra are normalized to the Ti edge peak intensity and are vertically separated for clarity. (d) XANES results of TiC-derived films together with those for anatase, Ti₃AlC₂, TiC and TiCl₃. Both TiC samples were reacted in TMAH at 50° C for 3d. Inset shows XANES derivative. [58]

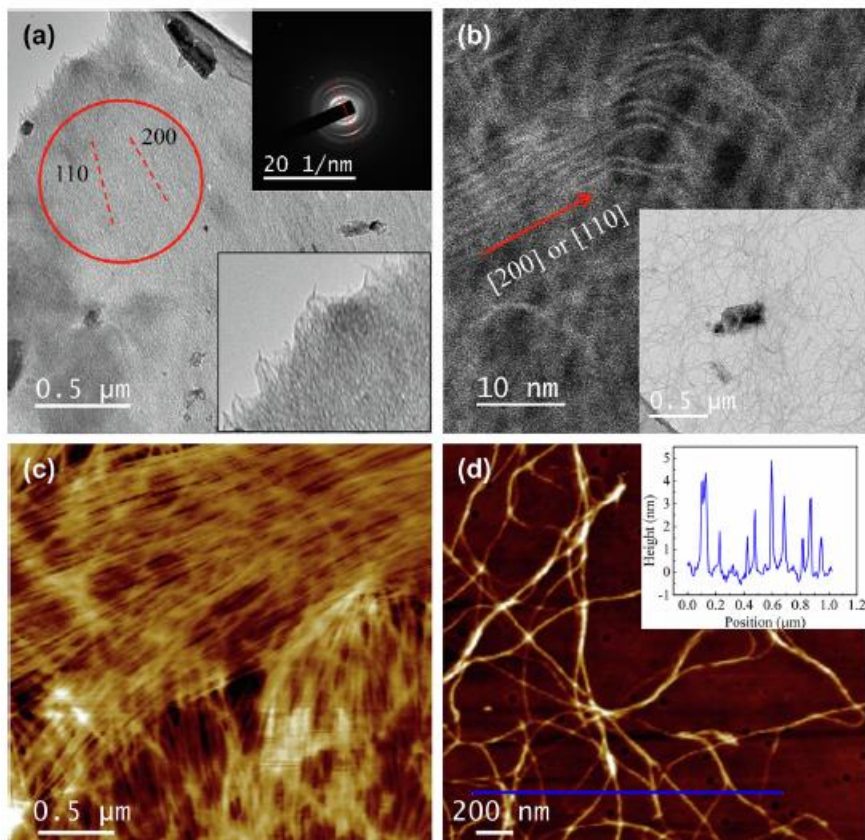


Figure II.16: TCO Flake morphology. (a) Typical TEM image of TCO flake > 4 μm in lateral size. SAD of area encircled in red is shown in top right inset. Two arcs indicate fiber texture along [110] and [200] directions. Bottom inset is a higher magnification of top left corner showing frayed nfs in a direction that is in accordance with the arcs. (b) STEM showing individual filaments, the width of which is 10 Å. Bottom inset shows nfs being chemically “drawn out” from a large central Ti₃AlC₂ particle. (c) AFM of TCO self-assembled nanofilaments derived from TiC heated in TMAH at 80 C for 3d and washed with water. (d) Same as (c) but after diluting the colloidal suspension 500x and drop casting on a glass slide. Inset shows height profile corresponding to blue line in (d); thinnest filaments are 1.5 nm high. [59]

Further investigation; The Ti: X ratio obtained from electron energy loss spectroscopy (EELS) suggests that the system is not necessarily homogeneous and exhibits variability in the composition. However, the conclusions regarding the structure of the flakes and the presence of carbon in the structure remain valid. The mechanisms involved in the formation of the (nfs) and 2D layers are discussed, drawing from previous research. The role of TMAH (tetramethylammonium hydroxide) in directing the polycondensation process and assembly of Ti octahedra into 2D layers is highlighted. The nfs are believed to be chemically drawn out of the precursor, and self-assembly into 2D flakes occurs. Films derived from TiC and the MAX phases exhibit conductivity, while those made with TiO₂ or TiB₂ do not. The conductivity is lower than that of MXenes but higher than typical oxides. The electronic structure of the flakes is characterized by measuring their UV-vis optical absorption spectra, which show an indirect band gap and a pronounced Urbach tail.

In general the properties and mechanisms that could understand is:

II .8.1.The Properties:

- The nanofilaments (NFs) have a fibrous nature, with an estimated width of around 1 nm and a thickness of approximately 5.9 Å.
- The NFs have a cross-section of about $6 \times 10 \text{ \AA}^2$ and can be micrometers long.
- The theoretical surface area of the NFs is greater than 1500 m²/g.
- TEM and AFM maps show the fibrous nature and self-alignment of the NFs.
- Raman spectroscopy indicates that all NFs exhibit peaks belonging to anatase.
- XPS analysis confirms the presence of titanium (Ti), carbon (C), and oxygen (O) in the NFs, with the O:Ti ratio closer to 3 than 1.

II .8.2.The .Mechanisms:

- The presence of tetramethylammonium hydroxide (TMAH) helps in the formation of regular arrangements of rectangle nanocrystalline anatase particles.
- TMAH assists in assembling Ti octahedra into 2D layers and intercalating the resultant sheets, leading to the formation of 2D flakes.
- The TMAH capping occurs on low energy (001) planes and a second surface perpendicular to the growth direction, confining growth to one dimension.
- The nfs are chemically "drawn" out of the precursor, and the polycondensation process may occur at the interface.
- The nfs self-assemble into 2D flakes, forming crystalline regions in certain areas.

another study discovered by scientists recently successfully synthesized one-dimensional (1D) TiO₂-based nanofilaments (NFs) by reacting water-insoluble, abundant, and non-toxic Ti-containing precursors like TiC, TiB₂, and TiSi₂ with quaternary ammonium hydroxides, primarily tetramethylammonium hydroxide, under near-ambient conditions. Initially, our analysis based on selected area diffraction, X-ray diffraction, and Raman spectroscopy led us to conclude that the structure of the NFs was anatase-based. However, through advanced techniques such as high-resolution scanning transmission electron microscopy, low-power Raman spectroscopy, and density functional theory modeling, we have now determined that the actual structure of the NFs is a 1D titania lepidocrocite-based structure with minimal cross-sections measuring approximately 3.5 Å. The NFs exhibit growth along the [100] direction and possess lattice parameters of approximately 3.78 ± 0.01 Å (a-axis) and 3.04 ± 0.06 Å (c-axis). By providing a comprehensive characterization using these advanced techniques, we have gained a more accurate understanding of the structural properties of the TiO₂-based nanofilaments, identifying them as a 1D titania lepidocrocite-based structure rather than the previously assumed anatase-based structure. [60]

The scientists discussed The XRD patterns show the diffraction peaks of the samples synthesized using TiB₂ powders and TMAH. The powders were washed with ethanol and then dehydrated, or further treated with a LiCl solution and rinsed with DI water before drying. The XRD patterns reveal low-intensity unreacted TiB₂ peaks as internal standards. The patterns also exhibit basal reflections with a d-spacing of approximately 11.5 Å, indicating the stacking of 2D flakes in an in-plane alignment of 1DL. After washing with LiCl, the d-spacing value decreases to around 9.5 Å, confirming the replacement of TMA⁺ cations with Li⁺ ions. The yellow/green bands in the XRD patterns correspond to lepidocrocite non-basal reflections, consistent with previous observations. The Raman spectra (Figure 2A) of the samples processed in different ways also show consistent patterns with lepidocrocite. The scientists note that the laser power used in previous spectra was too high, resulting in a lepidocrocite-to-anatase transformation. When the laser power was increased, the Raman spectra changed from lepidocrocite-like to anatase-like (Figure 2B). The authors mention the importance of reconciling the observed XRD patterns with the lepidocrocite structure. While some peaks in the XRD patterns align with standard lepidocrocite, others show deviations. The absence of a prominent (103) peak, typically seen in lepidocrocite, is particularly notable in the observed self-assembled NFs. The authors refer to previous work on lepidocrocite nanotubes, which also

exhibited a peak at $62^\circ 2\theta$ assigned to (002), suggesting that the absence of a (103) peak may be a characteristic of the 1DL structure.

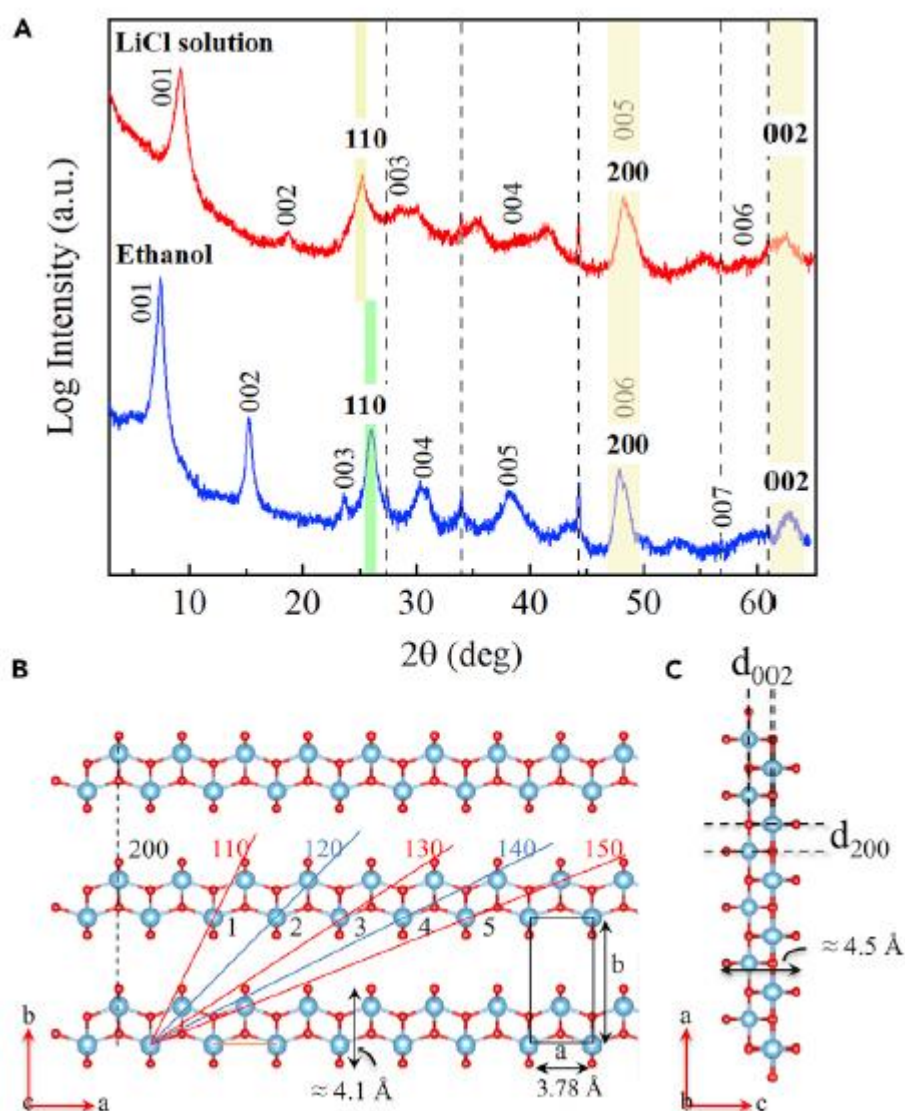


Figure II.17: XRD patterns and DFT-generated 1DL structure (A) XRD patterns of 2 samples: one washed with ethanol (bottom, blue), the other (red, top) washed with ethanol and then a 0.5 M LiCl solution (see Experimental procedures section). Positions of the (200) and (002) peaks at 2θ z 48 and z 62, respectively, are crystallographic and processing invariant; the positions of all other peaks are processing dependent. Note log scale on y axis. Yellow/green bands outline the 3 arcs/rings observed in SAD patterns of 2D flakes in TEM. Vertical dashed lines designate low-intensity unreacted TiB₂ peaks used as internal standards.¹² (B) Schematic of DFT-generated structure with TiO₂ ribbons stacked normal to b axis. Also traced by inclined red and blue are all non-basal planes predicted. Rectangle on bottom right denotes a unit cell with lattice parameters a , and b . Note a is crystallographic but b depends weakly on spacing between ribbons, here chosen to be 7.5 \AA .

The same is true of stacking along 00L.(C) Schematic of (001) plane assuming it is 2 Ti atoms wide. Spacing between 2 adjacent Ti atoms, along c, or d_{002} , is 1.5Å , which gives rise to peak at $2\theta = 62^\circ$ seen in XRD and SAD patterns.¹² Also shown in (B) and (C) are the approximate thicknesses—measured from outermost O to outermost O—of 2-atom-thick Ti ribbons according to DFT calculations. Note that DFT results assume a 2D structure where the width of the ribbon in along c is infinite .

The analysis of the STEM images, FFT simulations, and domain sizes of the TiB₂-derived bundle of NFs. **Figure II.18** shows an annular bright field (ABF) STEM image of the NF bundle, along with an FFT of the micrograph's center. The high-angle annular dark field (HAADF) STEM image reveals crystalline contrast. To simulate the FFT, the authors used a DFT-generated lepidocrocite structure and tilted it so that the c-axis became the zone axis.

The lepidocrocite layers were stacked along the b-axis to align with the bundle axis. The agreement between the FFT spots and the simulated selected area diffraction (SAD) patterns is excellent, indicating specific d-spacings. The calculated d-spacings for the (110) and (200) planes were found to be 3.6Å and 2.1Å , respectively, while the corresponding values derived from XRD patterns were slightly different. The authors attribute this discrepancy to factors such as image calibration accuracy, scan distortions, and the material potentially containing carbon (not accounted for in the DFT model). The XRD results provide more accurate information, showing consistent symmetry of the diffraction peaks. The calculated lattice parameter a was found to be 3.78Å , slightly smaller than the value reported by Tominaka et al. for 2D lepidocrocite synthesized using TMAH. The authors previously identified the 1D nature of their product through XRD, high-resolution TEM, and SAD patterns, some of which appeared as arcs. The d-spacing obtained from the innermost arcs corresponded to the XRD peak at $26^\circ 2\theta$, characteristic of anatase. This, along with Raman results, led them to believe they were dealing with an anatase structure.

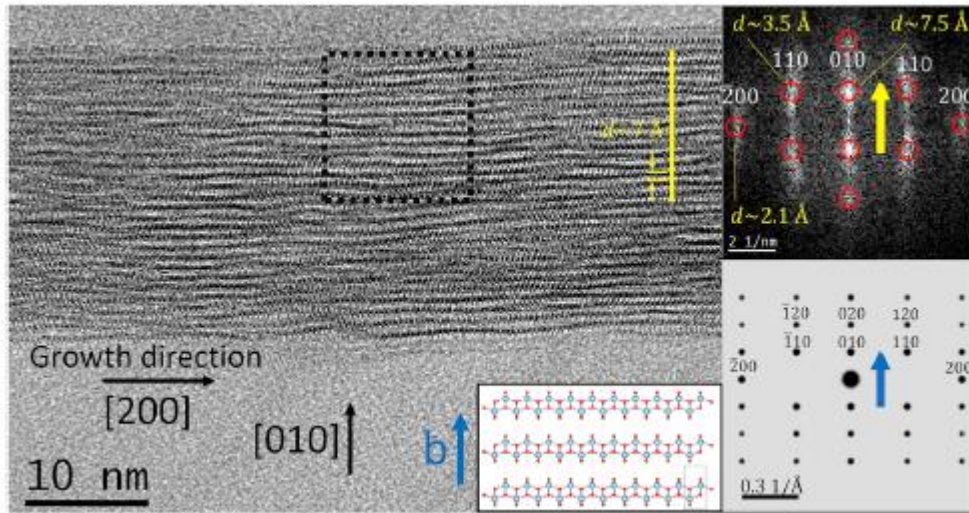


Figure II.18: ABF STEM micrograph of a bundle of individual 1DL NFs oriented along the fiber axis. Lower right inset is FFT of region outlined by black square. Lower middle inset shows schematic of lepidocrocite layers (not to scale) stacked along the b axis. Growth direction is along $[200]$, which coincides with bundle axis. Superimposed on FFT (upper right inset), as red circles, are the indices predicted from the lepidocrocite DFT structure assuming spacing along b is 7.5 \AA . Agreement between DFT-generated FFT and experiment is excellent. Planes $(1,n,0)$ outlined in Figure 1B are denoted by blue and yellow arrows. Precursor was TiB_2 , reacted in TMAH for 5 days at 80°C .

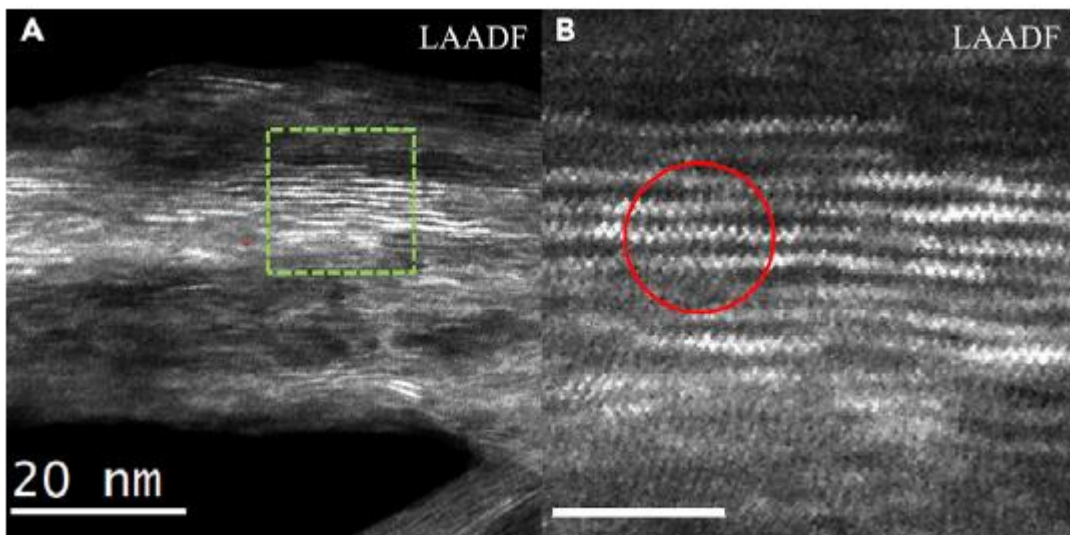


Figure II.19: Low angle annular dark field STEM micrograph of sample shown in Figure 3. Sample shown at (A) low magnification and (B) higher magnification of region enclosed in green square in (A). Scale bar is 5 nm . Zigzag and 2-layered nature of Ti atoms in the NFs in area enclosed by red circle are clearly shown.

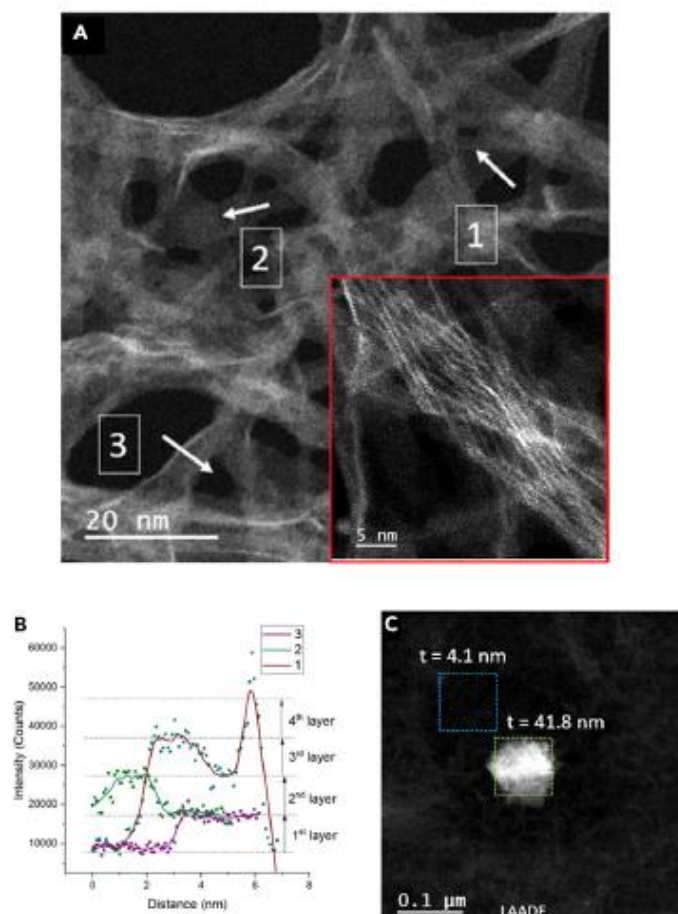


Figure II.20: STEM characterization of TiC-derived NFs, as well as unreacted particles (A) HAADF image of a loose bundle of NFs. Inset shows higher magnification image. Regions of reduced intensity without visible atomic contrast are likely NFs not oriented along a low zone axis.(B) Integrated line scans show the intensity of these regions scale as integer multiples of intensity measured in line scans denoted in (A) by respective numbers.(C) LAADF image of an unreacted TiC particle surrounded by a web-like structure composed of NFs; thickness estimates based on EELS spectra maps are shown to be 4.1 nm for web-like structure and 41.8 nm for unreacted TiC particle. Precursor was TiC, reacted in TMAH for 5 days at 80.

The scientists observe that in the HAADF image of the grids without carbon support, there is a lack of crystalline contrast. They propose that this absence of contrast is likely due to misoriented nanofilaments (NFs) rather than amorphous material. They suspect that these NFs are aligned along the [001] direction, and the increased contrast is a result of stacked NFs in integer multiples (1, 2, 3, etc.). To support their conclusion, the authors perform line scans on three regions indicated by white arrows in the HAADF image (Figure II.20A) and plot the

intensity profiles in Figure. As the contrast in HAADF images is influenced by specimen thickness, the intensity measured from the line scans correlates with the thickness in that region. Despite a low signal-to-noise ratio, distinct plateaus can be observed in the scan profiles. To enhance the visualization of these plateaus, the authors apply a smoothing technique using a Savitzky-Golay method with a window size of 15 points. The smoothed profiles are depicted as lines in **Figure II.20 B**, while the raw data is overlaid as a scatterplot. By considering the thinnest region as a single layer, the authors note that the other plateaus align with integer multiples of this thickness value. ^[60]

So generally The discussed research focuses on the synthesis and characterization of one-dimensional (1D) TiO₂-based nanofilaments (NFs) using Ti-containing precursors and quaternary ammonium hydroxides. The previous understanding was that the NFs had an anatase-based structure, but through advanced microscopy techniques and density functional theory modeling, it was discovered that the actual structure is a 1D titania lepidocrocite-based structure.

**CHAPTER III: EXPERIMENTAL PART
ELABORATION AND
CHARACTERIZATION**

III .1.Introduction:

The objective of this part generally about elaboration of new material called dimensional nanofilament derived from TiB_2 ; this study focuses on fabricating a solid lubricant using this new material through the spray coating technique. The primary objective is to investigate the lubrication properties of this new material by subjecting the resulting samples to tribological testing. The study aims to evaluate whether the TiB_2 nanofilament exhibits excellent lubrication performance, specifically in terms of reducing friction and wear. By conducting comprehensive tribological tests, the researchers seek to gain insights into the potential of this new solid lubricant for practical applications aimed at minimizing friction and wear.

Also investigate the effectiveness of using a solid material, called Cr_2CTx specifically in oil lubrication. To explore the lubricating properties and assess the potential of it in reducing friction and wear in oil lubrication applications. and evaluating the performance of TiB_2 in oil lubrication too , valuable insights can be gained to further advance the understanding and utilization of solid lubricants in enhancing the effectiveness of oil lubrication for various mechanical systems.

III .2.Materials:

We used materials for our investigation:

- 100 cr6 steel treated : with a composition primarily consisting of chromium (Cr) and carbon (C)
- 430 c stainless steel: characterized by its high chromium (Cr) content and added carbon (C) element.
- 316 L stainless steel: which boasts superior corrosion resistance due to its composition, comprising low carbon (C) levels, high chromium (Cr) content, and the inclusion of molybdenum (Mo) for enhanced performance.

III .3.Stability tests:

A stability test is a process or set of experiments conducted to assess and evaluate the stability of a product or solution or substance under various environmental conditions over a defined period.

The stability test is by comparing four mediums (Water; ethanol; acetone; propanol) + TiB_2 the objective was to determine which is better and suitable medium for our spray coating test which is important step.

- Compare results:
- propanol + TiB_2 :

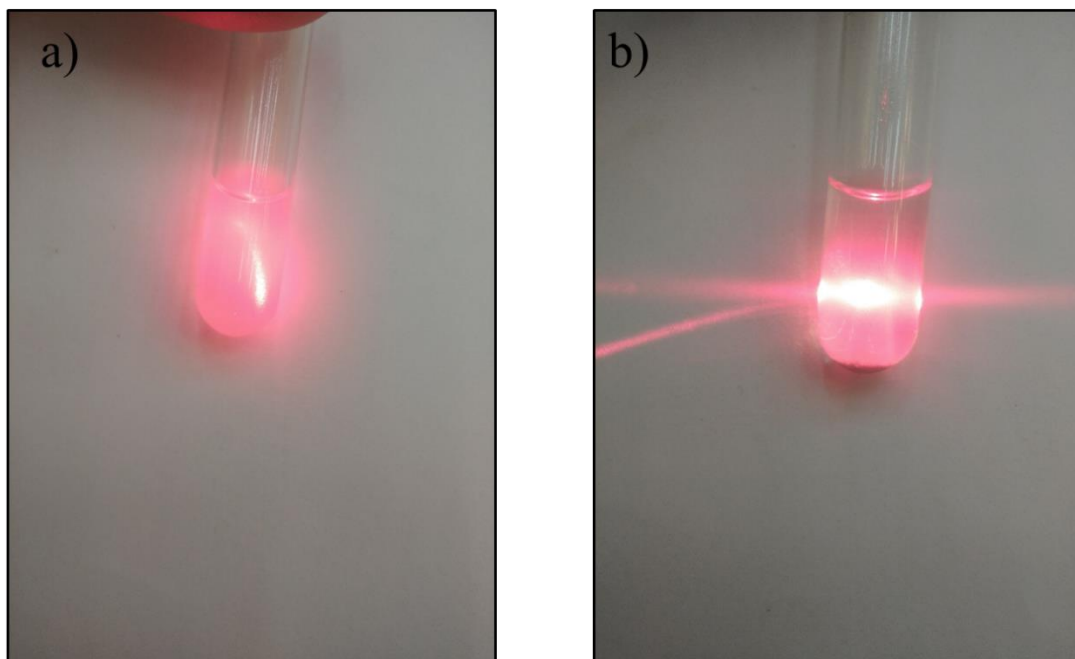


Figure III.1: Propanol + TiB_2 ; a) in few seconds and b) after 15 min

- Acetone + TiB_2 :

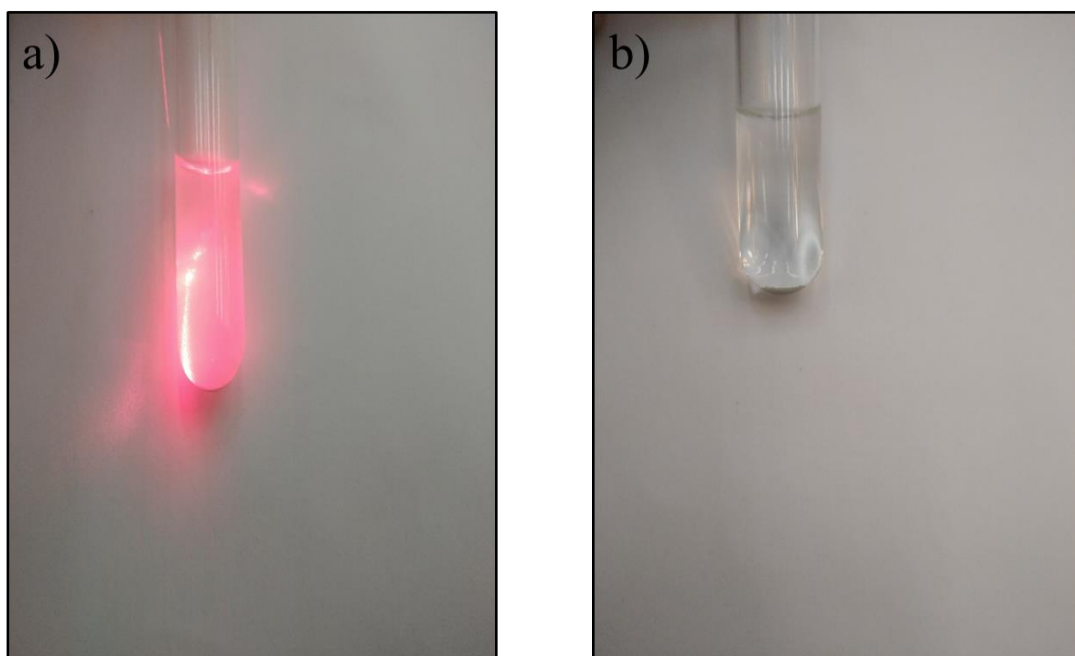


Figure III.2: Acetone+ TiB_2 ; a) in few seconds and b) after 15 min

- **Water+TiB₂:**

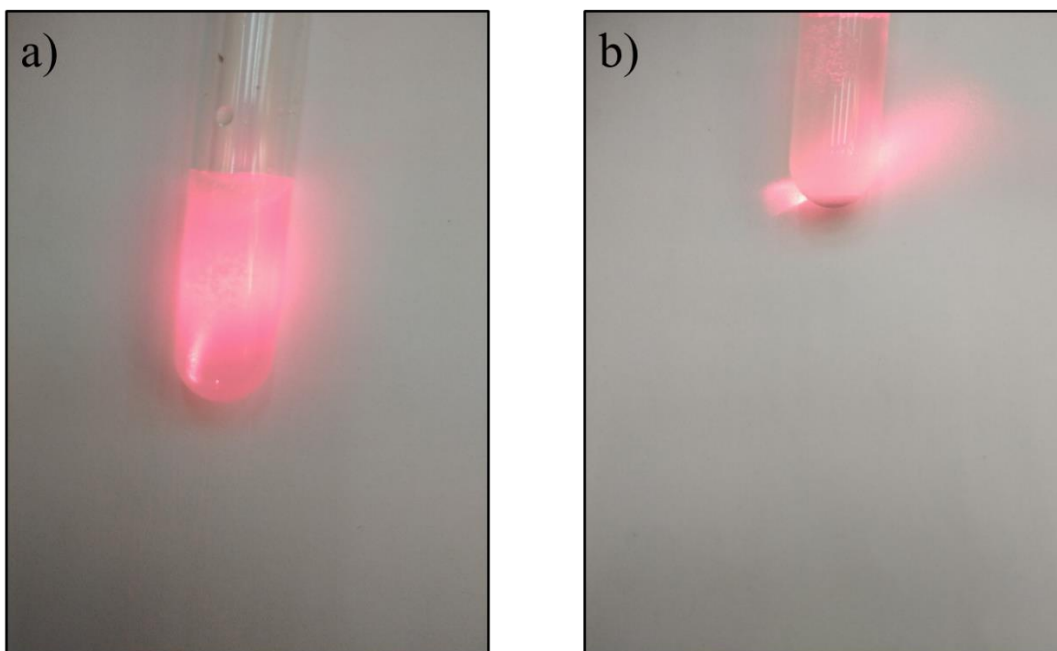


Figure III.3: Water+TiB₂; a) in few seconds and b) after 15 min

- **Ethanol + TiB₂ :**

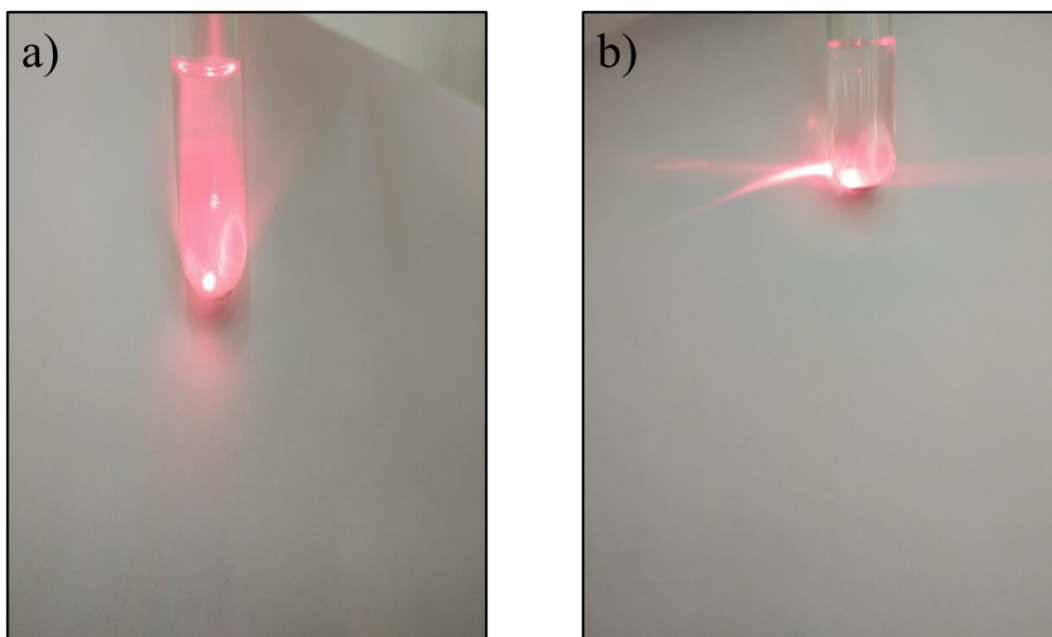


Figure III.4: Ethanol+TiB₂; a) in few seconds and b) after 15 min

- **After comparing mediums :**

After analyzing the results, it was evident that ethanol emerged as the optimal choice for our tests because the deposits performance were better of water, acetone, and propanol, demonstrating its effectiveness as a medium for spray coating.

III .4.Methods :

The lubrication test certainly is method we using it by two lubrications called:

III.4.1. Oil lubrication:

Oil lubrication is a widely used method for reducing friction and wear in mechanical systems. It involves the use of oil as a lubricant to create a thin film between moving surfaces, thereby reducing direct contact and allowing smoother operation.

Also oil lubrication generally systems are often employed to ensure a continuous supply of oil to the moving parts.

III.4.2. Dry lubrication:

Dry lubrication, also known as solid lubrication or dry film lubrication, is a method of reducing friction and wear between surfaces without the use of liquid lubricants such as oil or grease. Instead, a solid lubricant is applied in the form of a dry film coating.

Application Methods: Dry lubricants can be applied to surfaces through various methods, including spraying, drop casting, immersion, and immersion assisted by ultrasonation.

Benefits of Dry lubrication: offers several advantages, including resistance to high temperatures, reduced maintenance requirements, avoidance of contamination, and compatibility with certain environments.

III .5.Understanding steps by these methods:

First starting by the dry lubrication including by four methods that we worked by (spray coating; drop casting; immersion and immersion by ultrasonication):

III .5.1.Spray coating:

Is a widely used technique for applying thin films or coatings onto surfaces by making it a good and uniform and thickness coating on the surface. It involves the use of a spray gun or nozzle to disperse a coating material in the form of droplets, which are then directed onto the target surface. For example we use a Small perfume flask which is useful for our testing.

III .5.2.Drop casting:

Also known as drop deposition or drop coating, is a technique used to deposit liquid or dissolved materials onto a substrate by carefully placing or "dropping" the liquid droplets onto the surface. It is a simple and low-cost method commonly used for thin film deposition and coating processes.

Drop casting involves depositing small droplets of a liquid or dissolved material onto a solid substrate. The liquid is typically a solution or suspension containing the desired material to be deposited; also is good method that make a uniform and thickness coating.

III .5.3.immersion :

The immersion method typically refers to a technique or experimental approach that involves immersing a specimen, sample, or object in a specific medium or solution for analysis, testing, or processing purposes which is also a useful technique .

And here using immersion assisted by laboratory oven for Immersing an object or sample in a liquid or solution and subsequently subjecting it to controlled heating in a laboratory oven can aid in processes like curing, drying, or solidification of coating.

III .5.4.immersion assisted by ultrasonication :

Immersion assisted by ultrasonication; implies that the immersion process is enhanced or supported by the application of ultrasonic waves in the liquid medium. The ultrasonic waves provide additional benefits or effects during the immersion process, such as improved a good coating by Immersing an object in a liquid coating solution while applying ultrasonic waves can assist in achieving better coating uniformity, adhesion, or penetration into porous substrates.

III.6. Preparation coating of nanofilament derived from TiB₂ dry lubrication:

III .6.1.Spray coating:

- **first test:**

A 100Cr6 steel disk was used as substrate, whose surface was polished to mirror-like, Then sequentially ultrasonically cleaned in ethanol, shows in **figure (a)** and pre-heated to 60°C before the spray coating. in other hand the solution was prepared containing 15 mg of TiB₂ nanofilament re-dispersed in 10 ml of ethanol using this solution was applied using a simple sprayer for example a perfume bottle under room temperature which mixed ultrasonication for 10 min ; shows in **figure (b)**.

The Spray coating involved spraying a 30 cycles onto the prepared sample before and allowing it to dry for 120 seconds after each cycle; the first 15 cycles consisted of one spraying with near distance of (3-5) cm; while the last 15 cycles involved three sprays with a longer distance of (10-15) cm; the end of spray coating will let the sample out of laboratory oven make it dry more on the temperature room for 17 h.

As results of this process The TiB₂ nanofilament were staked tightly to the surface of 100 Cr6 steel disk; after 30 cycles a well coated surface was achieved shows in **figure (c)**.





Figure III.5: (a) sample ultrasonically cleaned in ethanol;(b)solution mixed in ultrasonication;(c)coating sample .

- **The second test:** used the same type of steel (100Cr6) disk and same method and measurement except while the spray coating involved a 30 cycles were consisted all with three sprays and longer distance of 20 cm .; The results of coating on the surface were also good .
- **third and fourth tests:** used the same type of steel (100Cr6) and method and measurement except the shape of steel were different as shows **in figure**.

While spray coating involved spraying a 30 cycles onto the prepared sample before and allowing it to dry for 120 seconds after each cycle consisted of three sprays with longer distance of 10 cm all cycles.

The results of coating as it shows **in figure (a and b)** were not achieved like the first test and second which looks that TiB_2 were not good stacked on the surface of steel .

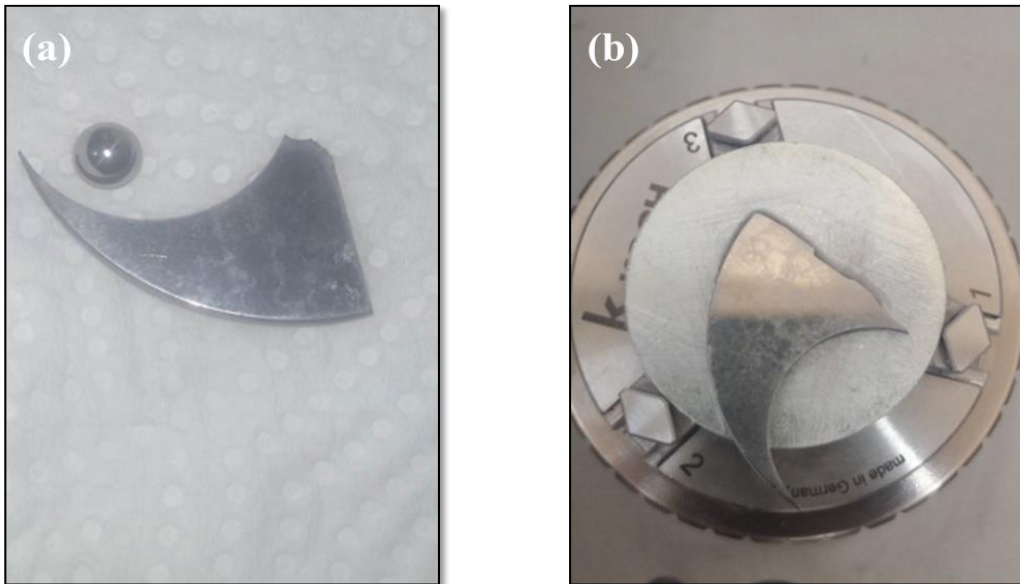


Figure III.6: coating tests of 100 Cr6 with different shape that aren't achieved

- **The fifth test:**

Before applying the spray coating, the steel 100 Cr6 was placed inside the laboratory oven at a temperature of 60 degrees for 23 minutes.

The same spraying method as the first test was used for the spray coating, and all; the tribology test were conducted on the same day. The coating results were good, as indicated by **the figure a and figure b with much more detail look.**

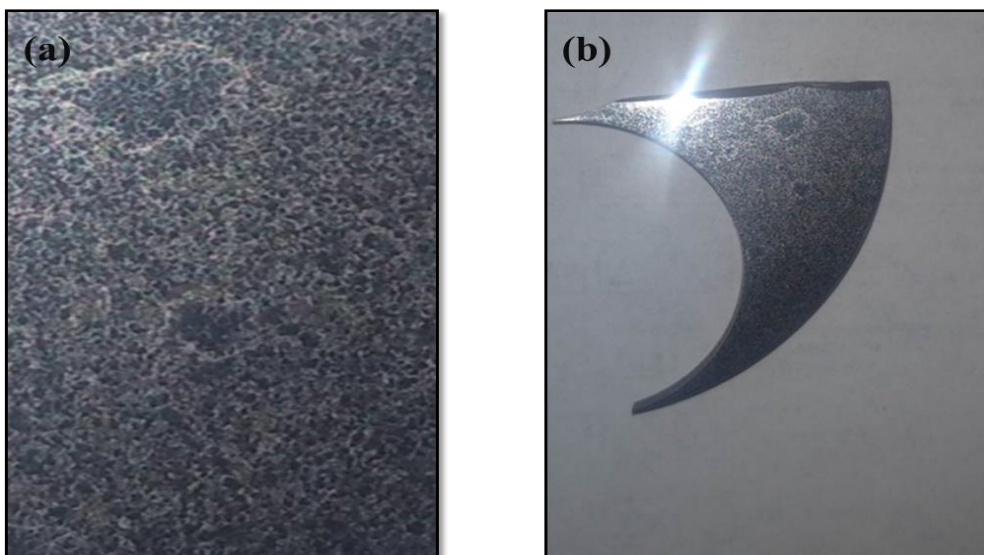


Figure III.7: The spray coating in the fifth test were achieved

- **The sixth test:**

The usual method was employed, using the same temperature and cycle parameters as the first test, and allowing it to dry more on the temperature room for 17 hours.

However, the desired coating results were not achieved on the surface of the 100 Cr6, as depicted in the figure.



Figure III.8: For the sixth test of spray coating are not achieved

- **Another test by:** stainless steel 430 C used it for spray coating and as usual did the same method like the first test.

The results of the coating of the surface stainless steel 430 C wasn't as same as the first test it shows **in the figure 36** before and after spray coating.



(a) before spray coating



(b) after spray coating



After spray coating with a , more detailed look

Figure III.9:(a) before spray coating , (b) after spray coating ; (c) coating surface with more detailed look

- **In another test:** we employed a different type of stainless steel known as 316 L. The preparation method was consistent with the previous tests, following the same procedure. However, the results of the coating appeared to be unsatisfactory, **as depicted in the figure III.10:**

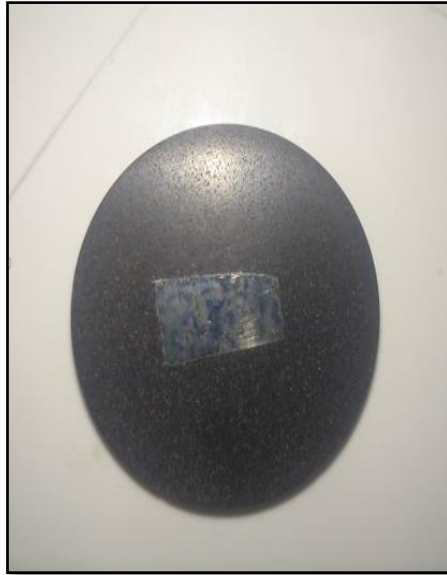


Figure III.10: a stainless steel 316L coating surface .

III .6.2.Test with drop casting:

Using the drop casting method, to determine the feasibility of the process. We prepared a stainless steel 430C substrate by polishing it and subjecting it to ultrasonication with ethanol for 5 minutes.

In the first step, we mixed 10 ml of ethanol with 15 mg of TiB_2 powder and subjected the mixture to ultrasonication for 10 minutes; then we loaded the prepared mixture into a syringe for application.

In the second step, the stainless steel 430C was heated to 70 degrees using a laboratory hot plate before initiating the application method. Using the pre-loaded syringe, we carefully applied 5 drops total of the mixture onto the substrate surface with distance 6 cm, with each drop being dispensed for 3 seconds. This process was repeated until a well-formed surface coating was observed.

- **The resulting figure (h) and (i) part of with demonstrates the successful achievement of a coating on the surface of the stainless steel 430C substrate; Figure III.11 :**

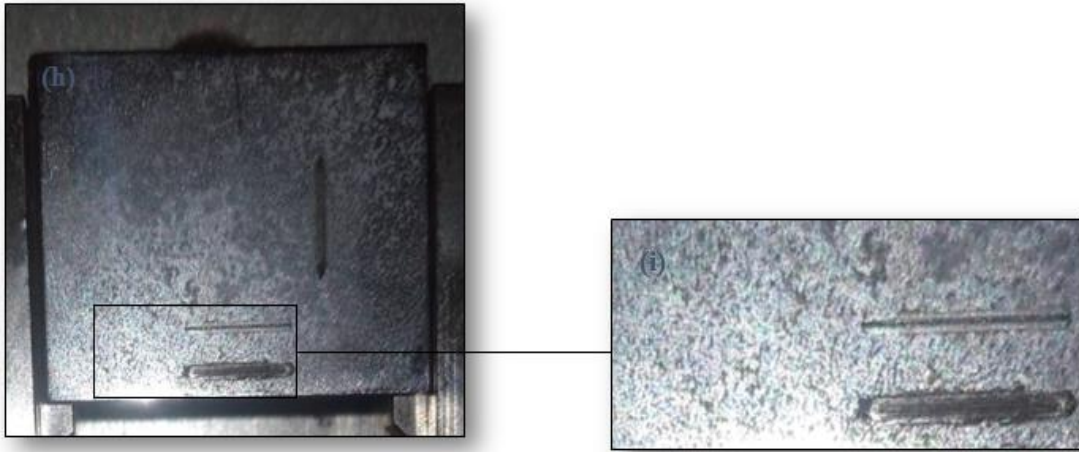


Figure III.11: coating surface of stainless steel 430C with drop casting succeed

- For another test, we followed the same method as the initial test, but this time we increased the concentration to 20 mL of ethanol combined with 30 mg of TiB_2 powder. The resulting coating is depicted in the **Figure III.12** below:

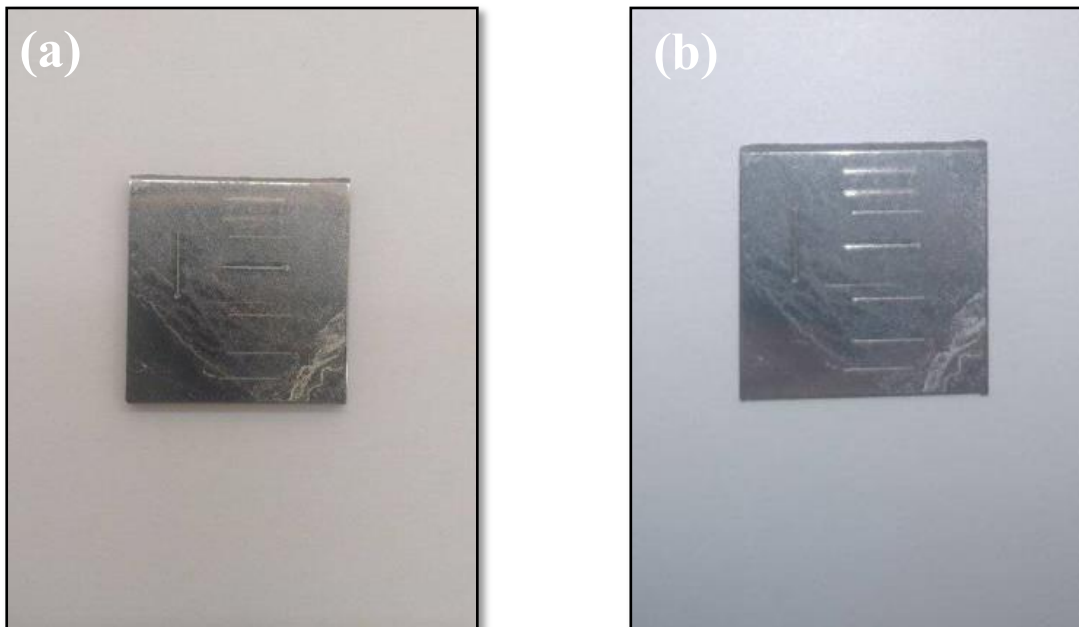


Figure III.12: coating surface of 430C with drop casting failed

III .6.3.Method the immersion assisted by ultrasonication:

The immersion-assisted ultrasonication method was employed for the testing process; In the first test, two different mediums, namely water and ethanol, were used The method involved preparing a solution of 7.5 mg of TiB_2 powder mixed with 5 ml of ethanol in a beaker. The stainless steel 430C specimen was then immersed in the solution and subjected to ultrasonication for 40 minutes at a temperature of 50 degrees, **as depicted in the figure III.13:**



Figure III.13: method of immersion the sample assisted by ultrasonication .

Subsequently, the ethanol was allowed to evaporate, revealing that the TiB_2 powder did not adhere properly to the surface of the 430C specimen, **as observed in the figure III.14:**



Figure III.14: coating results of the surface 430C

The second test utilized water as the medium. Similar to the first test, we employed the same concentration as before, preparing a solution by mixing the TiB_2 powder with water. The solution was then subjected to ultrasonication for 30 minutes at a temperature of 75 C degrees by immersion the stainless steel on the beaker, **as it shows in the figure :**



Figure III.15: solution subjected to ultrasonication

Following the ultrasonication process, the water wasn't good allowed to evaporate. Unfortunately, the results of the second test were unsuccessful.

III .6.4.method immersion by laboratory oven:

Two different mediums, water and ethanol, were used to evaluate the effect of multiple concentrations of the TiB_2 solution (7.5 mg, 5 mg, 2.5 mg, 1 mg) for both mediums:

- **Water:**

The experiment began by preparing a 5 ml solution of water and mixing it with 7.5 mg of TiB_2 powder. The resulting solution was then placed in a small beaker and subjected to heat in a laboratory oven at a temperature of 50 degrees Celsius. The process continued until all the water had evaporated, leaving the TiB_2 powder adhered to the surface of the 430C specimen, **as illustrated in the figure III.15 :**

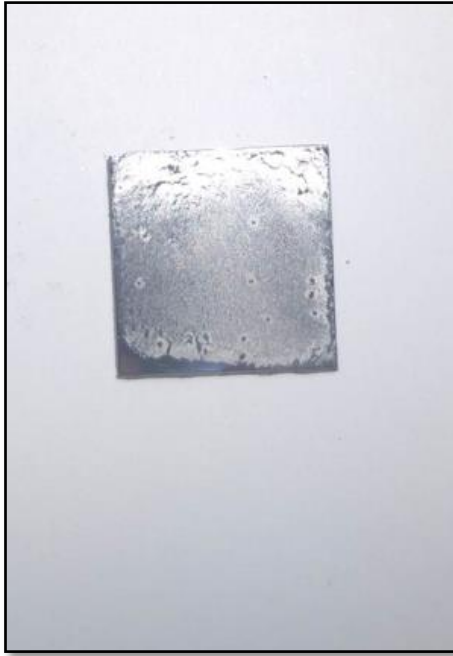


Figure III.16: coating surface with 7.5mg TiB_2 powder results by laboratory oven

Next, the experiment was repeated using a concentration of 5 mg of TiB_2 powder mixed with the same 5 ml of water. The solution was treated similarly, undergoing evaporation in the laboratory oven at 50 degrees; **the results of this experiment are illustrated in Figure III.16** :



Figure III.17: coating surface with 5mg of TiB_2 powder results by laboratory oven

Similarly, a concentration of 2.5 mg of TiB_2 powder mixed with 5 ml of water was tested. The solution underwent the same evaporation process, resulting of the coating outcome **captured in Figure:**



Figure III.18:coating surface with concentration 2.5mg of TiB_2

Finally, the experiment was conducted using a concentration of 1 mg of TiB_2 powder mixed with 5 ml of water. Following the evaporation step, the results were **documented in Figure :**



Figure III.19: coating surface with concentration 1 mg TiB_2 powder mixed with 5 ml of water

Using the identical method and TiB_2 powder concentration, we prepared solutions with the following concentrations: 5 mg, 2.5 mg, and 1 mg in 5 ml of water. However, we modified the temperature parameter to 75 C degrees. Subsequently, we observed the outcomes for each concentration, which are displayed in the order figures a; b and c:

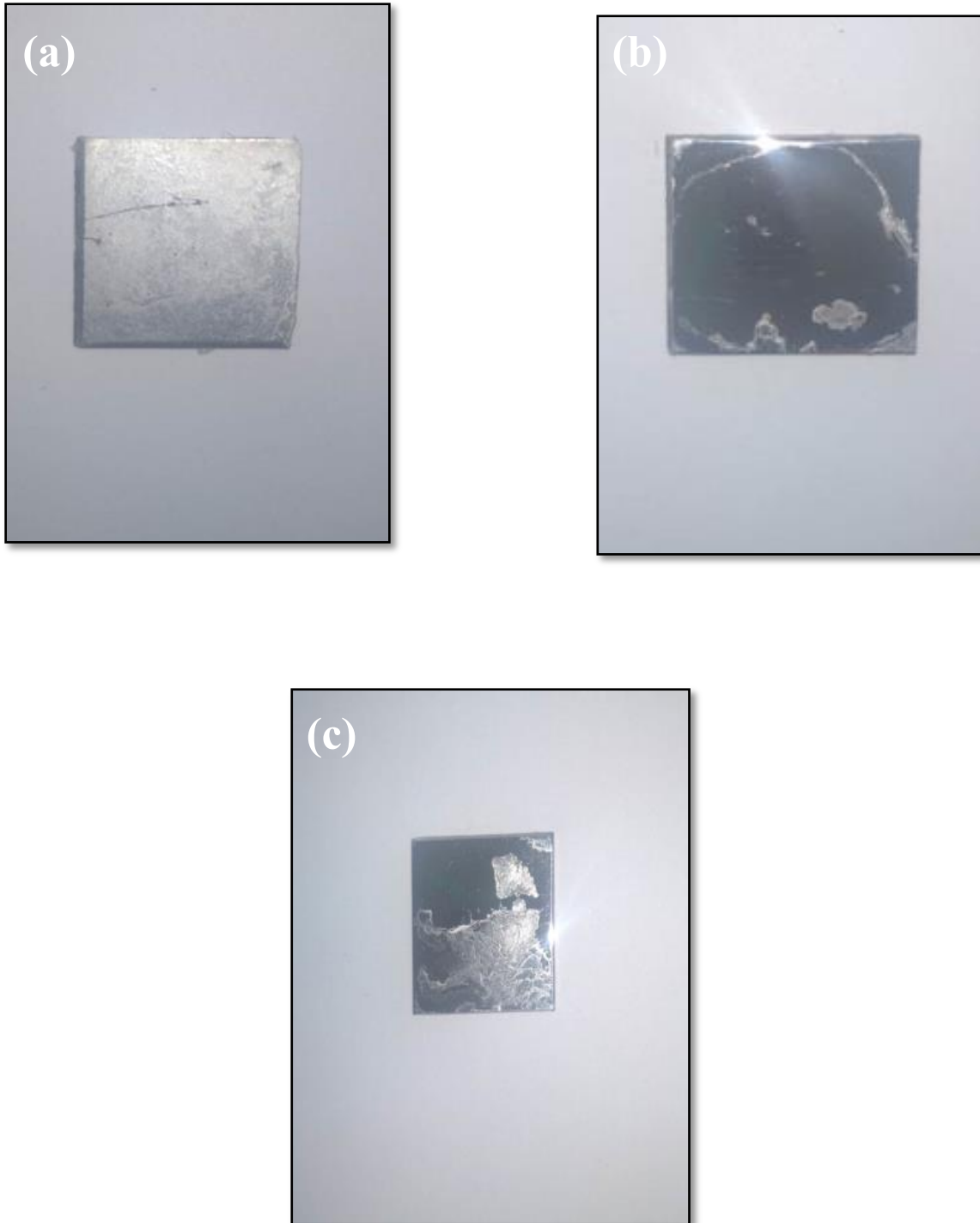


Figure III.20: different coating results with (a):5mg TiB_2 ;(b) 2.5mg TiB_2 ;(c)1mg TiB_2

- **Ethanol:**

Following our customary procedure, we prepared 5 mL of ethanol solution with varying concentrations of TiB₂ powder. The concentrations used were as follows:

7.5 mg, was then placed on a laboratory oven set at 50 C degrees to facilitate the evaporation of ethanol. The obtained results for each solution **concentration are in the figure below :**



Figure III.21: results of coating with 7.5mg concentration TiB₂ of ethanol

Oil lubrication:

Starting with an analytical balance, we measured the mass of the "test glass tube" along with 25 ml of paraffin oil, **as shown in Figure** ; the total mass was 20.06g:



Figure III.21: measured the mass of the "test glass tube"with oil paraffin

Next, we prepared various concentrations of TiB_2 powder (1%; 0.5%; 0.25%; 0.75%; 0.1%):
For the 0.5% concentration, we measured 0.156g of the powder, as depicted in Figure :



Figure III.22: TiB_2 misured

We then mixed it with the previously measured paraffin oil and placed it in a plastic tube to initiate our tests. The preparation method involved initially mixing the solution using a magnetic stirrer for 5 minutes.

Subsequently, we utilized a homogenizer to mix the solution for 2 minutes, repeated five times, while also employing ultrasonication for 2 minutes, repeated five times alternatively. Finally, we mixed the solution for an additional 5 minutes using the homogenizer to ensure thorough mixing, **as shown in Figure :**



Figure III.23: 0.5%TiB₂ solution with homogenization .

We then proceeded to conduct tribology tests for a duration of 2 hours and 45 min on our sample 100Cr6steel.

We did same method for the others concentrations 1%; 0.25%; 0.75%; 0.1% then produced for the test tribology for 2 hours and 45 minutes on the samples 100Cr6 steel.

On the other hand, we also evaluated another material known as Cr₂CTx 2D to compare its tribology test results with those of TiB₂ 2D. We followed the same method as in the first test, including the same concentrations of 0.5%, 0.25%, and 0.1%.

We initiated our experiment with a 0.25% concentration of Cr₂CTx 2D, equivalent to 0.0516g. To ensure thorough mixing, we combined the measured amount with paraffin oil and subjected

it to a magnetic stirrer for a duration of 5 minutes, **as illustrated in the accompanying figure** :



Figure III.24: 0.25%Cr₂CTx solution on magnetic stirrer

Subsequently, we followed the identical methodology employed in our initial approach for the TiB₂ testing, **as depicted in the figure below** :



Figure III.25: mixed the solution 0.25%Cr₂CTx on homogenization

After that preparing the same preparation to others concentration of 0.5% and 1 %.

Acid oleic:

In oil lubrication, acid oleic is commonly used as a lubricant additive due to its favorable properties. Acid oleic, also known as oleic acid, is a monounsaturated fatty acid that is derived from natural sources such as vegetable oils.

Lubricating properties: Acid oleic exhibits excellent lubricating properties, making it a desirable additive in oil lubrication. It forms a thin, protective film on metal surfaces, reducing friction and wear between moving parts.

Attempting to replicate the preparation method used for previous solutions, we aimed to create past solutions of TiB_2 with the addition of 2.7 ml of acid oleic. By following the same procedure as employed in previous experiments, we sought to assess the impact of acid oleic on the test results. The preparation process involved blending the desired quantities of TiB_2 with the predetermined amount of acid oleic. This mixture was subjected to rigorous mixing and homogenization to ensure thorough dispersion and uniformity. Subsequently, the resulting paste solutions were characterized and evaluated in our tests. Our objective in conducting these experiments was to investigate how the inclusion of acid oleic on these solutions we aimed to ascertain any notable differences or improvements in terms of factors such as lubricating efficiency, friction reduction, wear resistance, and corrosion inhibition.

III .6.5.generally laboratory materials are used :

1. polisher machine :



Figure III.26: polisher image

The specific polishing process and materials used depend on the type of object being polished. Common applications include polishing metals (such as stainless steel, aluminum, or brass) to remove scratches or oxidation, refining gemstones or jewelry, and smoothing the surfaces of wooden objects .

- **the ultrasonication :**



FigureIII.27: the ultrasonication image

Ultrasonication, also known as ultrasonic cleaning, is a process that utilizes high-frequency sound waves to clean and treat objects. It involves the use of an ultrasonic cleaning machine or ultrasonic bath that generates ultrasonic waves in a liquid medium.

- **magnetic stirrer:**

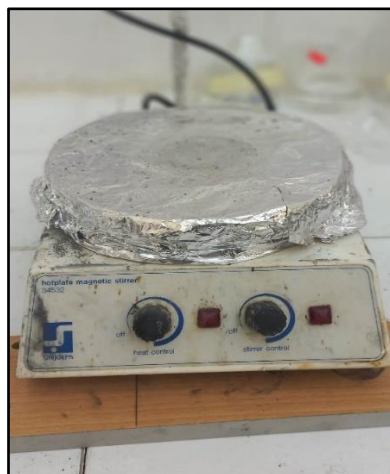


Figure III.28: magnetic stirrer image

A magnetic stirrer is a laboratory device used for stirring and mixing liquids. It consists of a rotating magnetic field generated by a magnetic stir bar or flea, usually made of Teflon-coated magnetic material, placed within the liquid to be stirred. The magnetic stir bar is driven by a magnetic stirrer plate or hot plate, which contains an electromagnet that produces the rotating magnetic field.

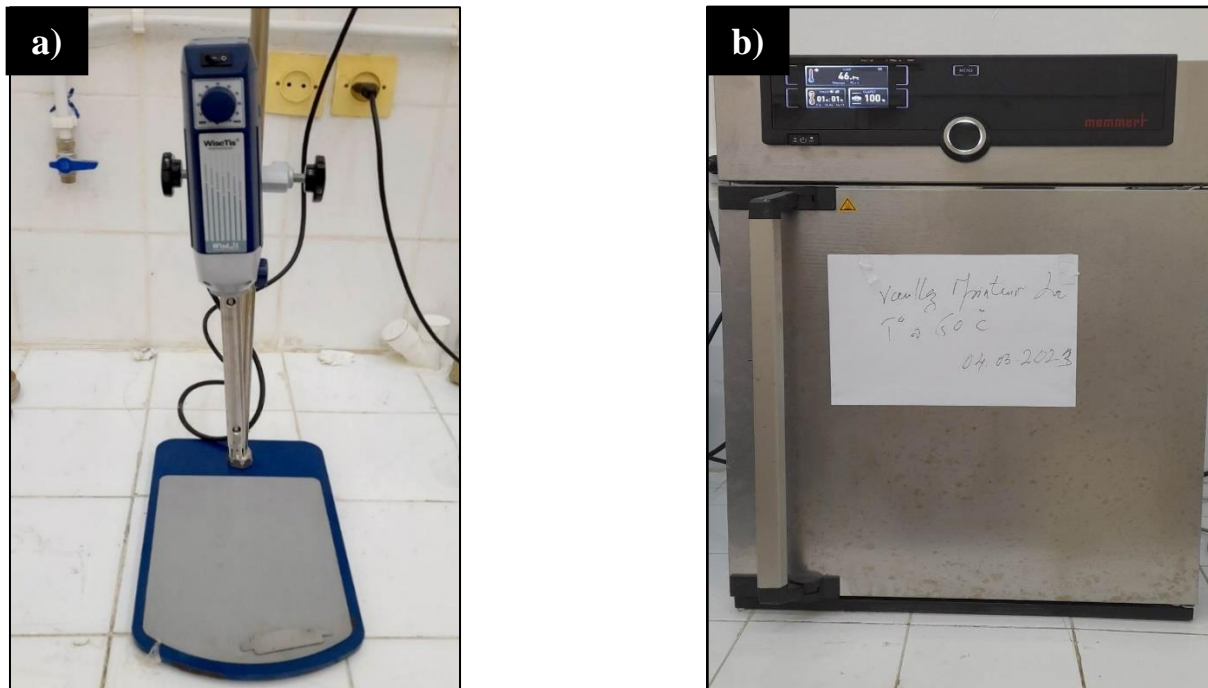


Figure III.29: (a) homogenization image ; (b) laboratory oven

- Homogenization, also known as homogenizing or homogenization process, is a technique used to make a mixture or solution uniform and consistent in composition. It is commonly applied to emulsions or suspensions containing two or more immiscible substances, such as oil and water, where the goal is to achieve a stable and homogeneous mixture.
- laboratory oven A laboratory oven, also known as an industrial oven or scientific oven, is a specialized piece of equipment used in laboratories and research facilities for heating, drying, sterilizing, or performing various other thermal processes on samples or materials.

- oil paraffin :



Figure III.30:oil paraffin image

Paraffin oil can act as a lubricant in laboratory equipment and instruments where a non-reactive, non-volatile, and non-toxic lubricant is needed. It can be used to reduce friction and facilitate smooth movement in various mechanical components, such as sliding joints, rotating parts, or piston systems. Cleaning and Disinfection: Ethanol is an effective cleaning agent and disinfectant. It is commonly used to clean laboratory glassware, surfaces, and equipment.

- ethanol :

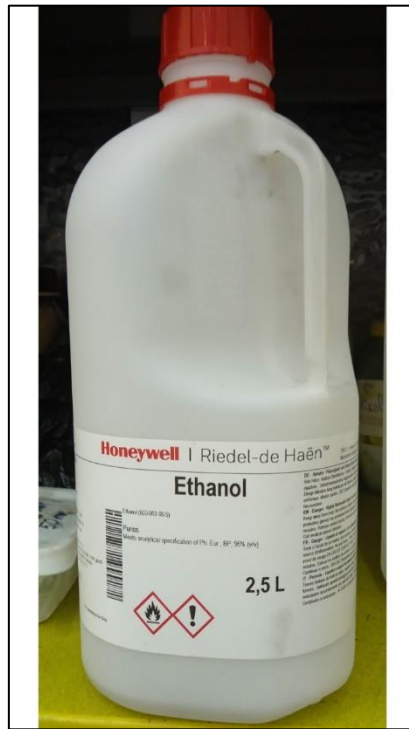


Figure III.31:ethanol image

Ethanol, also known as ethyl alcohol or grain alcohol, is a volatile and colorless liquid compound. It is the principal type of alcohol found in alcoholic beverages and is commonly used in various laboratory applications also using for Cleaning and Sanitization.



Figure III.32: a)tribometry images; b) optical microscope

- An optical microscope, known as a light microscope or compound microscope, is a widely used instrument that utilizes visible light and a system of lenses to magnify and observe small samples or objects.

- Tribometry is a scientific field that deals with the measurement and study of friction and wear properties of materials. It focuses on understanding the interactions between surfaces in contact and the forces involved in relative motion or resistance to motion. The word "tribometry" is derived from the Greek word "tribos," meaning rubbing or friction. Tribometry encompasses various techniques and methods used to evaluate friction, lubrication, and wear characteristics of materials. These measurements are crucial in fields such as engineering, materials science, manufacturing, and product development.

Chapter IV

Results and discussion

IV.1 Introduction:

In this chapter, we present and discuss the results obtained from the experimental investigation involving these new materials nanofilaments (NFS) titanium carbo-oxides derived from TiB_2 by TMAOH as solid lubricants in spray coating and oil lubrication as well as Cr_2CT_x in oil lubrication applications. The main objective of this study was to evaluate the performance and effectiveness of nfs from TiB_2 and Cr_2CT_x in reducing friction and wear in different lubrication conditions. The obtained results offer valuable insights into the tribological behavior and lubricating properties of TiB_2 in both spray coating and oil lubrication as well as Cr_2CT_x in oil lubrication.

This chapter followed by a detailed presentation and discussion of the key findings and their implications. Furthermore, we compare the results obtained from the spray coating experiments with the others relevant experimental approaches while also comparing the TiB_2 and Cr_2CT_x oil lubrication experiments.

By examining and comparing these results, we aim to gain a deeper understanding of the performance and potential applications of nanofilaments titanium carbo-oxides derived from TiB_2 BY TMAOH and Cr_2CT_x as solid lubricants.

IV .2 Spray coating results:

IV .2 .1 the first and second test results:

Summary: Martensitic 100Cr6 samples with a 62 HRC hardness were coated by 1D nanofilaments titanium carbo-oxides derived from TiB_2 by TMAOH.

Wear tests: sliding speed: 10cm/s, load: 1 and 2N, radius: 5mm, rotating ball on disk mode, 6mm hardened 100Cr6 ball; the humidity: 52%; the followings are the results:

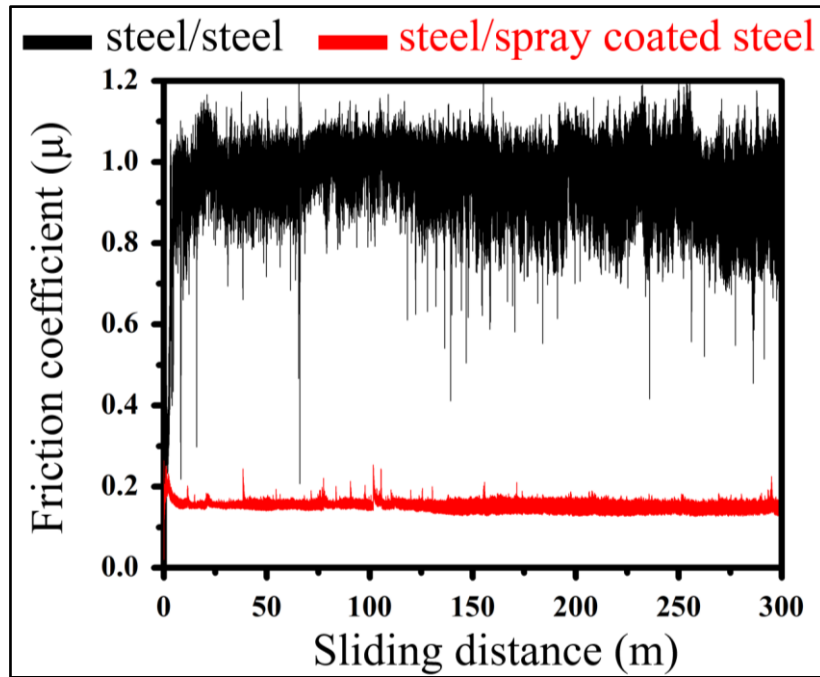


Fig. IV .1 Friction coefficient variation versus sliding distance. 1N load.

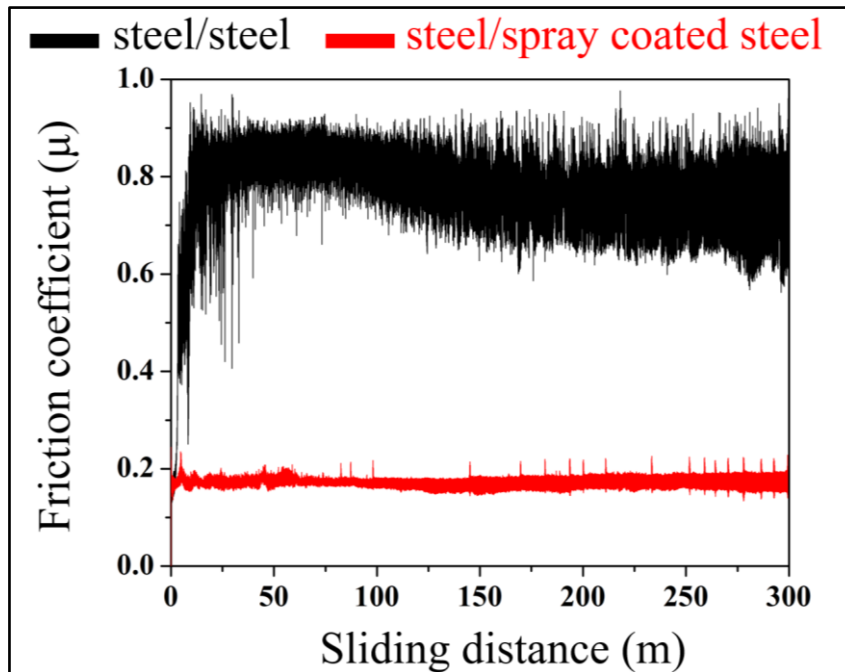


Fig. IV .2 Friction coefficient variation versus sliding distance. 2N load.

IV .2 .2 Discusses the results of tribological testing:

The tribological testing behavior of coated samples with nanofilament derived from TiB_2 dimensional coating is to explore effects of it during the friction and wear process; the two

models were experimental first one steel ball against steel and the second steel ball against TiB₂ nanofilament spray coated steel.

The fig .1 and the fig.2 shows the friction coefficient of the two models under the load 1N and 2N the initial coefficient for the steel ball against steel was low then increases rapidly to reaches the value about (1.1-1.2) load **1N and** more then (0.9) load **2N** until the end of test .

The COF for the test of steel ball against nanofilament derived from TiB₂ coatings steel decreases 0.15 and 0.18 under the load of **1N** and **2N** respectively.

By comparing between these two models it shows the effect of TiB₂ nanofilament presence which means it has excellent and favorable lubricant effects. It effectively reduces the friction coefficient, resulting in smoother sliding between the steel ball and the coated surface. This finding highlights the potential of TiB₂ nanofilament coatings as a means to improve lubrication and reduce friction in various applications

Remarque: the others tests of spray coating did fell because of high humidity wish was more then 60%.

IV .2 .3 optical microscope as part of investigation:

Microscope optical tests were conducted to examine the surfaces of the steel ball against steel and the steel ball against nanofilament derived from TiB₂ coatings on steel under loads of 1N and 2N. **The figures below illustrate the results of these tests**, providing insights into the condition of the surfaces and any changes that may have occurred during the friction test.

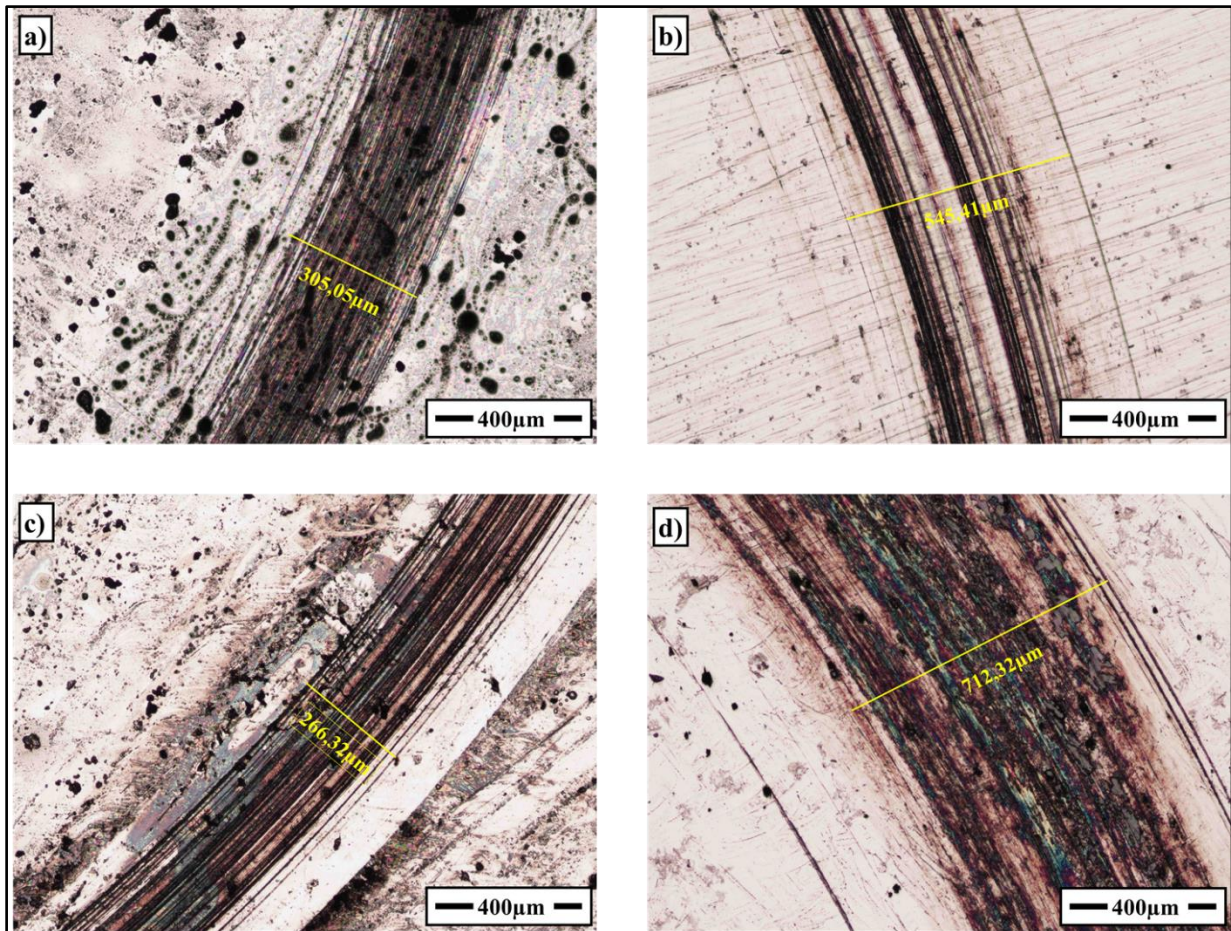


Figure IV .3 (a) and (c) show the surfaces of the steel ball against nanofilament derived from TiB_2 coating under loads of 1N and 2N, respectively. On the other hand, (b) and (d) depict the surfaces of the steel ball against steel under loads of 1N and 2N, respectively.

IV .2.4 discusses the results:

In Figure (a), the wear track measurement with coating at (a) load of 1N was 305.05um, significantly lower than the wear track measurement without coating in Figure (b), which was 545.41um. Similarly, in Figure c, the wear track measurement with coating at a load of 2N was 206.32um, again substantially lower than the wear track measurement without coating in Figure (d), which was 712.32um.

The significant difference in wear track measurements between the coated and non-coated samples can be attributed to the protective properties of the coating. When the coating is present, it forms a barrier between the steel ball and the surface, acting as a lubricant and reducing direct contact between the materials. This protective layer minimizes friction and wear, resulting in a lower wear track measurement.

IV. 3 Oil lubrication:

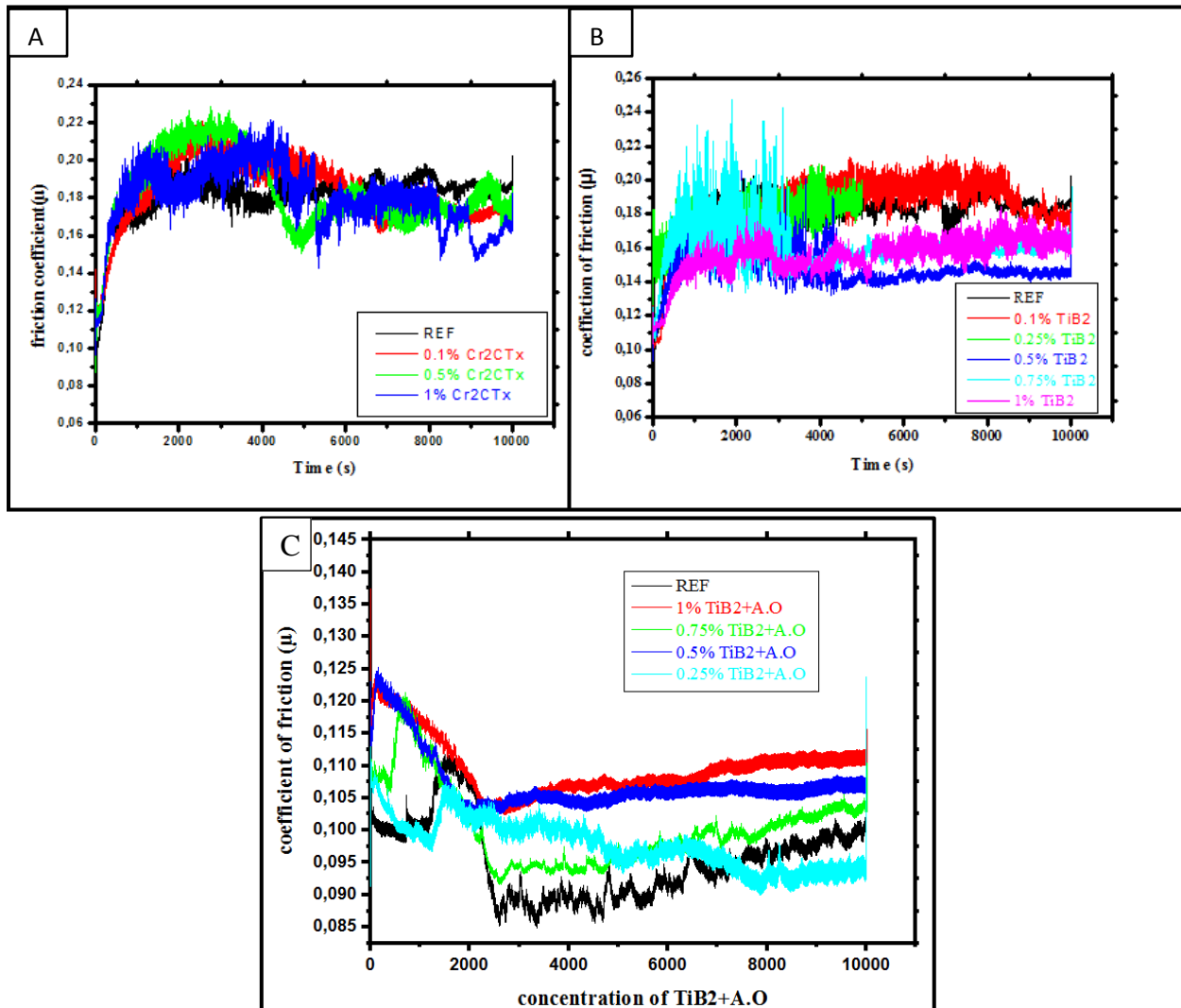


Figure IV .4 Friction coefficient variation versus time of (A) Cr₂CTx%; (B) TiB₂% and C % of acid oleic (A.O) + TiB₂

It shows the different coefficient between concentration of Cr₂CTx 2D and nanofilament TiB₂ dimensional in oil lubrication tests.

IV .3.1 discusses the tribological tests:

Tribological study conducted on as-prepared samples under a load of 20N, using different concentrations of Cr₂CTx and nano filament TiB₂ dispersed in oil paraffin.; For the reference samples of both materials, the CoF was initially 0.20. In the case of the 0.1% concentration of Cr₂CTx, the CoF decreased from 0.2 at 1500s to 0.17 at 6000s and remained constant until the end of the test. On the other hand, for the 0.1% concentration of TiB₂, the CoF remained constant at 0.2 from 2500s to 9000s and then decreased to 0.17. For the 0.5% concentration of Cr₂CTx, the CoF increased to 0.22 initially and then decreased to 0.15 at 5000s. It was then fixed at 0.17 until the end of the test. In contrast, for the 0.5% concentration of TiB₂, the CoF increased from 0.16 to 0.17 and remained constant at that level until the end of the test. For the

1% concentration of Cr₂CTx, the CoF initially increased to 0.22 and then decreased to a range between 0.16 and 0.17 towards the end of the test. As for the 1% concentration of TiB₂, the COF started at 0.16 and increased to 0.17 by the end of the test. Both of two materials shows a better results generally versus of the reference.

Also by comparing between this two materials the Concentration Effect of both Cr₂CTx and TiB₂ influenced the coefficient of friction (COF); higher concentrations of Cr₂CTx generally resulted in higher initial COF values, whereas TiB₂ showed a more stable COF across different concentrations.

And as it shows in figure C it looks the tribological tests has better results of TiB₂+A.O.

IV .3.2 microscope optical results:

Microscope optical tests were to figure out the wear track both of these new materials Cr₂CTx 2D and nfs derived from TiB₂ dimensional and comparison between them, and the figures below shows the wear track concentrations of both new materials versus reference sample:

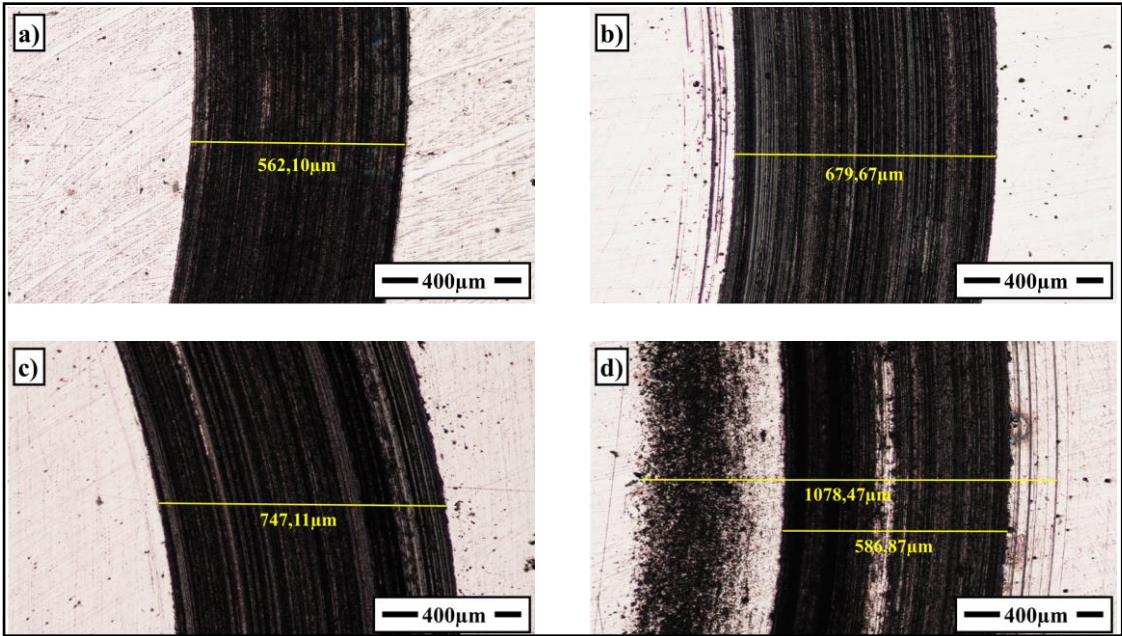


Figure IV .5 Microscope optical of Cr₂CTx 2D in multiple concentrations; (a) reference sample; (b) 0.1%Cr₂CTx; (c) 0.5%Cr₂CTx; (d) 1%Cr₂CTx.

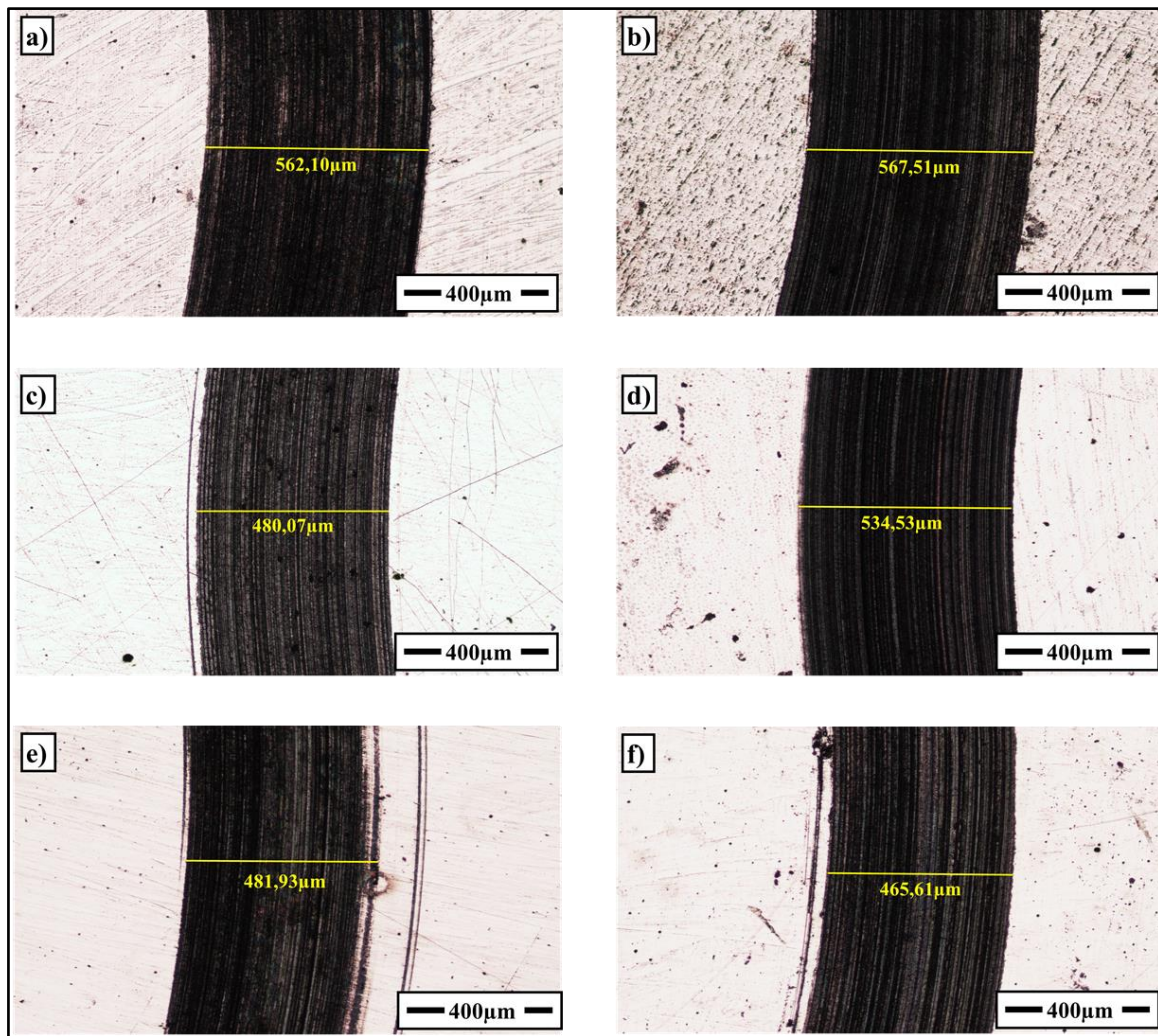


Figure IV .6 Microscope optical of nfs derived from TiB_2 in multiple concentrations; (a) reference sample; (b) 0.1% nfs from TiB_2 ; (c) 0.25%: (d) 0.5% nfs from TiB_2 ; (e) 0.75% nfs from TiB_2 ; (f) 1% nfs from TiB_2 .

IV .3.3 discusses the results:

Based on the microscopic optical results, it is evident that the wear track of the Cr_2CTx 2D material was significantly higher compared to the reference sample (a). The figures clearly demonstrate that as the concentrations of Cr_2CTx 2D increased, the wear track also increased. For instance, when the concentration was at 1%, the wear track reached 1078 um, whereas the reference sample had a wear track of only 562.10 um. This observation suggests that higher concentrations of Cr_2CTx 2D material lead to a substantial increase in wear track. The wear track is a measure of the material loss due to friction and wear, indicating the deterioration of the surface. In this case, the higher wear track values indicate that the Cr_2CTx 2D material is more prone to wear and is less resistant to friction compared to the reference sample.

The results observed in TiB₂ nfs material present an opposite trend compared to the Cr₂CTx 2D material. In the case of TiB₂ nfs, as the concentration of the material increases, the wear rate actually decreases. This can be seen from the figures, where at a concentration of 1%, the wear rate is significantly lower at 465.61 um compared to the reference sample's wear track of 562.10 um. This indicates that higher concentrations of TiB₂ nfs material lead to improved wear resistance. As the concentration increases, the material exhibits a higher ability to withstand friction and wear, resulting in reduced material loss and a lower wear track.

By comparing this two results it shows that nfs TiB₂ Lubrication Effect means the presence of TiB₂ nfs particles in the material may introduce lubrication properties, reducing friction and wear between the sliding surfaces. This lubrication effect can contribute to the lower wear track observed.

The Cr₂CTx 2D material may possess properties, such as lower hardness or poor adhesion strength, which make it more susceptible to wear and friction. These properties can result in accelerated material loss and higher wear rates.

Also it may the possibilities why the wear track of Cr₂CTx get high more when the concentration of it get high:

In 2014, Yang et al. conducted a study on the use of MXene, specifically 2D Ti₃C₂, as an additive in paraffin base oil for liquid lubrication. They prepared the 2D Ti₃C₂ by HF etching and ultra-sonication, and then dispersed it in liquid paraffin through ultrasonic vibration to create suspensions with varying mass fractions. Their findings, illustrated in Figure 9a, demonstrated that the addition of 2D Ti₃C₂ significantly improved the friction reduction and anti-wear properties of the paraffin base oil, particularly at a 1.0 wt% Ti₃C₂ concentration. The researchers also analyzed the effect of applied load on the coefficient of friction (COF)., the COFs exhibited a slight increase when the load was raised from 8 to 20 N, indicating the formation of oil films under relatively low loads. However, at higher applied loads (20 N–30 N), the COFs remained constant due to the formation of a Ti₃C₂ lubricant film.

The dispersibility of additives in lubricants plays a crucial role in determining their tribological properties. MXenes have hydrophilic groups distributed on their surfaces, which hinders their dispersibility and stability in oil-based lubricants. However, these hydrophilic surface functional groups of MXenes can serve as anchor points for surface engineering. To address this issue, surface modification techniques have been employed as an effective approach to enhance the dispersibility of MXenes in oil.

Huang and colleagues conducted a study where they grafted tetradecylphosphonic acid (TDPA) onto the surface of 2D Ti₃C₂ through a condensation reaction. This process resulted in the formation of TDPA-Ti₃C₂ nanosheets with a high grafting density. The TDPA-Ti₃C₂ nanosheets demonstrated improved dispersibility and stability in castor oil and could be stored for 7 days without significant degradation. The researchers further investigated the tribological performance of TDPA-Ti₃C₂ in castor oil at various concentrations. As expected, the modified TDPA-Ti₃C₂ exhibited superior tribological properties compared to unmodified Ti₃C₂. When using a concentration of 0.1 wt% TDPA-Ti₃C₂, the coefficient of friction (COF) was reduced by 27.9%, and the wear rate decreased by 55.1%. These improvements in tribological properties can be attributed to the formation of a uniform TDPA-Ti₃C₂ film during the friction process. This film acts as a protective layer, preventing direct contact between the friction pairs and reducing friction and wear. So this condition it may including the new material Cr₂CTx 2D specially it is a nature Mxene, To overcome the researches still challenge, ongoing efforts are focused on modifying the surface chemistry of MXenes.

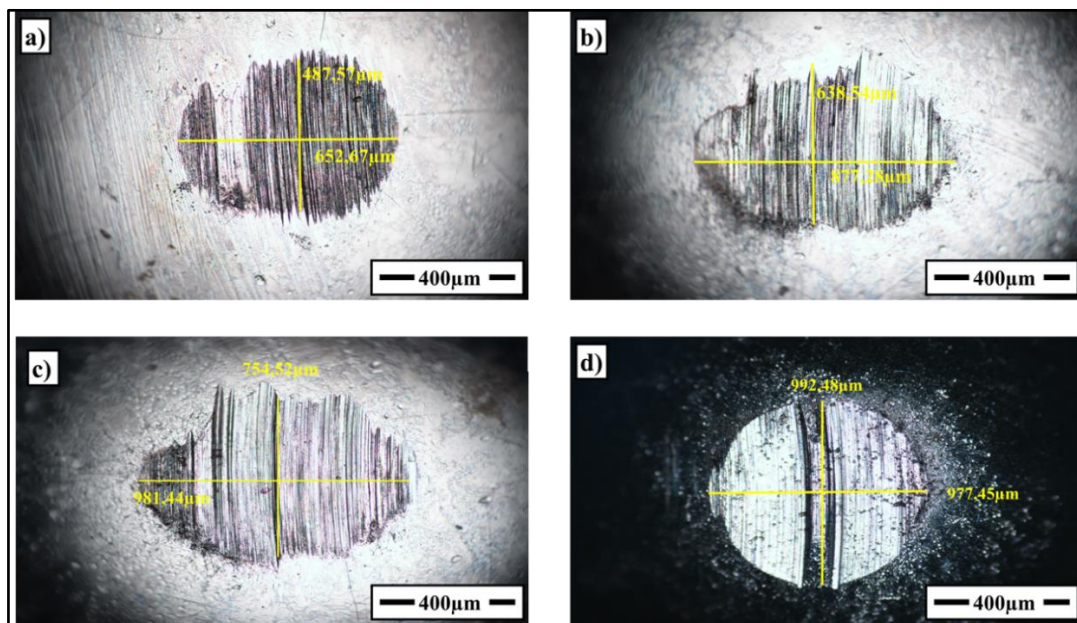


Figure IV.7 Microscope optical of balls Cr₂CTx; (a) sample REF; (b) 0.1% Cr₂CTx; (c) 0.5% Cr₂CTx; (d) 1% Cr₂CTx.

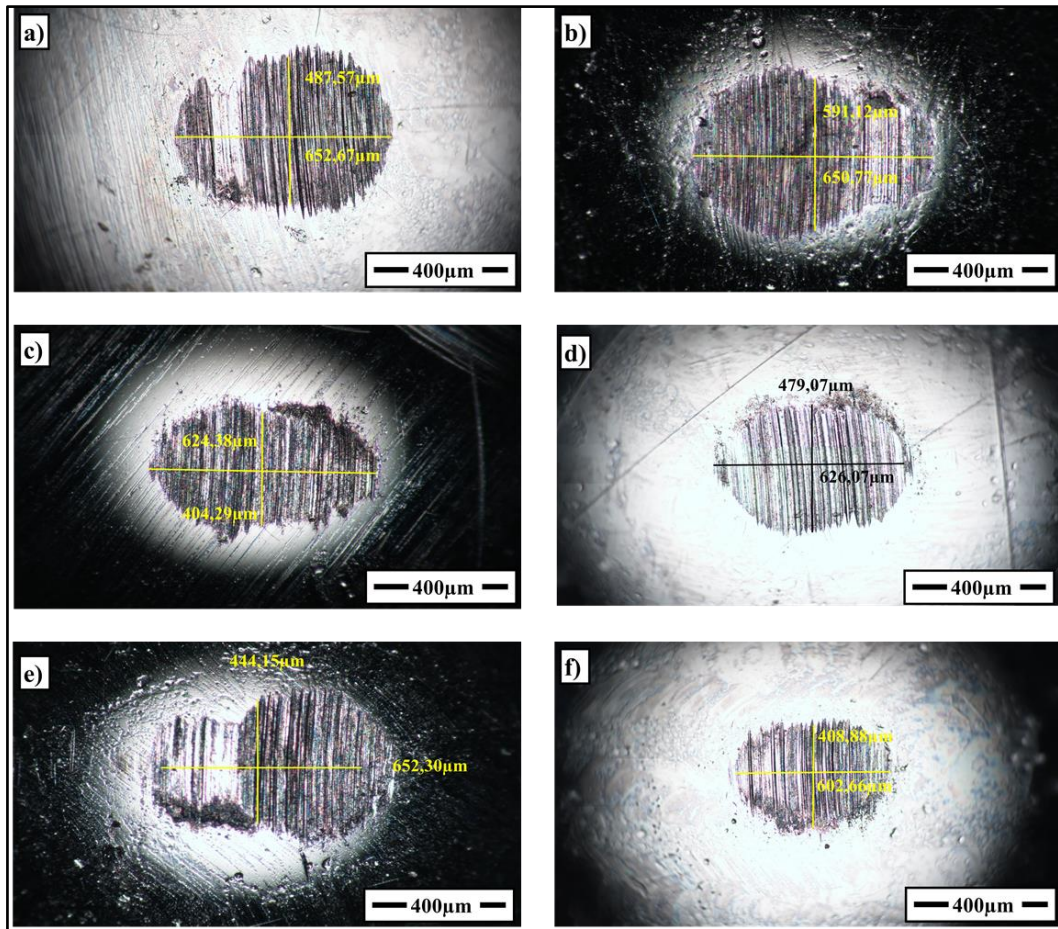


Figure IV .8 Microscope optical balls of TiB2 (a) sample ref; (b) 0.1% TiB2; (c) 0.25% TiB2; (d) 0.5% TiB2; (e) 0.75% TiB2; (f) 1% TiB2.

According to figures IV.7 and IV.8, it is evident that TiB2 exhibits better wear resistance than Cr2CTx. For instance, in figures (d) and (e), the wear tracks of TiB2 were noticeably smaller compared to the reference sample shown in figure (a). Conversely, the wear tracks of Cr2CTx were significantly larger compared to the reference sample a.

IV .3.4 different concentration between TiB2 and Cr2CTx:

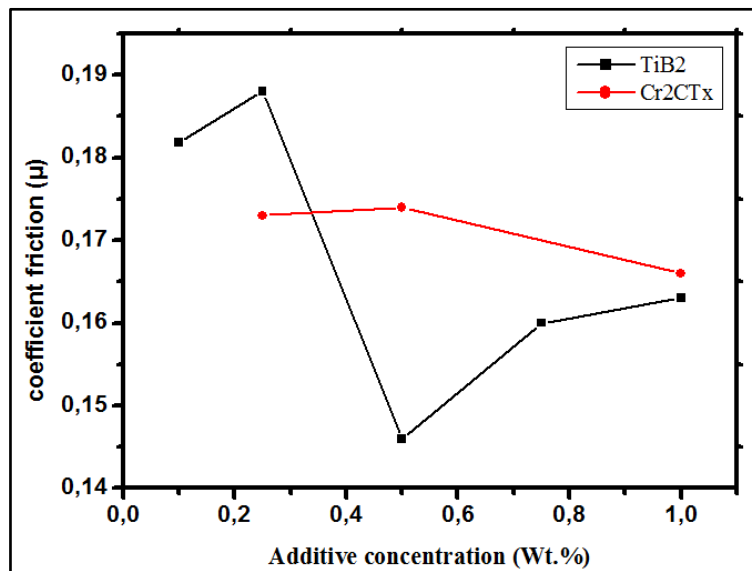
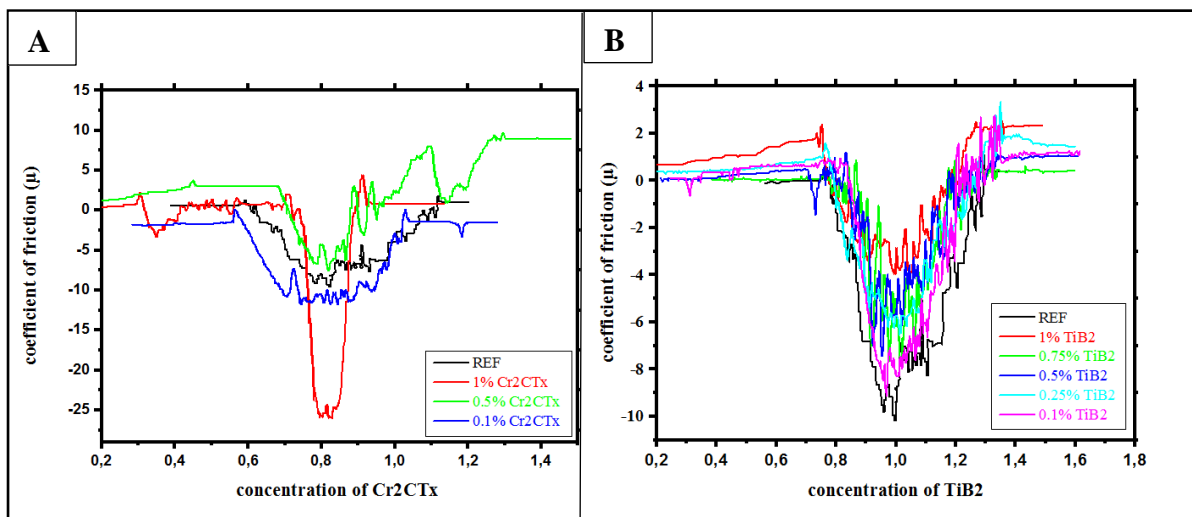


Figure IV. 9 The coefficient friction (μ) versus additive concentration (Wt. %) between TiB2; cr₂ctx

IV .4 the wear rate tests: Let's now proceed to analyze the graph, which presents the coefficient of friction plotted against the concentration of both materials. This graph will provide us with valuable insights into how changes in concentration impact the frictional behavior and, consequently, the wear rate of the materials.



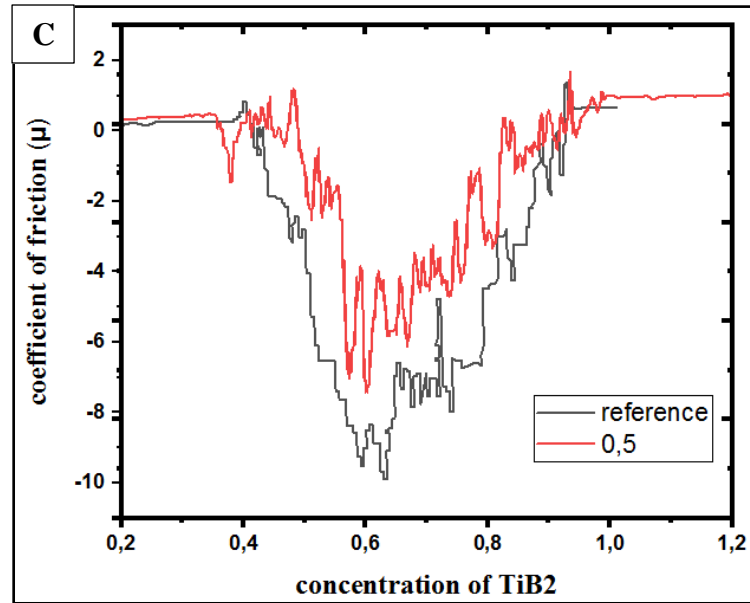


Figure IV. 10 Coefficient friction versus concentration both of (A) Cr₂Ctx % and (B) TiB₂ also (c) concentration 0.5 % TiB₂ of the wear rate test.

IV .5 calculate different wear rate:

We calculate the wear rate by this rule: $WR = \text{mm}^3 / \text{Nm}$

S: track area (mm²) R: radius (m): constant F: charge (N) d: distance (m).

To show the different between of wear rates for different concentrations of TiB₂, Cr₂CTx, and TiB₂+A.O represent in the table:

Concentrations	The wear rate (mm ³ /N.m)		
	TiB2	Cr2CTx	TiB2+A.O
REF	4.7×10^{-6}	4.7×10^{-6}	5.1×10^{-7}
1%	3.75×10^{-6}	4.95×10^{-6}	9.5×10^{-7}
0.75%	2.25×10^{-6}		8.5×10^{-7}
0.5%	1.12×10^{-6}	5.35×10^{-6}	6.65×10^{-7}
0.25%	2.84×10^{-6}	5.43×10^{-6}	
0.1%	3.8×10^{-6}		6.5×10^{-7}

Table 1: the wear rate in different concentration of materials.

In this table, "Concentrations" represents the different concentrations of TiB₂, Cr₂CTx, and TiB₂+A.O (acid oleic) being tested. The wear rates are calculated:

- At a concentration of 1%, TiB₂ has a wear rate of 3.75×10^{-6} mm²/N.m, while Cr₂CTx has a higher wear rate of 4.95×10^{-6} mm²/N.m, suggesting that TiB₂ performs better in terms of wear resistance at this concentration.
- At a concentration of 0.75%, TiB₂ has a wear rate of 2.25×10^{-6} mm²/N.m, while there. TiB₂+A.O has a wear rate of 8.5×10^{-7} mm²/N.m, indicating improved wear resistance compared to the reference concentration.
- At a concentration of 0.5%, TiB₂ shows the lowest wear rate of 1.12×10^{-6} mm²/N.m, while Cr₂CTx has a higher wear rate of 5.35×10^{-6} mm²/N.m. TiB₂+A.O has a wear rate of 6.65×10^{-7} mm²/N.m, suggesting enhanced wear resistance compared to the reference concentration.
- At a concentration of 0.25%, both TiB₂ and Cr₂CTx exhibit higher wear rates compared to the reference concentration.
- At a concentration of 0.1%, TiB₂ has a wear rate of 3.8×10^{-6} mm²/N.m, while there. TiB₂+A.O has a wear rate of 6.5×10^{-7} mm²/N.m, indicating improved wear resistance compared to the reference concentration; etc.

the table highlights the variations in wear rates among different concentrations of TiB₂, Cr₂CTx, and TiB₂+A.O. TiB₂ generally exhibits better wear resistance compared to Cr₂CTx, and the acid oleic improves the wear resistance of TiB₂.

Here the graph shows the wear rate calculated for concentrations of new materials:

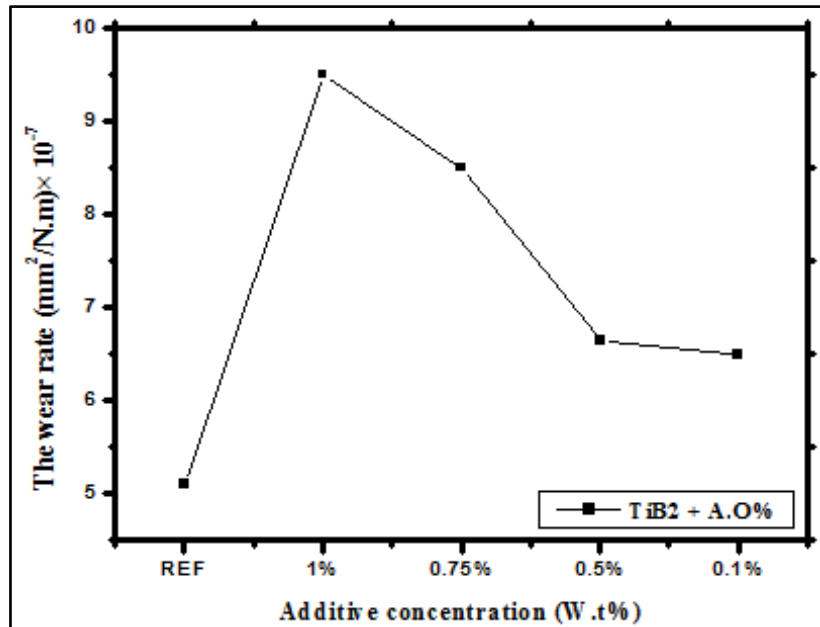


Figure IV .11 The wear rate (mm²/N.m) × 10⁻⁷ calculated versus additive concentration W.t% of TiB₂+Acid oleic (A.O).

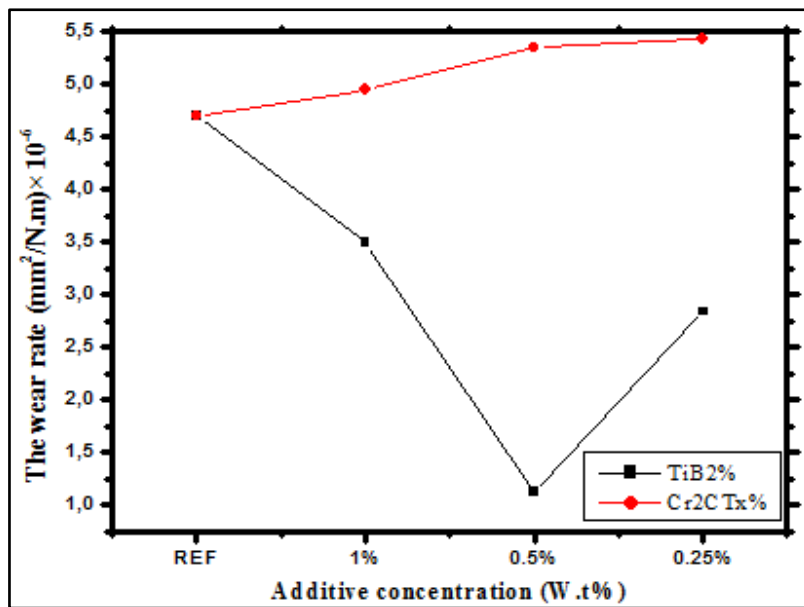


Figure IV .12 the wear rate (mm²/N.m) × 10⁻⁷ calculated versus additive concentration W.t% between TiB₂ and Cr₂CTx.

CONCLUSION GENERAL:

The objective of this work was to investigate the tribological behavior and lubricating properties of nanofilaments titanium carbo-oxides derived from TiB_2 as solid lubricants in spray coating and oil lubrication also Cr_2CTx in oil lubrication applications. Through experimental testing, is to find out the evaluate of their effectiveness in reducing friction and wear between sliding surfaces or are they promising materials or not the results discusses:

In spray coating showed that the presence of TiB_2 nanofilament coatings effectively reduced the friction coefficient and wear in comparison to the steel ball against steel model. The TiB_2 nanofilament coatings acted as a lubricant, forming a protective layer between the steel ball and the coated surface, resulting in smoother sliding and improved lubrication.

In the oil lubrication; the comparison between TiB_2 and Cr_2CTx indicated that the nfs TiB_2 exhibited better lubrication effects, reducing friction and wear between sliding surfaces. The TiB_2 nfs particles introduced lubrication properties, contributing to the lower wear rate observed. In contrast, the Cr_2CTx 2D material showed higher wear rates, possibly due to its lower hardness or poor adhesion strength.

The TiB_2 coatings showed excellent lubricating properties and wear resistance, while the Cr_2CTx material requires further improvement to enhance its lubrication and friction-reducing performance.

References:

- [1] Arun kumar, s., Ram sevak, s., & Anar singh. (2023). EMERGING TWO DIMENSIONAL MATERIALS AND APPLICATIONS . Material science and engennering .
- [2] Lu, X. K.; Yu, M. F.; Huang, H.; Ruoff, R. S. *Nanotechnology* 1999,10, 269
- [3] Athanasios Dimoulas, Alessandro, M., & Michel, H. (2016). 2D materials for nanoelectrones. *science in materials and engeneering*.
- [4] Bin, L., Gang, L., & Lianzhou, W. (2016). Recent advances in 2D materials for photocatalysis. *Nanoscale*, 17.
- [5] Krätschmer, W., Lamb, L. D., Fostiropoulos, K. & Huffman, D. R. *Nature* **347**, 354–358 (1990).
- [6] Y. Li, H. Zhang, Y. Chen, Z. Shi, X. Cao, Z. Guo, P.K. Shen Nitrogen-doped carbon-encapsulated SnO₂@Sn nanoparticles uniformly grafted on three-dimensional graphene-like networks as anode for high-performance lithium-ion batteries *ACS Appl. Mater. Interfaces*, 8 (2016), pp. 197-207
- [7] Novoselov, K. S. et al. Twodimensional atomic crystals. *Proceedings of NationalAcademy of Sciences* 102, 1045110453 (2005).
- [8] Jaemyung , K., , Laura J, .., & Jiaxing, H. (2012). Two Dimensional Soft Material: New Faces of Graphene Oxide. *ACS publications* .
- [9] JAEMYUNG, K., , LAURA J, C., & JIAXING , H. (2012). Two Dimensional Soft Material: New Faces of. *acount of chemical research* .
- [10] Maurizio , D., & Luca , O. (2018). 2D Materials for Gas Sensing Applications: A Review on Graphene Oxide, MoS₂, WS₂ and Phosphorene. *chemical sensors* .
- [11] Fu Z, Wang N, Legut D, et al. Rational design of flexible twodimensional MXenes with multiple functionalities. *Chem Rev*2019; 119:11980–2031
- [12] Zongyu, h., Xiang, Q., & jianxin, Z. (2022). 2D Monoelemental materials Xenes and related yechнологies beyond graphene. *deanta global publissing services , chennai india* .
- [13] Li, Z. and Y. Wu, 2D early transition metal carbides (MXenes) for catalysis. *Small*, 2019. 15(29): p. 1804736

- [14] Tianjie , X., , Yuhua , W., Zuzhao , X., & Yitong , W. (2022). A Rising 2D Star: Novel MBenes with Excellent Performance in Energy Conversion and Storage.
- [15] M. Ade, H. Hillebrecht, Ternary borides Cr₂AlB₂, Cr₃AlB₄, and Cr₄AlB₆: the first members of the series (CrB₂)_nCrAl with n = 1, 2, 3 and a unifying concept for ternary borides as MAB-phases. *Inorg. Chem.* 54(13), 6122–6135 (2015).
- [16] M. Naguib, O. Mashtalir, J. Carle, V. Presser, J. Lu, L. Hultman, Y. Gogotsi, M. W. Barsoum, *ACS Nano* 2012, 6, 1322.
- [17] Anasori, M. R. Lukatskaya, Y. Gogotsi, *Nat. Rev. Mater.* 2017, 2, 16098.
- [18] K., L., S., K., & T.-C., J. (2023). Emerging borophene two-dimensional nanomaterials for hydrogen storage. Department of Mechanical Engineering Science, University of Johannesburg, Johannesburg, Auckland Park, 2006, South Africa.
- [19] Boustani, Ihsan (January 1997). "New quasi-planar surfaces of bare boron". *Surface Science*.
- [20] Pranay , R., Jang Mee , L., Prashant , K., & Ajayan, V. (2020). Borophene: New Sensation in Flatland. Department of Physics.
- [21] C. Maani, A. McKinley, R. H. Williams, *J. Phys. C.: Solid. State Phys.*
- [23] S.Zhang, M.Xie, F.Li, et al., Semiconducting group 15 monolayers: a broad range of bandgaps and high carrier mobilities, *Angew. Chem.* 128(5)(2016)1698.
- [24] Charlotte, T.-C. (2019). Optical reconfiguration of microwave functionalities.
- [25] K. Ledwaba , S., K., & T.-C., J. (2022). Emerging borophene two-dimensional nanomaterials for hydrogen storage. Department of Mechanical Engineering Science, University of Johannesburg, Johannesburg, Auckland Park, 2006, South Africa.
- [26] Manzeli, s., Dmitry , O., Diego , P., & , Oleg . (2017). 2D transition metal dichalcogenides.
- [27] Narayanasamy, s., & vellalalayam, d. (2019). two-dimensional transition metal dichalcogenides synthesis properties and applications. college of information science and electronic engineering .
- [28] Hussein O. Badr 1, T. E.-M. (2021). Bottom-up, scalable synthesis of anatase. 1 Department of Material Science and Engineering, Drexel University, Philadelphia, PA, USA .

- [29] M.C. Şenel, M. Gürbüz, E. Koç, *Engineer & the Machinery Magazine* (2015).
- [30] kazuyuki, t., seiya, t., feiyu, k., & michio, i. (2020). graphene preparation properties applications and prospects.
- [31] Y W Sun, D. G. (2021). Mechanical properties of graphene. School of Engineering and Materials Science, Queen Mary University of London,.
- [32] Lim, C. S.; Sofer, Z.; Mazánek, V.; Pumera, M. Layered Titanium Diboride: Towards Exfoliation and Electrochemical Applications. *Nanoscale* 2015, 7, 12527–12534.
- [33] Park, H.; Lee, E.; Lei, M.; Joo, H.; Coh, S.; Fokwa, B. P. T. Canonical-Like HER Activity of Cr_{1-x}MoxB₂ Solid Solution: Overpowering Pt/C at High Current Density. *Adv. Mater.* 2020
- [34] Heine, T. Transition Metal Chalcogenides: Ultrathin Inorganic Materials with Tunable Electronic Properties. *Acc. Chem. Res.* 2015, 48, 65–72.
- [35] Mengrao, T., Jiaming, L., Yu, W., Wenjuan, h., Shichong, X., Ming Lu, . . . ORCID and Ha. (2022). Surface Terminations of MXene: Synthesis, Characterization, and Properties. china.
- [36] G. Tai, T. Hu, Y. Zhou, X. Wang, J. Kong, T. Zeng, Y. You, and Q. Wang, “Synthesis of atomically thin boron films on copper foils,” *Angewandte Chemie International Edition*, vol. 54, no. 51, pp. 15473–15477, 2015.
- [37] B. Peng, H. Zhang, H. Shao, Y. Xu, R. Zhang, and H. Zhu, “The electronic, optical, and thermodynamic properties of borophene from first-principles calculations,” *Journal of Materials Chemistry C*, vol. 4, no. 16, pp. 3592–3598, 2016
- [38] J. Yang, R. Quhe, S. Feng, Q. Zhang, M. Lei, and J. Lu, “Interfacial properties of borophene contacts with two-dimensional semiconductors,” *Physical Chemistry Chemical Physics*, vol. 19, no. 35, pp. 23982–23989, 2017
- [39] Shao, L.; Li, Y.; Yuan, Q.; Li, M.; Du, Y.; Zeng, F.; Ding, P.; Ye, H., Effects of Strain on Mechanical and Electronic Properties of Borophene. *Mater. Res. Exp.* 2017, 4, 045020.
- [40] Feng, B.; Zhang, J.; Zhong, Q.; Li, W.; Li, S.; Li, H.; Cheng, P.; Meng, S.; Chen, L.; Wu, K., Experimental Realization of Two-Dimensional Boron Sheets. *Nat. Chem.* 2016, 8, 563.

- [41] Mortazavi, B.; Rahaman, O.; Dianat, A.; Rabczuk, T., Mechanical Responses of Borophene Sheets: A First-Principles Study. *Phys. Chem. Chem. Phys.* 2016, 18, 27405-27413.
- [42] Xiao, H.; Cao, W.; Ouyang, T.; Guo, S.; He, C.; Zhong, J., Lattice Thermal Conductivity of Borophene from First Principle Calculation. *Sci. Rep.* 2017, 7, 45986.
- [43] R. Raccichini, A. Varzi, S. Passerini, B. Scrosati, The role of graphene for electrochemical energy storage, *Nature materials* 14(3) (2015) 271-279.
- [44] V. Eswaraiyah, V. Sankaranarayanan, S. Ramaprabhu, Graphene-Based Engine Oil Nanofluids for Tribological Applications, *ACS Applied Materials & Interfaces* 3(11) (2011) 4221-4227.
- [45] D. Berman, A. Erdemir, A.V. Sumant, Graphene: a new emerging lubricant, *Materials Today* 17(1) (2014) 31-42.
- [46] M. Ratoi, V.B. Niste, J. Walker, J. Zekonyte, Mechanism of Action of WS₂ Lubricant Nanoadditives in High-Pressure Contacts, *Tribology Letters* 52(1) (2013) 81-91.
- [47] X. Shi, S. Song, W. Zhai, M. Wang, Z. Xu, J. Yao, A.Q.U. Din, Q. Zhang, Tribological behavior of Ni₃Al matrix self-lubricating composites containing WS₂, Ag and hBN tested from room temperature to 800 °C, *Materials & Design* 55 (2014) 75-84.
- [48] Zhou, X.; Liu, Y.; Hu, X.; Fang, L.; Song, Y.; Liu, D.; Luo, J. Influence of elastic property on the friction between atomic force microscope tips and 2D materials. *Nanotechnology* 2020, 31, 285710.
- [49] Berman, D.; Erdemir, A.; Sumant, A.V. Graphene: A new emerging lubricant. *Mater. Today* 2014, 17, 31-42.
- [50] Lee, C.; Wei, X.; Kysar, J.W.; Hone, J. Measurement of the Elastic Properties and Intrinsic Strength of Monolayer Graphene. *Science* 2008, 321, 385-388.
- [51] Yao, Q.; Qi, Y.; Zhang, J.; Zhang, S.; Zhao, P.; Wang, H.; Feng, X.-Q.; Li, Q. Impacts of the substrate stiffness on the anti-wear performance of graphene. *AIP Adv.* 2019, 9, 075317.
- [52] Y. Huang, Q. Yao, Y. Qi, Y. Cheng, H. Wang, Q. Li, et al., Wear evolution of monolayer graphene at the macroscale, *Carbon* 115 (2017) 600-607.

- [53] P. Wu, X. Li, C. Zhang, X. Chen, S. Lin, H. Sun, et al., Self-Assembled graphene film as low friction solid lubricant in macroscale contact, *ACS Appl. Mater. Interfaces* 9 (25) (2017) 21554–21562.
- [54] Y. Liu, X. Chen, J. Li, J. Luo, Enhancement of friction performance enabled by synergistic effect between graphene oxide and molybdenum disulfide, *Carbon* 154 (2019) 266–276.
- [55] H.-J. Kim, D-E. Kim, Water lubrication of stainless steel using reduced graphene oxide coating, *Sci. Rep.* 5 (2015) 17034.
- [56] H.J. Kim, D.G. Shin, D-E Kim, Frictional behavior between silicon and steel coated with graphene oxide in dry sliding and water lubrication conditions, *Int. J. Precision Eng. Manuf.-Green Technol.* 3 (1) (2016) 91–97.
- [57] Xiaonan, M., Zhangpeng, L., Shuwen, L., Jinqing, W., & Shengrong, Y. (2023). MXenes in tribology: Current status and perspectives. keaipublishing.
- [58] Y. Chen, et al., *J. Colloid Interface Sci.* 310 (2007) 171-177.
- [59] F. Labat, P. Baranek, C. Adamo, *J. Chem. Theory Comput.* 4 (2008) 341–352.
- [60] Hussein, O., Francisco, L., Daniel E. Autrey, Jacob Cope, Takayuki Kono, Takeshi Torita, Michel W. Barsoum. (2023). On the structure of one-dimensional TiO₂ lepidocrocite. *Matter*.